STUDY OF ELECTROSTATIC EFFECTS ON CONDENSING HEAT TRANSFER

HARRY Y. CHOI

TUFTS UNIVERSITY

JOHN M. REYNOLDS III

MASSACHUSETTS INSTITUTE OF TECHNOLOGY

FOREWORD

This report was prepared at Tufts University and Massachusetts Institute of Technology by Dr. Harry Choi and Dr. John Reynolds respectively, under USAF Contract No. AF33(657)-10908. The contract was initiated under Project No. 6146, "Thermal and Atmosphere Control," Task No. 614615, "Internal Thermal Management." The work was administered under the direction of the Air Force Flight Dynamics Laboratory, Vehicle Equipment Division, Mr. Eugene A. Zara, Project Engineer.

This report covers work conducted from February 1963 to May 1964 and was submitted by the authors in October 1964.

ABSTRACT

During the past year the program of study on the effects of strong electric fields on condensation heat transfer and two-phase flow has provided some valuable knowledge. It has been confirmed that significant changes in the flow regimes and heat transfer are possible with negligible electrical power expenditure. Over 100 per cent increase in heat transfer has been attained with pressure drop increases which are of the order of 15 per cent in the annular flow regime. These investigations were performed on two separate apparatus: one at Tufts University in which heat transfer phenomena in condensation were investigated and one at the Massachusetts Institute of Technology in which hydrodynamic phenomena in two-phase flow were studied.

Results show that the slug flow regime is substantially suppressed. In essence, slug flow occurs only in the region of very low gas flows in which the system is almost entirely gravity dependent. The increase in heat transfer rates is gradual up to a certain threshold value of the applied voltage; beyond this value, the increase is steep. Some progress has been made in analytical and physical modeling of the phenomenon both from the viewpoint of determining pressure drop and heat transfer and of aiding in the determination of the fluid configuration at the heat transfer surface.

This technical report has been reviewed and is approved.

T. J. BAKER
Asst. For Research & Technology
Vehicle Equipment Division
AF Flight Dynamics Laboratory

TABLE OF CONTENTS

ILLUSTRATIONS

ILLUSTRATIONS (CONT'D)

NOMENCLATURE

a	liquid film thickness: inch
A	area: ft^2
b	vapor film thickness: inch
c_l	specific heat of liquid: Btu/lbm^oF
c_p	specific heat of vapor at constant pressure: Btu/lbm^oF
D	diameter: inch
D_h	hydraulic diameter: inch
E	electric field intensity: volts/in
f	friction factor
F	electric force: Newtons/meter^3 or lbf/ft^3
g	gravitational acceleration: ft/sec^2
g_o	constant: 32.2 lbm-ft/lbf-sec^2
h	heat transfer coefficient: Btu/hr-ft^2-^oF
h_{fg}	latent heat: Btu/lbm
h''_{fg}	$h_{fg} + c_p \Delta T_{sup} + \frac{3}{8} c_l \Delta T_{lm}$
I	Bessel function
I'	derivative of Bessel function with respect to r
j	$\sqrt{-1}$
J	current density: amperes/meter^2
k	thermal conductivity: Btu/hr-ft-^oF
K	wave number: 1/ft
K^*	characteristic wave number: 1/ft
K	Bessel function
K'	derivative of K with respect to r

p	pressure: lbf/in^2
q	electrostatic charge: coulombs
Q	rate of heat transfer: Btu/hr
R	radius: inch
R^*	radius to liquid-vapor interface: inch
t	time
T	temperature: ^oF
V	applied voltage: volts
V	velocity: ft/sec
V_g^*	parameter defined as: $V_g^* = V_g \frac{g}{g(\quad - \quad g)D_h}$
V_c	phase velocity of capillary wave: ft/sec
V_e	phase velocity of an electrohydrodynamic wave: ft/sec
V_g	phase velocity of gravity wave: ft/sec
w	surface charge density at one side of interface: coulombs/m^2
W	net surface charge density: coulombs/m^2
ΔT_{lm}	logarithmic mean temperature: ^oF
ΔT_{sup}	superheat temperature difference: ^oF

Greek letters

γ	perturbation parameter
δ	film thickness: inch
δ	charge separation
ϵ	dielectric permittivity: farads/meter
ϵ_o	permittivity in vacuum: 8.854×10^{-12} farads/meter
κ	relative dielectric constant

λ	wave length: ft
λ^*	characteristic wave length: ft
μ	viscosity: lbm/hr-ft
ν	kinematic viscosity: ft^2/hr
ξ	equivalent body force: lbf/ft^3
ρ	density: lbm/ft^3
ρ_e	electrostatic charge density: $coulombs/meter^3$
σ	surface tension: lbf/ft
σ	electric conductivity: mhos/meter
τ	shear stress: lbf/in^2
τ^*	dimensionless shear stress
ϕ	reading of flowrator meter: %
ϕ	free energy
φ	potential
ω	angular frequency: 1/sec
Σ	stress tensor
Δ	perturbation parameter

Subscripts

bottom	bottom chamber
cond.	condensation
e	electrostatic field quantity
eq	equivalent
g	gas phase in two phase flow
i	inner tube (electrode)
l	liquid phase
o	outer tube (condenser)
sat.	saturation condition

top top chamber

v vapor phase

Superscripts

(1),(2) phases (1) and (2) respectively

$\sim$ perturbed quantity

Overscripts

0,1,2 zero, first and second order terms respectively in stability analysis

Added Note

In the momentum boundary condition, on page 113

$\delta_{\alpha\beta}$ is the unit matrix, i.e. $\delta_{\alpha\beta} = 1$ if $\alpha = \beta$

$\delta_{\alpha\beta} = 0$ if $\alpha \neq \beta$

σ is the surface tension.

γ is a third subscript that takes on the values r, θ and z. We have followed the standard practice of using repeated subscripts to mean summation over all values of the subscript, so the $E_\gamma E_\gamma$ means sum of squares of components of E over all values of γ .

1.0 INTRODUCTION

This report describes the results of an investigation of the effects of strong electric fields on two phase flow and condensation phenomena. Essentially, this program has been undertaken to predict the values of internal heat transfer and fluid flow parameters which are required to determine the feasibility and practicality of electrostatic condenser designs. This program has been suggested by earlier exploratory work (Refs. 1 and 2) which indicated that application of electrostatic fields offer a promising and practical means of improving the performance of certain types of condensers.

Since the principles underlying electro-fluid interactions may not be familiar to the reader, we propose to outline, in some detail, the pertinent fundamental concepts of electrohydrodynamics.

The basis of electrohydrodynamics is the Coulomb force (Eq) experienced by a charge of q coulombs in a field of E volts/meter. To adopt the viewpoint of fluid dynamics, it is a simple extension of this concept to state that an element of a fluid containing a charge density of ρ_e coulomb/meter^3 in a field, E, is subject to a body force of $\rho_e E$ newtons/meter^3. A more subtle manifestation of the Coulomb force is that a body can experience a force in an electric field even though there is no net electric charge on the body. This is a consequence of the fact that all material bodies contain charges even though the sum of the negative charges exactly cancels the sum of the positive charges in the body. In the presence of a field, the positive and negative charges experience forces of opposite sign which tend to separate them as illustrated in Fig. 1a. This is the polarization phenomenon.

If the body is in a uniform electric field, it will experience two equal and opposite Coulomb forces. Consequently, the body will remain in equilibrium. If, however, the field is non-uniform, the small but finite separation between the lumped charges within the body must be considered. In this case one portion of the charge (-q) will be subject

to a field, E, while the other portion of the charge (+q) will be in a field of strength E + dE. Here dE refers to the change in field strength over the distance by which the positive and negative charge distributions are separated. That is, if the positive and negative charges can be considered as separated by the small distance, δ, then

$$dE = \delta \, dE/dx \tag{1}$$

Consequently, the body experiences a force

$$\begin{aligned} F &= (-q)E + (+q)(E + \delta \, dE/dx) \\ &= q \, \delta \, dE/dx \end{aligned} \tag{2}$$

The quantity ($q \, \delta$) is called the polar moment and is (Ref. 3) proportional to the field strength so that

$$F \sim E \frac{dE}{dx} = \frac{1}{2} \frac{dE^2}{dx} \tag{3}$$

Consequently, it is clear that it is possible to have a net electrical force on a fluid element even though that element carries no charge. This development can be extended to a fluid continuum (Ref. 4) with the result that

$$F = \rho_e E + \frac{1}{2} \rho \left(\frac{\partial \epsilon}{\partial \rho}\right)_T \text{grad } E^2 \tag{4}$$

for homogeneous fluids. The first term in this expression is simply the coulomb-force and the second is the "electrostrictive" force which is analogous to Eq. (3) with the coefficient of proportionality given by the quantity $\rho(\partial \epsilon/\partial \rho)_T$. This coefficient can be evaluated for any particular fluid by electrical equations of state relating the various properties of that fluid. One of these equations is the Clausius Mossotti law (Ref. 5) which states

$$\frac{\kappa - 1}{\kappa + 2} = c\,\rho \qquad (5)$$

where c is a constant for the particular fluid under consideration and κ is the permittivity relative to that of free space ($\epsilon = \kappa\,\epsilon_o$). Combining (4) and (5) and assuming $\rho_e = 0$ yields

$$F = (\epsilon_o/6)(\kappa - 1)(\kappa + 2)\ \text{grad}\ E^2 \qquad (6)$$

for the body force in a charge free and homogeneous fluid.

Some consequences of (6) are interesting. First, it is clear that if two fluids are present, the one having the greater dielectric constant (κ) will experience the greater force and will occupy those regions of space in which the field is strongest (see Fig. 1c). Secondly, the fact that the field enters (6) only as E^2 indicates that the direction of the force does not depend upon the polarity of the field; that is, the force is unidirectional even in an alternating field.

In addition to body forces, it is also necessary to consider forces acting at fluid surfaces. It is clear from Coulomb's law that an interface having a charge density of W coulomb/meter^2 in a field will experience a pressure of EW newton/meter^2. Again, it is less clear how an uncharged surface experiences a force. To see this, the fact must be recognized that the surface charge density is proportional to the jump across the interface in the quantity (ϵE) in the direction normal to the interface. Consequently, for a charge free surface, we must have (at the interface)

$$\epsilon_1 E_1 = \epsilon_2 E_2 \qquad (7)$$

As before, this does not mean that there are no charges on the interface, but simply that the sum of all the charges on the interface is zero. Actually, there is a layer of negative charge on one side of the interface (-w) and an equal layer of positive charge on the other side of the interface (+w). Consequently, an interfacial force is present of magnitude

$$E_1(-w) + E_2(+w) = w(E_2 - E_1) \tag{8}$$

this force has a net value since $E_1 \neq E_2$ from Eq. (7).

This discussion is meant merely to indicate the reasons for the existence of the force rather than to be a derivation. Actually, the expression for the interfacial stress is (Ref. 4)

$$\Sigma = \left[\frac{E^2}{2} \rho (\partial \epsilon / \partial \rho)_T - (\epsilon/2) E^2 + \epsilon E_n^2 \right] \tag{9}$$

where the square brackets indicate the magnitude of the discontinuity in the bracketed quantity across the interface. The subscript n refers to the field component normal to the interface. The first two terms in (9) are electrical "pressure" terms which are a consequence of the nature of the body forces discussed previously. The last term in the brackets is essentially a result of the interfacial charge distribution.

In practice, the fluid configuration is determined by both types of forces. The combined effect of these is often difficult to visualize. An alternative approach which is often helpful to the qualitative picture is to recognize that a minimum free energy statement is valid here and that the free energy is given by (Ref. 4)

$$\phi = \phi_o - \frac{1}{2} \epsilon E^2 \tag{10}$$

where ϕ_o is the free energy in the absence of a field. Consequently, a system is in equilibrium when that fluid having the highest available dielectric constant occupies that portion of the volume under consideration in which the field is greatest (as in Fig. 1c). For example, the free energy in a gravity field (ϕ_o) is simply ρgh where h is the height of a fluid element. Therefore, a parallel plate capacitor which is dipped into the interface between a gas ($\kappa_g \approx 1$) and a liquid ($\kappa_l \approx 2$) will become partially filled with liquid as in Fig. 2. The filling stops when the next increment of rise results in an increase of the system's gravitational free energy which is just balanced by the decrease of electrical free energy.

In the discussion above, it has been tacitly assumed that the field is known. Actually, it may be quite difficult to compute the field distribution for a given system. Conceptually, however, the procedure is quite simple. One of Maxwell's equations states that, in the absence of a magnetic field

$$\text{curl } E = 0 \tag{11}$$

Therefore, the field has a potential (φ, volts) such that

$$E = -\text{grad } \varphi \tag{12}$$

For perfect nonconductors which are charge free, another Maxwell equation requires that

$$\text{div } (\varepsilon E) = 0 \tag{13}$$

For perfect conductors, on the other hand, the current is conserved so that

$$\text{div } J = \text{div } (\sigma E) = 0 \tag{14}$$

where σ is the electrical conductivity (mho/meter) and J is the (vector) current density (amps/meter^2). If the properties (ϵ and σ) are constant, Eqs. (13) and (14) combined with Eq. (12) both yield Laplace's equation of the potential

$$\text{div (grad } \varphi) = 0 \qquad (15)$$

Thus, the nature of the fluid does not effect the governing equation of the system and both ideal dielectrics and ideal conductors are governed by Eq. (15). There are, however, important differences between these two classes of media and these are manifest in the boundary conditions, particularly the boundary condition at the interface between two fluids.

At the charge free interface between two perfect dielectrics we must have Eq. (7) satisfied. At the interface between two perfect conductors, the current must be continuous, or

$$\sigma_1 E_1 = \sigma_2 E_2 \qquad (16)$$

In general, the conditions (7) and (16) yield different results. Most of the classical literature divides the universe into dielectrics which satisfy Eqs. (15) and (7) and conductors which satisfy Eqs. (15) and (16). We will find, however, that this arbitrary division does not give a realistic physical picture of the nature of real systems. In fact, real fluids do have a finite conductivity. Even a very poor conductor must satisfy (16) in the steady state. If (16) is satisfied, (7) is not, so that a charge free interface does not exist in the actual steady state.

To illustrate the behavior of real fluids, consider the system shown in Fig. 3. This is simply a parallel plate capacitor in which a fluid-fluid interface is parallel to the electrodes. We will consider this system

from the instant that a voltage (V) is applied to the top plate so that φ is a function of time. Using the terms defined in Fig. 3, the appropriate boundary conditions are

$$\varphi_1(0,t) = 0 \tag{17}$$

$$\varphi_2(H,t) = V \tag{18}$$

$$\varphi_1(h_1,t) = \varphi_2(h_1,t) \tag{19}$$

These can be used to evaluate three of the four constants of integration which result from solving Eq. (15) in each of the two fluids. Since Eq. (15) simply requires a linear potential distribution, we have

$$\varphi_1(y,t) = A_1(t)y + B_1(t) \tag{20}$$

$$\varphi_2(y,t) = A_2(t)y + B_2(t) \tag{21}$$

Elimination of A_1, B_1 and B_2 with the aid of the above boundary conditions gives

$$\varphi_1 = \frac{y}{h_1}\,(V - A_2h_2) \tag{22}$$

$$\varphi_2 = V - A_2(H - y) \tag{23}$$

Another boundary condition is required to evaluate A_2. This comes from the conservation of charge at the interface, i.e.,

$$\left[\sigma \frac{\partial\varphi}{\partial y} + \epsilon \frac{\partial^2\varphi}{\partial y \partial t}\right] = 0 \tag{24}$$

where, as before, the bracket indicates the jump in the value of the enclosed quantity across the interface. The first term in (24) is the discontinuity in the current density across the interface. This discontinuity must be accompanied by a rate of charge accumulation on the interface which is given by the second term of (24). Substitution of Eqs. (22) and (23) into Eq. (24) results in a differential equation in $A_2(t)$ which has the solution

$$A_2(t) = c\, e^{-(\sigma^*/\epsilon^*)\, t} + \frac{\sigma_1}{\sigma^*}\, V \qquad (25)$$

where c is an arbitrary constant and

$$\sigma^* = \sigma_1\, h_2 + \sigma_2\, h_1 \qquad (26)$$

$$\epsilon^* = \epsilon_1\, h_2 + \epsilon_2\, h_1 \qquad (27)$$

Finally, an initial condition is required to evaluate c. Let us take the case that there is no charge on the interface at time zero. That is, at t = 0, Eq. (25) must satisfy condition (7). The final result is

$$-E_2 = \frac{\partial \varphi_2}{\partial y} = V\left(\frac{\epsilon_1}{\epsilon^*} - \frac{\sigma_1}{\sigma^*}\right) e^{-(\sigma^*/\epsilon^*)\, t} + \frac{\sigma_1}{\sigma^*}\, V \qquad (28)$$

In order to interpret the implications of this result, consider the case in which fluid 2 is a gas having a very low conductivity compared to that of fluid 1 which is a liquid. Then, Eq. (28) indicates that initially (t = 0)

$$E_2 = -\frac{\epsilon_1}{\epsilon^*}\, V \qquad (29)$$

which is the field distribution that would result if both fluids were ideal dielectrics. After a time equal to a few "relaxation times", ϵ^*/σ^*, the field is

$$E_2 = -\frac{\sigma_1}{\sigma^*} V \rightarrow -\frac{V}{h_2} \qquad (30)$$

for

$$\sigma_1 >> \sigma_2$$

which is the field distribution which results if the liquid is considered to be a perfect conductor.

Consequently, Eq. (28) indicates that the effective nature of the fluid changes with time during a transient of the order of ϵ^*/σ^* sec. Since this time varies from 10^{-1} to 10^{+4} sec for typical "dielectric" liquids, this is clearly an important practical consideration in determining the field distribution and, hence, the forces in real systems.

With the results discussed above, it is possible to predict electrical forces in the simpler geometries. In the present problem, however, it is not obvious what should be done with the forces once they are computed. Here we are concerned with an electrostatic condenser which, consists of a pair of concentric cylindrical electrodes forming an annular flow passage. Assume that there is a liquid film on the outer surface of the annular passage and that the remaining area is occupied by vapor. In this system, the electrical forces act in the radial direction normal to the flow direction.

The problem is complicated by the fact that any effect of the transverse electrical force field on the fluid configuration must also be a consequence of an alteration in the shape of the fluid interface. If one writes the axial force balance for the two fluid streams,

it becomes clear that the shear stress on the interface determines the fluid configuration. This interfacial shear is not simply a viscous stress, but may include a form drag due to the gas flow over the wavy interface. Anything which alters the nature of the waves on the interface will, in turn, cause a readjustment of the total fluid configuration. An analytical approach to wave phenomena necessarily involves a stability analysis of the system. This is done in detail in Appendix C. Here, we intend to summarize the thinking which goes into such an analysis. Essentially, the goal of stability analyses is the prediction of wave lengths as a function of system parameters.

The method of stability analysis is to assume that some particular interface shape is stable, the cylindrical shape in this case, and to investigate the behavior of this interface after an arbitrary disturbance. If, for example, a plane interface is perturbed so that it has a sinusoidal shape about its equilibrium position in the x-z plane, it will not, in general, remain stationary. That is, if the interface is initially given by $y = y_o$, then the perturbed interface is given by the real part of

$$y = y_o + \gamma\, e^{jKx} \tag{31}$$

where γ is a small perturbation parameter and K is a constant (the wave number). Since the interface given by Eq. (31) is not in equilibrium, it will move. Moreover, for a stable non-dissipative system, it will oscillate about its equilibrium position ($y = y_o$) with some frequency ω. That is, the interface will be given by the real part of

$$y = y_o + \gamma\, e^{j(Kx - \omega t)} \tag{32}$$

Since the motion is in response to the disturbance, however, it is clear that K and w cannot be independent. In fact, there is a characteristic w associated with each wave number. These values are determined from the equations of motion which the system must obey subsequent to its deformation.

It often happens, however, that there are no real values of w consistent with a given value of K. In such cases w becomes imaginary and the amplitude of the motion grows exponentially (like e^{wt}). This indicates that a disturbance having that wave number will increase without limit and the system is unstable. Moreover, of all the values of K for which the system is unstable, that K which yields the greatest (imaginary) value of w will grow the fastest. This value, then, is the characteristic wave number and is obtained from a solution of the equation

$$\frac{d\, w\ (K)}{dK} = 0 \qquad (33)$$

2.0 TWO PHASE FLOW PROGRAM

2.1 Summary

An experimental program has been undertaken to investigate the behavior of two phase (liquid-gas) flows in vertical tubes. The experiments have consisted of a study of the upward flow of silicone oil (Dow 200) and nitrogen in an annular flow passage having an outside diameter of 3/4" and an inner diameter of 1/2". The original intent of the program involved a study of the behavior of Freon 113 as the liquid phase rather than silicone oil. However, the use of Freon presents such significant experimental difficulties that it was felt that the basic data in the field of electrohydrodynamic two-phase flow would be more reliable if taken on a silicone oil system. The properties of silicone oil (except for density) are sufficiently close to those of Freon so that no important differences are anticipated between them with regard to frictional pressure drop and the flow regime map.

The effect of the field on the flow can be summarized as:

a) The transition from annular to slug flow is significantly suppressed, particularly at low liquid Reynolds number.

b) The pressure drop in annular flow is increased by the electric field.

These effects, in conjunction with visual observations of the flow, indicate that the liquid film thickness is significantly reduced by the electric field. This film reduction indicates that improvement in condensation heat transfer coefficients is to be expected in electrohydrodynamic condensers.

A considerable body of data has been obtained and a correlation of this data is presented. It appears from these results that it is possible to estimate the pressure drop of an electrohydrodynamic annular flow from data taken under ordinary conditions. The method is simply to perform ordinary two phase flow experiments at gas kinetic energy levels $(1/2)\rho_g V_g^2$ which correspond to the desired value of the total energy $(1/2)\rho_g V_g^2 + (1/2)\epsilon_o E_o^2$ in the electrohydrodynamic case.

2.2 Test Apparatus

2.2.1 General Discussion

A basic two phase flow apparatus was designed and constructed for the study of two phase flow under the influence of electrostatic fields. The apparatus is suitable for related studies in EHD such as single phase flow, free and forced convection by appropriate changes of test sections and details of the instrumentation. A schematic of the system is given in Fig. 4.

All materials used are compatible with Freon-113 and silicone oil which means that glass, copper, brass, stainless steel, Buna-N rubber, nylon, teflon and plexiglass have been used exclusively in the flow systems.

2.2.2 Test Section

The test section consists of an approximately four foot long vertical glass tube .742" I.D. In the present arrangement, flow is upwards for both phases. The inside of the tube is coated with a transparent, electrically conducting layer of tin oxide. Centered in the glass tube is the electrode, a .500" O.D. steel tube with good surface finish. The high voltage is applied to the electrode with the coated surface on the glass tube grounded. The radial spacing for the field is 1/8". The annular flow channel formed has a hydraulic diameter of 1/4" and a cross sectional area closely corresponding to that of a 1/2" I.D. pipe.

The glass tube is divided in two parts to provide a pressure tap in the middle. The two pieces are joined together in a brass body (Fig. 5). To insure an uninterrupted field, the coating is brought around the end of the tubes and one inch up on the outside. A thin aluminum foil connects the coating with a screw on the flanges. A second pressure tap is located before the outlet in a similar arrangement (Fig. 6).

The first two feet of the test section is an entrance and calming region, all measurements are made over the remaining two feet of length. A square one foot long box of plexiglas with one side white opaque is placed around the test tube and sealed at the bottom. It is used for photographic purposes to provide a reflecting surface for the light and may be filled with a proper fluid to reduce the distortion of the picture from the glass tube and liquid inside acting as a cylindrical lens.

2.2.3 Inlet Section

The inlet section (Fig. 7) provides the liquid and gas supply to the test section, and supports the glass tube and center electrode. It consists of a cylindrical plexiglas body 6.5" dia. with a large opening in the bottom and an opening on the gas inlet side to furnish a possibility to change inlet configurations and test section geometries.

Preliminary runs with a simple slug flow inlet (a piece of pipe bent at the end for the gas flow, meeting the liquid flow, forming a T-inlet) revealed that bubbly flow and slug flow show minute changes with electrical field applied. For annular flow, however, especially at low liquid flow rates, merely visual observations brought out spectacular changes in the flow pattern and measurements showed an accompanying considerable field effect on the pressure drop. Consequently, the effort was concentrated on this promising flow regime.

It was desired to produce better defined inlet conditions than those the simple T-mixing chamber would provide. A porous cylinder, made from molded cellulose filter material and with the same I.D. as the test tube is inserted in a plexiglas housing (Fig. 7) in the liquid inlet chamber and the electrode and gas inlet pipe are sealed off from the chamber with O-rings. The liquid flows through the plug, the gas stream rushes by and the result is an annular liquid film flowing on the glass tube wall and virtually no film on the electrode, provided that the flow rates are such that annular flow is possible. This simulates the gradual build up of a liquid film on the inside of a cooled condenser tube with saturated vapor flow.

The electrode is centered in the housing for the porous cylinder, and sealed off in a plexiglas bottom plate which is free to move radially. It is firmly supported by a steel device provided with set screws for accurate centering and lining up of the electrode. The plexiglas body is an effective and safe insulator for the high voltage. The connection between the power supply and the electrode is made in a glass container filled with transformer oil, the level of which covers all metal parts of the inlet section connected with the electrode.

The inlet section can with minor alterations accommodate test tube sizes up to 1.5" I.D. and electrodes from thin threads and up.

2.2.4 The Outlet Section

The outlet from the test section (Fig. 6) is a brass body to which the test section glass tube is connected and extending some eight inches up in the liquid collecting tank. The field is uninterrupted all the way to the actual outlet point. The two phase

mixture is exhausted up in a chamber with appropriate drain passages formed in a cylinder of plexiglas. The plexiglas cylinder is a film support and a centering device for the electrode and insulates it electrically from the grounded tank. The liquid level in the tank is kept a couple of inches below the outlet, thus the test section experiences a constant outlet head.

The gas exhausts from the tank via a separator through a control valve on the control board. With this valve the outlet pressure from the test section can be set at any desired value thus providing a possibility to test with different gas densities by merely changing the system pressure.

Liquid is circulated (Fig. 4) by a centrifugal pump equipped with a variable speed drive providing a discharge pressure corresponding to 20 feet of head at 20 gpm. When running the system under elevated pressure the whole liquid system is pressurized and the pump only has to make up for headlosses in the system.

A full flow filter is installed to keep impurities from entering the test section and reduce the breakdown voltage for the system. Two tapered glass tube flow rators are connected in such a way that only the control valves have to be operated on to switch from the large to the small one, shut off valves are provided to accomplish changes of floats or tubes. Make up liquid is introduced by pouring directly to the collecting tank, a sight glass yields information when addition is necessary.

Before the apparatus is put into operation with silicone oil the piping systems were thoroughly cleaned by pumping F-113 through for several hours. The systems were drained and nitrogen blown through to dry out any remaining solvent. A new filter cartridge was installed and the system filled with silicone oil. At shut off both systems are closed from communication with the atmosphere.

2.2.5 Power Supply

A 120 KV - 5 mA power supply is installed. By changing connections in the transformer it can produce DC with positive or negative polarity and 60 cycles AC.

2.2.6 Instrumentation

The static pressure drop in the test section, gas and liquid flow rates, outlet pressure and applied voltage are the prime quantities to be measured.

The static pressure drop is measured by the difference in liquid levels in two vertical glass tubes (Fig. 4) directly connected with the two pressure taps 24.00" apart along the test section. To keep the common level on eye level for convenience, the free ends of the manometer tubes are connected to a manifold supplied with pressure from a nitrogen bottle.

Two flow rator meters measure the liquid flow rate by position of a float in a vertical tapered glass tube. The range is 0.2 to 9.5 gpm with three different floats for the 1" flowmeter, 5 cc/min to 200 cc/min for the smaller one with 1/8" and 1/4" tube sizes. The accuracy is approximately 2% of full scale reading for any float or tube. The 1/8" and 1/4" flowmeters have a spherical float and are working on viscous forces. Since the viscosity of the silicone oil is a function of temperature, the temperature of the liquid is measured before the inlet to the smaller flow meter.

The pressure taps and liquid flow rates were checked by single phase pressure drop measurements (Fig. 8) which indicated that the instrumentation is sufficiently accurate for the purposes of the current project.

The gas flow rate is measured by the pressure drop over an ASME square-edged orifice .1875" dia. in a 1 1/4" I.D. pipe. The pressure drop is measured on two u-tube manometers, filled with silicone oil and mercury respectively, to cover the whole range of flow rates. Temperature and pressure are measured before the orifice.

2.3 Experimental Results

The effect of an electric field on the upward flow of silicone oil (Dow 200, 2 centistoke) and nitrogen is shown on Fig. 9. It is clear that the wavelength of the interfacial disturbances is reduced by the application of the field. Ultimately, at this flow condition, the film is no longer continuous on the outer wall as shown in Fig. 9c.

A direct manifestation of the decreased film thickness can be observed when the electric field is shut off. Then the film runs down the tube wall indicating that the interfacial stress is no longer adequate to maintain such a thin film. Eventually, a new film of the conventional type becomes reestablished by rising up from the inlet section.

The consequences of this change in flow configuration would be expected to involve an increased friction factor and a reduced gravity head. This is apparently what actually does occur as shown by the data of Figs. 10 through 14. At low gas flow the gravitational terms are important, and it is clear that the pressure gradient is reduced by application of the field. At higher gas flows, however, the gravitational term loses importance relative to the frictional effects at the interface and the pressure gradient is increased by the application of the field.

The data taken indicates that the effect of electric fields on two phase flow is to increase the interfacial friction factor in annular flow. This in turn:

a) delays the slug-annular transition so that annular flow is obtained at significantly lower gas velocities,

b) decreases the overall pressure gradient at the lower gas velocities where the gravity head is important,

c) increases the overall pressure gradient at higher gas velocities where the gravity head is relatively small,

d) dramatically reduces the liquid film thickness on the outer wall. At modest liquid flow rates, the field virtually reduces the film thickness to zero. This reduction has obvious application to improving heat transfer to condensate films.

2.4 Correlation of the Data

Although the data taken to date suffers from the serious deficiency that void fractions have not been measured, some attempt has been made to put the overall pressure drop data into a rational form. This can be accomplished by considering the result of the stability analysis. Essentially this is that the characteristic wave number is given by (see Appendix C)

$$K^* = \frac{3}{4\sigma}\left[\rho_g (V_1 - V_g)^2 + (1 - \frac{\epsilon_g}{\epsilon_1})^2 \epsilon_1 E_1 E_g\right] \qquad (2.1)$$

For the two phase flow experiments, it is reasonable to assume that $V_g > V_1$. In addition, if the flowing media are nonconductors $\epsilon_1 E_1 = \epsilon_g E_g$ at the interface and the wave number (2.1)

$$K^* = \frac{3}{2\sigma}\left(\frac{1}{2}\rho_g V_g^2 + \frac{1}{2}(1 - \frac{\epsilon_g}{\epsilon_1})^2 \epsilon_g E_g^2\right) \qquad (2.2)$$

Equation (2.2) represents the desired result, that is, the group of terms in the brackets represents a rational means of combining electrical and hydrodynamic parameters. Actually, this rule of combination is only approximate since the kinetic energy is based upon a mean velocity and the value of E_g used must account for the fact that there are actually two liquid films present, one on each electrode surface. Consequently, we assume that it is sufficiently accurate to simply add the kinetic and electrical energy densities, i.e., $1/2\ \rho_g V_g^2 + 1/2\ \epsilon_g E_g^2$,

to form the correlation parameter. On this assumption, the pressure drop data were plotted against the total energy density that is $(1/2)\rho_g V_g^2 + (1/2)\epsilon_o E_o^2$. This plot is shown in Fig. 15. It seems clear from this plot that this is a powerful correlating factor for sufficiently large flow rates.

The curves for various voltages are in fact separate at low energy densities. This is due to the fact that transition to slug or wavy flow occurs at different values of the energy density for different field strengths. This is unavoidable in the plotting scheme. The important feature of Fig. 15 is, however, that all the constant field curves ultimately come together. This indicates that a friction factor based upon the total energy density rather than simply the kinetic density is an appropriate one for electrohydrodynamic flow. That is, after an undefined transition region it appears appropriate to define a new friction factor by

$$\Delta p = f_e \left(\frac{L}{D}\right) \left(\frac{1}{2} \rho_g V_g^2 + \frac{1}{2} \epsilon_o E_o^2\right) \qquad (2.3)$$

This definition indicates clearly the behavior of the data shown in Fig. 15. That is, the pressure drop in an electrohydrodynamic flow can be determined from the ordinary pressure drop by considering the two at equal values of total energy and liquid flow rate. There are clearly limitations to this statement. However, the tendency seems clear. It should be noted that similar correlations have also been obtained for liquid flow rates of 1.4 and 21.8 lbm/hr.

If now, fe is considered to be a function of the dimensionless gas velocity

$$V_g^* = \rho_g^{\frac{1}{2}} V_g \, g \, D_h (\rho_1 - \rho_g)^{-\frac{1}{2}} \qquad (2.4)$$

defined by Wallis (Ref. 6), the results shown in Figs. 16 through 18 are obtained. It is seen that, at least for the lower flow rates, the modified friction factor approaches a constant value which is apparently independent of applied voltage. This correlation is the suggested form of the limited range of data on which it is based.

2.5 Applicability of the Results

From a design viewpoint, it is clear that an appropriate energy density must somehow be maintained in the system. The present result indicates that, as far as flow configuration is concerned, the form of this energy is immaterial. That is, for sufficiently high values of the total energy density, it is immaterial whether the energy is supplied in the form of kinetic energy or electrical energy, and the flow configuration depends only on the value of total energy density. Consequently, since the power expenditure in maintaining the field is minute, the total power expenditure (pump work) will be lower when high fields are employed rather than high velocities.

This fact is clear from Fig. 15 as well as Figs. 16 through 18. There it is seen that the pressure drop is, ultimately, a function only of energy density. Consequently, the flow work (approximately $V_g \Delta p$) will decrease the field when it is applied. This result indicates that the use of electric fields is, indeed, a promising practical method of altering the flow conditions.

It is important to note in closing that the field is relatively unimportant in energetic considerations. Throughout the present program the current has remained below 10^{-4} amperes which is the limit of the present instrumentation. Consequently the power requirement has always been less than 1.5 watts.

3.0 CONDENSER PROGRAM

3.1 Summary

Simultaneously with the two phase flow program, an experimental program was undertaken to study the effect of an electrostatic field on condensation heat transfer. The experimental system is shown in Fig. 19 and described in Section 3.3. Freon-113 is condensed inside a vertical tube and the condensate interface is stressed by a radial DC field.

The effect of the field on condensing heat transfer can be summarized as follows:

a) The condensing heat transfer coefficient increases significantly with the electric field.

b) The increase is related to the appearance of instability waves at the liquid film interface.

These effects in conjunction with the visual studies in the two-phase flow program suggest that the average liquid film thickness is significantly reduced at high electric field intensities.

Without electric field, the film Reynolds number suggests laminar flow condensation throughout at least eighty per cent of the tube, and the heat transfer data shows an acceptable degree of correlation with theory taking into account the interfacial shear. A tentative correlation is presented for the high-field data. The correlation is presented in terms of a Nusselt number and a Grashof number in which the characteristic length is the most unstable wave length in the system and the driving force acting on the film is an equivalent electrohydrodynamic body force.

3.2 Visual Condensation Study

Preliminary studies were conducted in a visual apparatus in an attempt to identify the type of electrohydrodynamic instability under actual condition of forced convection condensation. Details of the visual system are shown in Fig. 23 and described in Section 3.3.8. Freon vapor was condensed on the inner wall of a vertical electrically-conducting glass tube and a radial electric field was applied normal to the condensate film interface.

The stages of development of the wave pattern with increasing field are shown in Fig. 24 and might be described as follows. As the voltage is increased, the condensate film becomes dynamically unstable and develops ridges. The ridges in turn become unstable and droplets form. The wave lengths observed are of the order of 1 mm. It is anticipated that at even higher values of the electric field intensity the droplets would break away as sprays into the vapor stream. This final stage was not observed because of the experimental limitation of the visual system. Pictures A through D in Fig. 24 were taken with a strobe light at 4200 cpm and clearly show the drop pattern on the condensate film. Picture E in Fig. 24 was taken under identical experimental conditions as Picture D, but with natural lighting and shows the phenomenon as would be seen by human eyes. The pictures lack somewhat in clarity, but allowance should be made for the difficulty of focusing on the condensate film inside a glass condenser tube.

It may be noted that a similar type of wave pattern can be produced by letting a thin film of water flow down the underside of a glass plate inclined at a small angle from the horizontal, as shown in Fig. 25. In this situation, there is a gravitational acceleration component normal to the flowing film. Figure 26 (Ref. 8) shows the instability of a liquid film on the outside surface of a vertical, rotating cylinder, at accelerations of the order of 3 to 8 gees normal to the flowing film. The pictures were apparently taken under natural lighting conditions, and may be compared with Picture E of the electrohydrodynamic (EHD) waves in Fig. 24.

Since the EHD waves on the condensate film were essentially identical to those observed in the two-phase flow system, no visual work was planned for the condenser loop.

3.3 Test Apparatus and Procedure

3.3.1 General Discussion

A condenser loop was built to perform experimental investigation of the electrostatic effects on condensing heat transfer inside a vertical tube with forced convection. Freon-113 was chosen as the test fluid. A schematic diagram of the test loop is shown in Fig. 19 and a brief description on the loop operation is presented below.

Freon is boiled inside a 10 gallon cylindrical tank, heated by a water bath equipped with a temperature control and a 4 KW heater. The boiler has a vapor generation capacity of 160 lbm/hr. A direct immersion of an electric heating element in the freon was avoided to prevent any possible dissociation of the freon at the high surface temperature of the heating element. Freon vapor from the boiler flows through a filter-drier unit and is slightly superheated before the inlet to a vertical condenser tube. Vapor is condensed on the inner wall of the tube by counter flowing cooling water in the condenser jacket. The condensed freon is collected and measured in the condensate collecting burette; excess vapor is trapped in the bottom chamber of the condenser tube and condensed in an auxiliary condenser. All the condensed freon, then, is pumped back to the boiler.

To evaluate the variation of the condensing heat transfer coefficient and the condenser wall temperature with the electrostatic field, the following quantities are measured:

Temperature and pressure of vapor at inlet and outlet of the test section.
Temperature of condenser tube wall at several locations.
Vapor flow rates before and after the test section (flowmeters).
Temperature and pressure of vapor in the flowmeters.
Time to collect 500 cc of condensate in the collecting burette.
Temperature of the condensate in the collecting burette.
Coolant flow rate (orifice).
Temperature rise of the coolant flow.
Applied voltage.

The loop was operated at slightly pressurized condition and air in the loop was scavanged carefully before each series of tests (see Section 3.3.7).

3.3.2 Test Section

The test section consists of three concentric vertical tubes: the inner tube is the electrode, the outer tube is the coolant jacket and the intermediate tube is the condenser. The condensing tube is made of 304 stainless steel, 53" long and 1" OD by 0.032" wall thickness, and is grounded. Five copper-constantan thermocouples are soldered into grooves on the outside surface of the tube, at distances of 4", 15.25", 26.5", 37.75" and 49" from the inlet. The grooves are cut in the wall to half the wall thickness. The central electrode is also made of 304 stainless steel tube of good surface finish. Three electrode sizes were used--1/4", 1/2", 3/4" OD. It is noted that as the electrode diameter is changed, both the annular flow channel of the vapor as well as the radial gap distance of the electric field are changed. The cooling jacket is made of a plexiglas tube, 50" long and 2" OD by 1-1/2" ID and flanged at both ends to enable bolting to the top and bottom chambers of the test section. The test section assembly is insulated with fiberglas insulation. The thermocouples leads are brought out over the rubber gasket between the cooling jacket flange and the top plate of the bottom chamber.

3.3.3 Inlet Section (Top Chamber)

The inlet section is made of 1/4" plexiglas, and measures 8 1/2" x 8 1/2" x 8 1/2" with 10" x 10" flanges at top and bottom. The details are shown in Fig. 21. The condenser tube extends into the chamber via an O-ring seal. A major problem in design was the end support for the electrode which would accommodate electrodes from wires to tubes, allow accurate centering, and maintain electrode rigidity under thermal expansion. The first design with spring support of the electrode proved unsatisfactory. The slightest eccentricity resulting from the different thermal expansion of the stainless steel and the plexiglas in the test section caused local shorting at high electrostatic fields. In the final design, instead of a spring, a 3" OD x 2.5" ID plexiglas cylinder with a 1/2" thick top plate is used and the electrode is bolted down through the center of the plate. Holes drilled in the top plate, as well as on the side of the cylinder allow uninterrupted passage of vapor into the condenser tube. After warm-up, the electrode is re-centered and tightened at the condenser operating temperature. The electrode is supported in an identical manner in the bottom chamber.

3.3.4 Outlet Section (Bottom Chamber)

The bottom chamber of the test section has similar dimensions as the top chamber and supports the coolant jacket, the condenser and the electrode. The details, including the electrode support, are shown in Fig. 22. A U-loop in the condensate outlet from the bottom chamber serves to trap the excess vapor. Occasionally, a rapid pressure rise in the bottom chamber as when the electric field is suddenly shut off blows down the condensate in the U-loop and some of the vapor escapes into the condensate collecting burette. Such a condition can be corrected merely by waiting a few minutes until the system regains steady state.

The condensate from the test section and the auxiliary condenser is pumped back to the boiler by a variable-speed centrifugal pump.

3.3.5 Power Supply

A 30 KV - 10 ma power supply (NJE Power Supply, Model HA-30-10A) is used and the high voltage lead is connected to the test section electrode through the top chamber. By changing connections in the transformer of the power supply, it can produce DC with positive or negative polarity and 60 cycles AC. All the test results in this report were obtained with DC fields.

3.3.6 Instrumentation

The quantities measured during an experiment are listed in Section 3.3.1. The pressures of the vapor in the top and bottom chambers of the test section and in the flowmeters are measured with mercury manometers which can be read to an accuracy of 1 mm Hg. The cooling water flow rate is measured with a calibrated orifice of 3/16" VDI standard type for 1" pipe flow. The pressure drop across the orifice is measured with a U-tube Hg manometer. The temperatures in the top and bottom chambers of the test section, of the condenser wall, of the coolant at inlet and outlet of the condenser jacket and of the condensate in the measuring burette are all measured with copper-constantan thermocouples and a highly sensitive potentiometer (Leeds and Northrup Type K-3 Potentiometer).

Two flowmeters are used, to measure the rate of vapor flow into the condenser and the excess vapor leaving the condenser. The 1" flowmeter measures up to 200 lbm/hr and the 1/2" meter measures up to 100 lbm/hr. The accuracy is approximately 1% of full scale reading. The calibration of both meters was checked before their use.

3.3.7 Experimental Procedure

It is well known that the presence of small amount of non-condensable gas can have large effect on the performance of a condenser. Since the objective of the present study is to identify the effect of an electric

field on the condensing phenomenon, the presence of air in the system would be an unnecessary and undesirable complication. Therefore, special precautions have been taken to scavange the system of air before each series of tests. The following procedure is used, taking advantage of the large density difference between the Freon vapor and air. The boiler is set to generate vapor at a moderate rate. The three way valve after the boiler is set to by-pass the test section and vapor is diverted into the auxiliary condenser and the bottom chamber. As the freon vapor level rises in the loop, air in the system is displaced upward. At this stage, the opening in the top chamber that normally serves as vapor inlet is opened to atmosphere, and air displaced by the freon vapor is evacuated through the opening. After letting freon vapor escape through the opening for some time, the three way valve is set to the test section, and air in the inlet lines is similarly evacuated. The opening in the top chamber is then closed and the loop is set for normal operation.

The attainment of steady state in the loop, monitored by the condenser tube wall temperatures, takes from two to three hours. During the transient period, some condensation occurs in the flowmeters (insulated with fiberglas), but as steady state is approached, the amount of condensate decreases and disappears completely at steady state.

In a given series of tests, the vapor generation rate and the coolant flow rate are set and tests are run at normal gravity and at different values of the electric field. At least two points are taken at a given value of the electric field to check reproductibility of data.

All the data taken without electrostatic field show an acceptable degree of correlation with theory taking into account the interfacial shear. This correlation provides a measure of confidence in the experimental procedure, particularly with respect to the effectiveness of scavanging of air from the system.

3.3.8 Visual Condensing Apparatus

At the beginning of this study, there was no information to guide the design of the electrode geometry in the test section. To permit a qualitative evaluation of the significant electrical field parameters under actual conditions of forced convection condensation, a simple, visual open-loop system was built as shown in Fig. 23.

The arrangement of the electrodes, condenser tube and coolant water jacket in this system is approximately similar to that in the main loop except for the use of an electrically-conducting glass tube for the condenser. A variety of electrodes from wires to tubes were tested in this unit. Photographs taken of the condensate configuration on the glass tube wall with varying electrostatic field is shown in Fig. 24.

3.4 Experimental Results

The operation of the condenser loop is described in Section 3.3 and the experimental data is tabulated in Appendix B. The heat transfer rates have been determined by two independent methods, i.e. the amount of the condensate and the enthalpy change of the coolant.

Without electric field, calculation suggests laminar film condensation throughout at least eighty percent of the tube. The data points show an acceptable degree of correlation with theory (Ref. 9) taking into account the interfacial shear, as shown in Fig. 27.

The first data obtained with a 1/4" electrode in a 1" ID condenser did not show any significant effect of the electric field on heat transfer, at least up to the maximum applied voltage of 30 KV. The increase in the heat transfer coefficient was about 10 to 20 percent over that obtained at normal gravity.

Most of the subsequent data were taken with a 1/2" OD electrode in a 1" ID condenser, and the results are shown in Figs. 28 and 29. Figure 28 shows that, at the maximum voltage of 30 KV, increases of the order of 100 per cent in the average heat transfer coefficient were attained. The data also shows an apparent decreasing effect of the electric field with increased vapor generation rates. The absolute increase in the heat transfer coefficient with electric field h_e is actually larger with increased vapor generation rates, but since the heat transfer coefficient without electric field h_o increases even faster, the ratios show an apparent decrease.

Figure 29 shows temperature measurements four inches downstream from the inlet T_1 and four inches upstream from the outlet T_5. It is seen that T_5 approaches T_1 at high field intensities. Temperature measurements at intermediate stations show a similar convergence to T_1. It is noted that as the heat transfer coefficient on the condensing side increases, the wall temperature distribution would approach the approximate constant temperature of the vapor. Thus, the wall temperature variation gives an indication of the variation of the <u>local</u> heat transfer coefficient with the electric field. Indications are that near the downstream end of the tube, increases in heat transfer significantly greater than 100 percent have been attained, since the increase of 100 percent that was noted earlier in connection with Fig. 28 applies to the heat transfer coefficient averaged over the length of the tube.

Figure 29 also shows a relatively sudden change in T_5 at approximately 16 KV for this particular geometry. The existence of this threshold point is supported qualitatively by visual observations which show that a marked instability of the interface develops at certain particular values of the field intensity. It is not possible to establish a quantitative relationship between measurements and visual observation, since the latter was performed on a different apparatus.

The tests with 3/4" OD electrode in 1" ID condenser concentrated on wall temperature measurement. The results are shown in Figs. 30 and 31. In Fig. 30, at moderate vapor generation rates, the local wall temperatures T_2, T_3, T_4, T_5 converge to T_1 with increasing voltage. By contrast, T_5 in Fig. 31, corresponding to a higher vapor generation rate, suddenly starts to drop at approximately 6 KV. This could indicate the appearance of slug flow near the tube exit due to the increased condensing rate brought about by increasing the electric field. At first glance, this would seem to contradict the findings of the two-phase flow study in which it was concluded that the electrostatic field suppressed the transition from the annular flow to the slug flow. Actually, in the two-phase flow system, there is no change in the relative amounts of liquid and gas flowing through the test section. In the condensing system, on the other hand, the condensate flow rate is increased by the electric field.

3.5 Effect of Electric Field on Condensation

It will be helpful at the start to review the state of art on condensation on a plane surface.

In condensation on a vertical surface and when the condensate film is laminar and stable, the classical Nusselt analysis applies, modified when necessary for the interfacial shear. When the surface is inclined at an angle θ to the horizontal plane and so long as the film remains stable, the Nusselt equation may still be assumed to apply if the gravitational acceleration g in the equation is replaced by $g \sin \theta$, the component of gravity acting along the surface. In the above cases, the force per unit volume of the film which acts to drive the liquid off the condensing surface is the gravity force ρg or $\rho g \sin \theta$. When condensation occurs on a surface facing down, the dominant phenomenon is that of interfacial instability (Taylor instability) and the characteristic length of the system is the wave length of the fastest growing instability. The driving force acting on the liquid film is still the gravity, but in this case, the gravity vector is normal to the interface. Now consider the rotation of the condensing surface from the horizontal

to the vertical position. Over a range of values of the angle θ, gravity force components act both in moving the condensate film and in generating instability. It is not clear a priori whether the two effects are simply additive as far as the heat transfer rates are concerned.

In the electrohydrodynamic condensation in a vertical tube, if it is assumed that at high field intensities the electrical effects predominate, then the phenomenon of interest at high field intensities may essentially be that of interfacial instability. The characteristic length might therefore be identified in terms of the fastest growing wavelength and the driving force in terms of electrically induced stresses in the system. Some insight into their nature is given by the dispersion relation for the EHD waves derived in Appendix C.

In applying the results of the stability analysis to the condensing system, the following assumptions have been made:

1. The effect of relative parallel motion at the interface is neglected. This assumption is necessary because the liquid and the vapor velocities vary along the length of the tube and are unknown in the present system. It may be justified because the inlet vapor velocities in the condenser tests are significantly lower than those in the two phase flow tests.

2. The condensing system is approximated as a plane case. This assumption avoids the complications resulting from non-uniform field intensities and the curvature of the interface. The resulting simplifications are detailed in Appendix C.

3. The effect on stability of condensation process at the interface is neglected.

For thin films, the characteristic wave number K* can be readily obtained from the dispersion relation by maximizing ω with respect to K. This gives (see Appendix C):

$$K^* = \frac{3}{4\sigma}\left(1 - \frac{\epsilon_v}{\epsilon_1}\right)^2 \epsilon_v E_v^2 \qquad (3.1)$$

The characteristic wavelength of instability is then

$$\lambda^* = \frac{2\pi}{K^*} \qquad (3.2)$$

To obtain an expression for the electrohydrodynamic driving force governing the EHD waves, it is noted that in the dispersion equation for the more familiar gravity waves (see for example Eq. C.5.3 in Appendix C), the corresponding force can be obtained by multiplying their phase velocity $\mathcal{V}_g$ by $K^*\rho_{eq}$, so that

$$g(\rho_1 - \rho_v) = K^*\rho_{eq}\,\mathcal{V}_g^2$$

The gravity waves do not appear in vertical films. In the case of the EHD waves of phase velocity $\mathcal{V}_e$, assuming that they dominate at high field intensities, their corresponding driving force can be similarly expressed as

$$\mathcal{F} = K^*\,\rho_{eq}\,\mathcal{V}_e^2 \qquad (3.3)$$

For thin films, K* is given by Eq. (C.5.7) and $\rho_{eq}\,\mathcal{V}_e^2$ by Eq. (C.5.3), so that

$$\mathcal{F} = K^*\left(1 - \frac{\epsilon_v}{\epsilon_1}\right)^2 \epsilon_v E_v^2 \qquad (3.4)$$

The force ζ given by this equation has the dimensions of a body force, lbf/ft^3.

Equation (3.1) gives the characteristic wave number K* for thin films. Alternately, K* can be determined as follows without making the thin film assumption. Equation (C.5.3) in the Appendix has been solved for the particular case of R_o = 0.5" and R_i = 0.25" and for the following values of the film thickness a: 0.001", 0.005", 0.01", 0.05" and 0.1". The solution was programmed on an IBM 1620 computer and the results are plotted in Figs. 32 and 34 with the wave number K as the independent variable. The maxima in these curves give the characteristic wave numbers K* corresponding to the most unstable waves, and Fig. 35 shows a plot of the most unstable wavelength $\lambda^*(= 2\pi/K^*)$ versus the mean film thickness. It is seen that at 20 KV and 30 KV, λ^* is relatively insensitive to the film thickness over the computed range.

Figure 36 is an alternate plot of the data presented in Fig. 28 and shows how the average condensing heat transfer coefficient varies with the wave number K*.

3.6 Condensation Heat Transfer Correlation

A complete heat transfer analysis of the electrohydrodynamic condensing system presupposes a knowledge of the actual shape of the liquid-vapor interface which, in the present system, is complicated by the gravitational flow of the film. In this first attempt at a correlation and based upon the discussion in Section 3.5, it is suggested that at high field intensities the drop spacing on the film is determined by the EHD waves and that the effect of the film motion can be neglected. The problem then becomes similar to that of film boiling on a surface facing up or film condensation on a surface facing down in a gravitational environment. It might therefore be expected that the condensation heat transfer data at high field intensities will correlate on the basis of a Nusselt number and a Grashof number in which the characteristic

drop dimension is given by the most unstable wavelength λ^* and the equivalent driving force acting on the film is the electrohydrodynamic force :

$$Nu = \frac{h_i \lambda^*}{k} \tag{3.5}$$

$$Gr = \frac{\rho \lambda^{*3} h_{fg}''}{k \mu \Delta T_{lm}} \tag{3.6}$$

where, for thin films, λ^* is given by Eq. (3.1) and is given by Eq. (3.3).

It is further noted that in the normal gravitational film boiling on a surface facing up (Ref. 10) and condensation on a surface facing down (Ref. 11), data has been correlated by the parametric ratio $Nu/(Gr)^{\frac{1}{4}}$ which, in the case of film boiling, has a value of 0.425. The ratio $Nu/(Gr)^{\frac{1}{4}}$ has been computed for the fifty odd data points obtained in the present study and plotted in Fig. 37 against the electrohydrodynamic driving force It is seen in Fig. 37 that above a certain value of , the ratio $Nu/(Gr)^{\frac{1}{4}}$ is essentially a constant estimated to be approximately 0.50. This suggests the following correlation equation:

$$Nu = 0.50\ (Gr)^{0.25} \tag{3.7}$$

The correlation should work only for those points at which interfacial instability is the dominant phenomena, namely the high field data. A direct plot of Nusselt versus Grashof numbers of all the E-field data will show a wide scatter and will be rather meaningless in terms of the present correlation. Those points that lie below the threshold ξ may perhaps correlate by some combination of the ordinary gravitational and the electrohydrodynamic forces. The problem would be qualitatively analogous to

that discussed in Section 3.5 of condensation on a plane surface facing down as it is rotated from the horizontal to the vertical position. A generalized correlation is not known at present for this latter case.

In summary, an "exact" heat transfer analysis would require a knowledge of the drop dimensions and arrangements on the flowing condensate film. This is a rather formidable task. As an initial effort, a correlation based upon an equivalent Grashof number is attempted, with the constant determined experimentally. The fact that this correlation seems to work successfully with the high-field data taken to date is encouraging. It is emphasized, however, that the equation is tentative and needs further verification analytically as well as experimentally for different fluids and geometries.

4.0 CONCLUSIONS

In general, the results of this program indicate that condensation inside tubes can be significantly improved by the application of steady electric fields. Moreover, this improvement is due to field effects without any special apparatus to introduce ions into the system. The increase in pressure drop which accompanies this improvement of heat transfer coefficient is moderate.

A number of specific conclusions can be listed:

1. In two-phase flow, the transition from annular to slug flow is significantly suppressed by an electrostatic field, particularly at low liquid Reynolds number.

2. The pressure gradient in annular flow is increased by the field. Tentatively, the pressure drop in the annular flow regime has been shown to be a function of the total energy density, $(1/2)\rho_g V_g^2 + (1/2)\epsilon_o E_o^2$

3. The condensing heat transfer coefficient increases significantly as the applied field is increased above a certain threshold value.

4. The increase in heat transfer coefficient and in pressure gradient can be related to the alteration in the wave patterns on the liquid-vapor interface. In effect, these results indicate that the effective film thickness is reduced if an electrostatic field is applied.

5. The high field heat transfer data has been correlated in terms of a Nusselt number and a Grashof number in which the characteristic length is taken as the most unstable wavelength in the system and the force acting on the film is an equivalent electrohydrodynamic driving force.

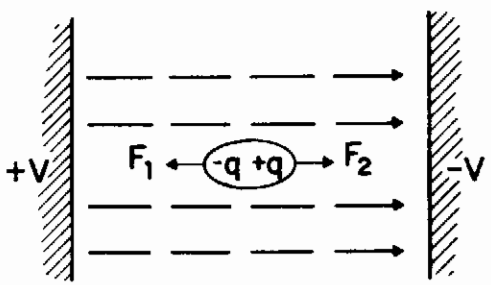

Fig. 1a - Molecule in a Uniform Electric Field (Equal Forces, i.e., $F_1 = F_2$

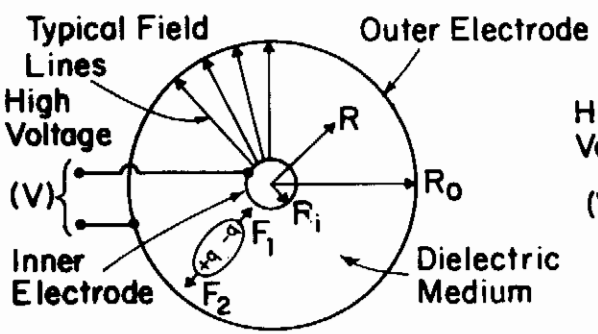

Fig. 1b - The Cylindrical Dielectrophoretic Cell. Unequal Forces $F_1 > F_2$.

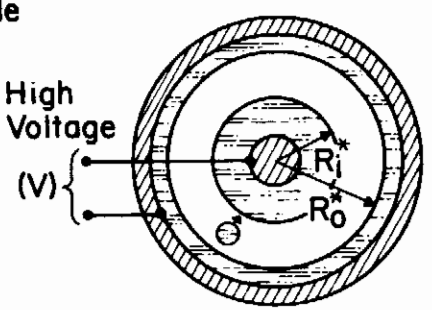

Fig. 1c - Equilibrium Configuration in the Simplest Dielectrophoretic Cell.

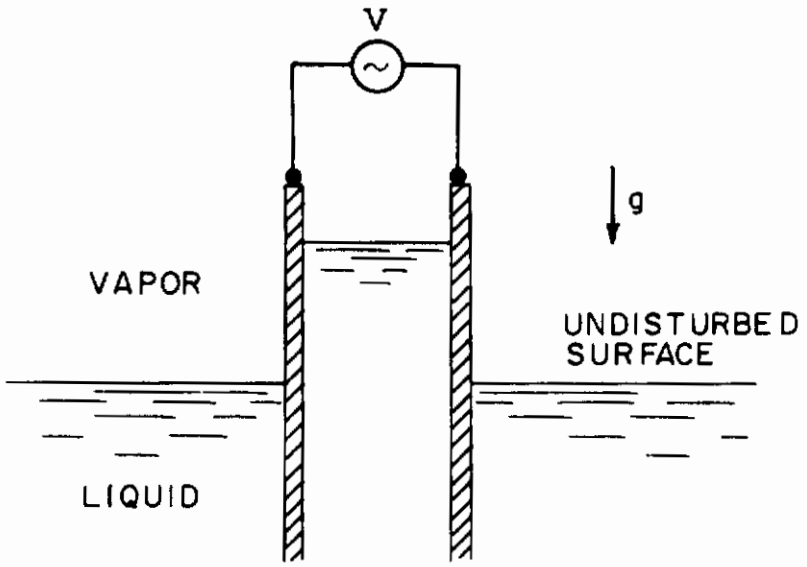

Fig. 2 Rise of Liquid Between Parallel Plates in Electric Field

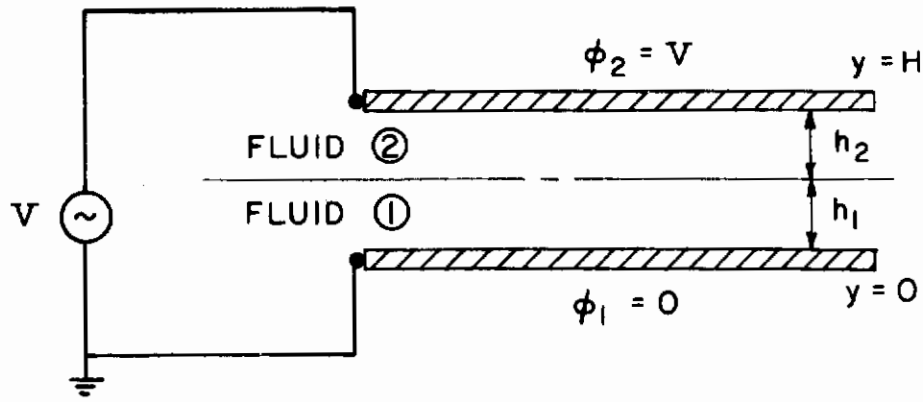

Fig. 3 Parameters for Discussion of the Field Between Parallel Plates

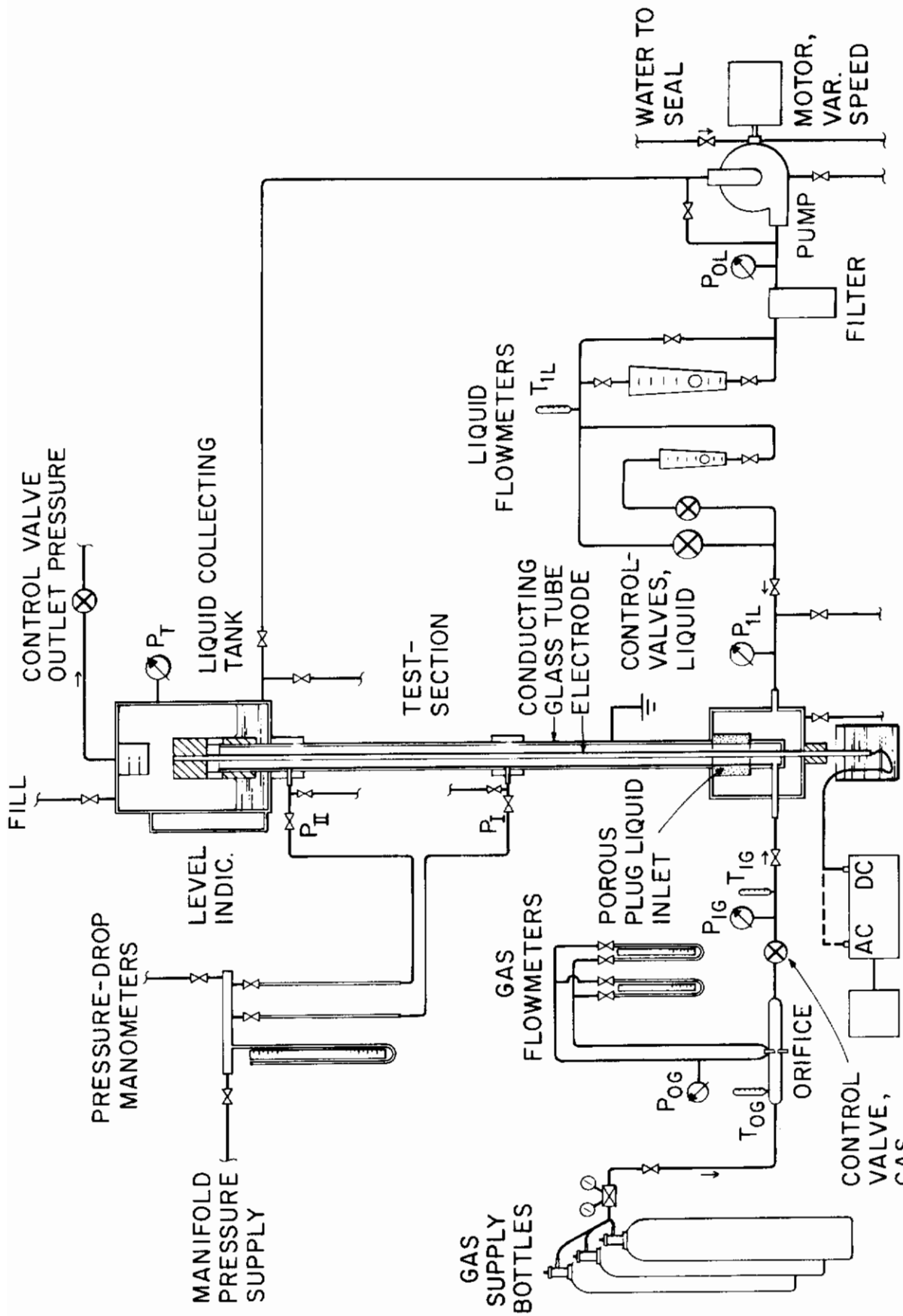

Fig. 4 Schematic of Experimental Equipment

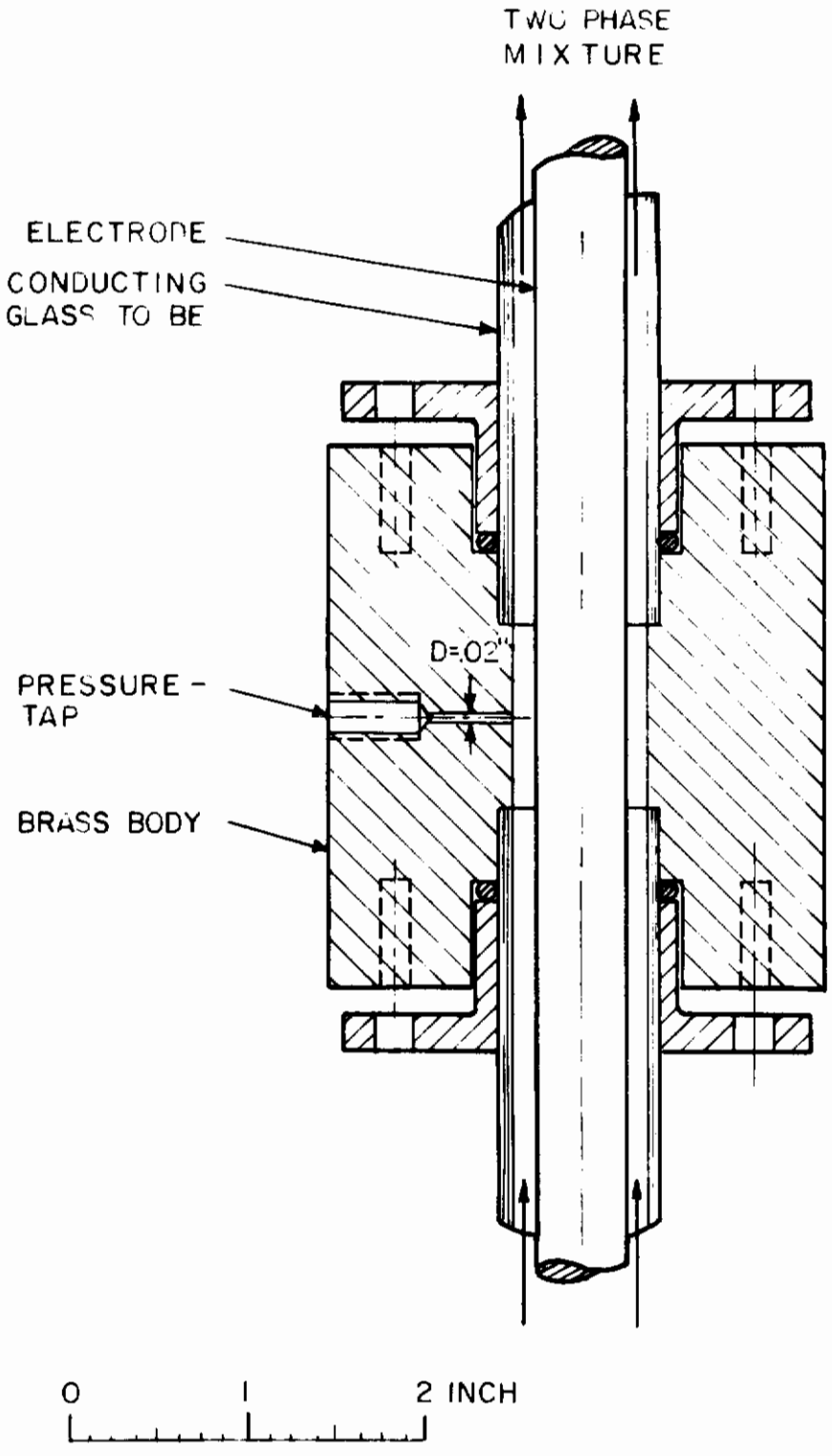

Fig. 5 Pressure Tap and Glass Tube Joint

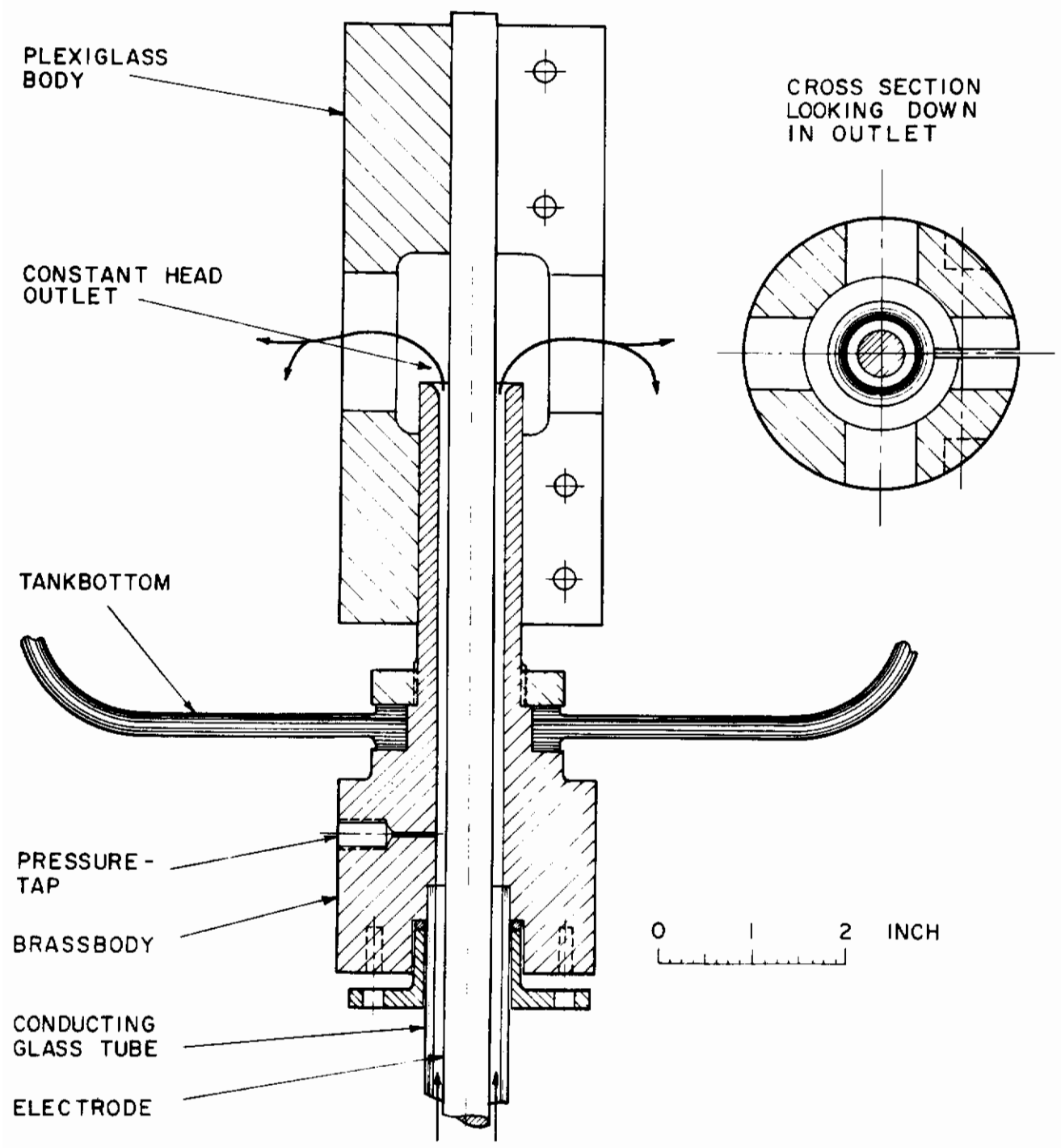

Fig. 6 Outlet Section and Top Electrode Support

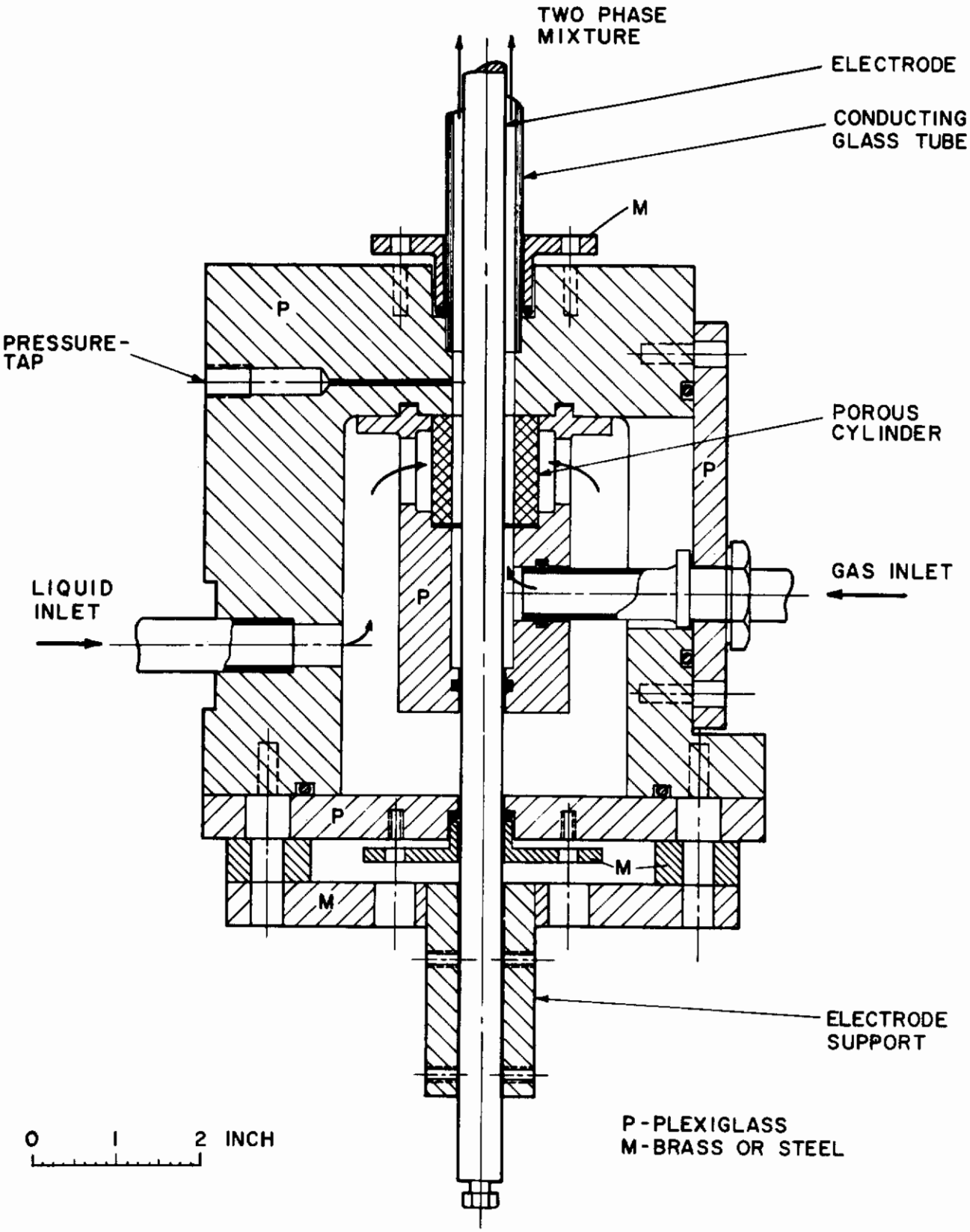

Fig. 7 INLET SECTION AND BOTTOM ELECTRODE SUPPORT

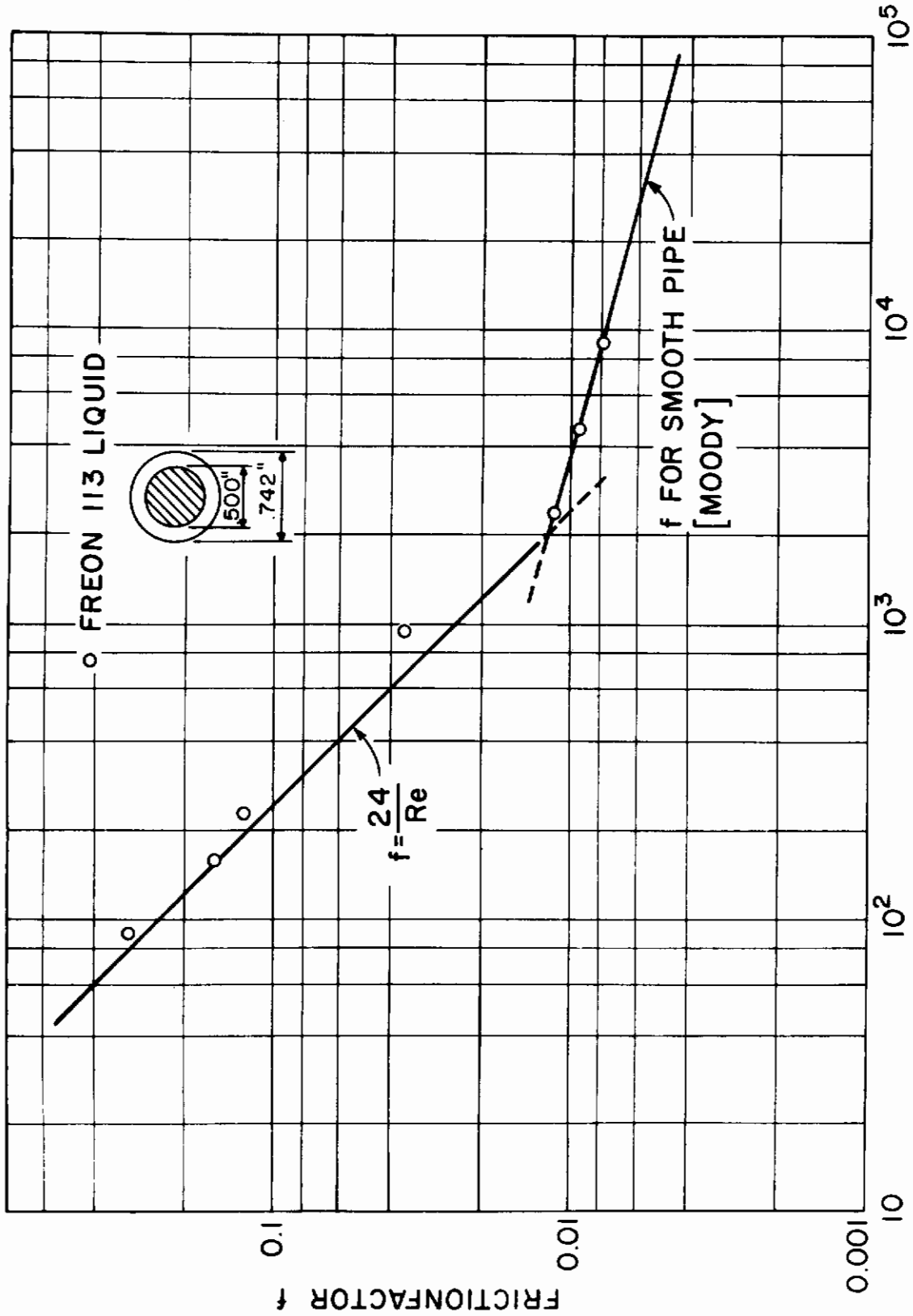

Fig. 8 Single Phase Pressure Drop

(a) 0 KV

(b) 8.5 KV

(c) 15.0 KV

FIGURE 9 Photograph of Annular Flow Near the Transition Region
w_L = 5.2 lbm/hr w_G = 11 lbm/hr p_T = 14.5 psig

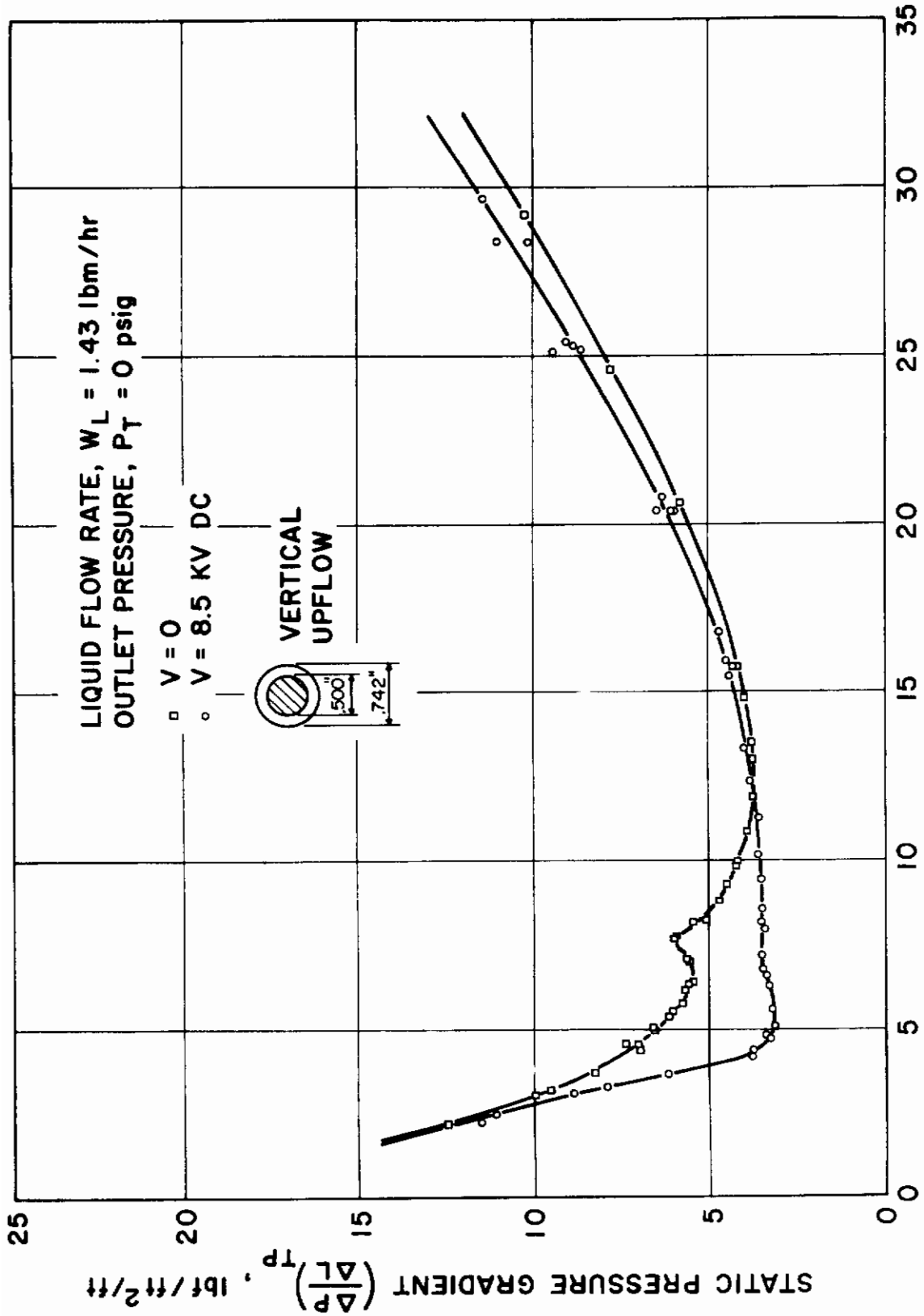

Fig. 10 Two Phase Flow Pressure Drop Versus Gas Flow Rate
w_L = 1.43 lbm/hr p_T = 0 psig

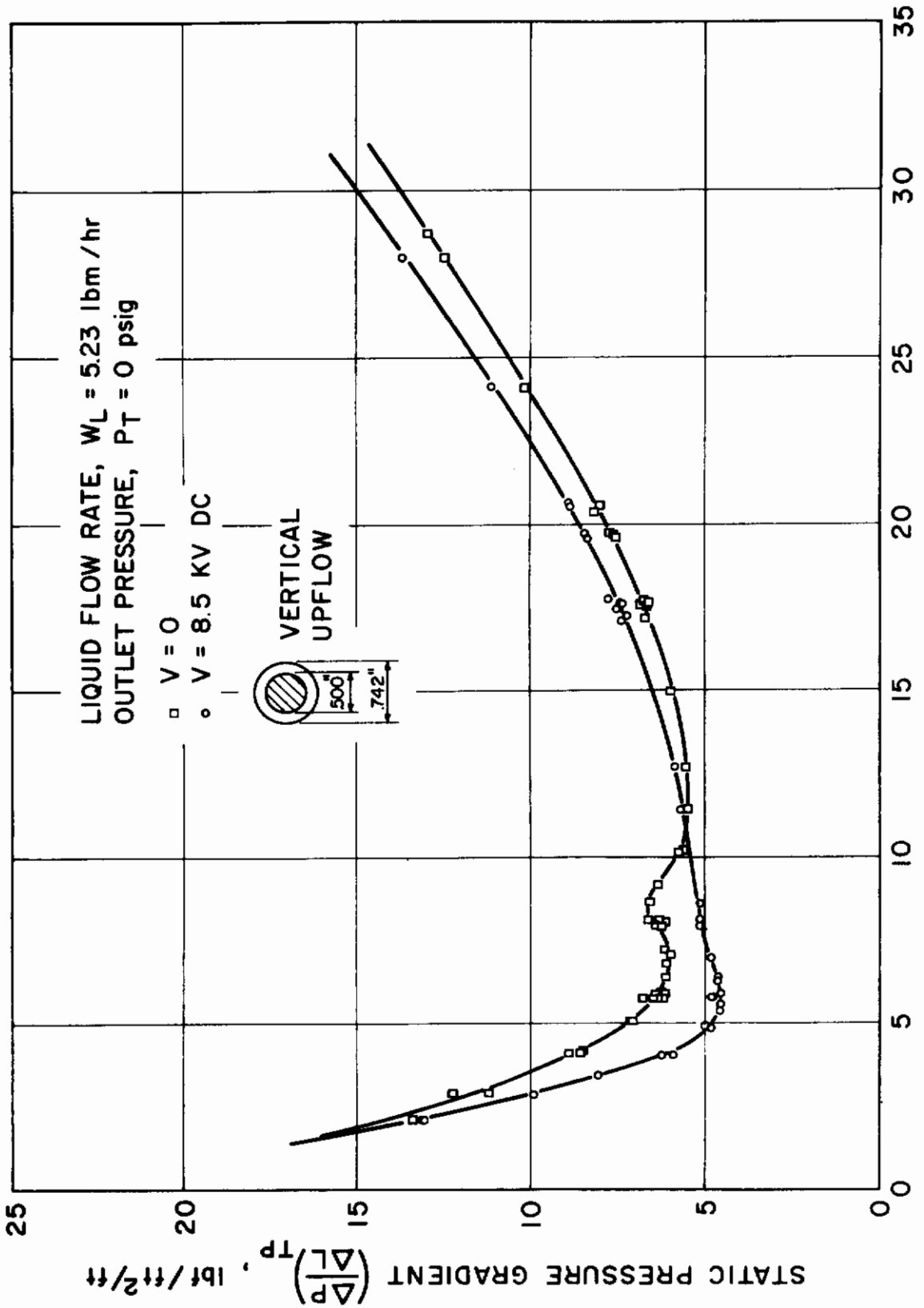

Fig. 11 Two Phase Flow Pressure Drop Versus Gas Flow Rate
w_L = 5.2 lbm/hr p_T = 0 psig

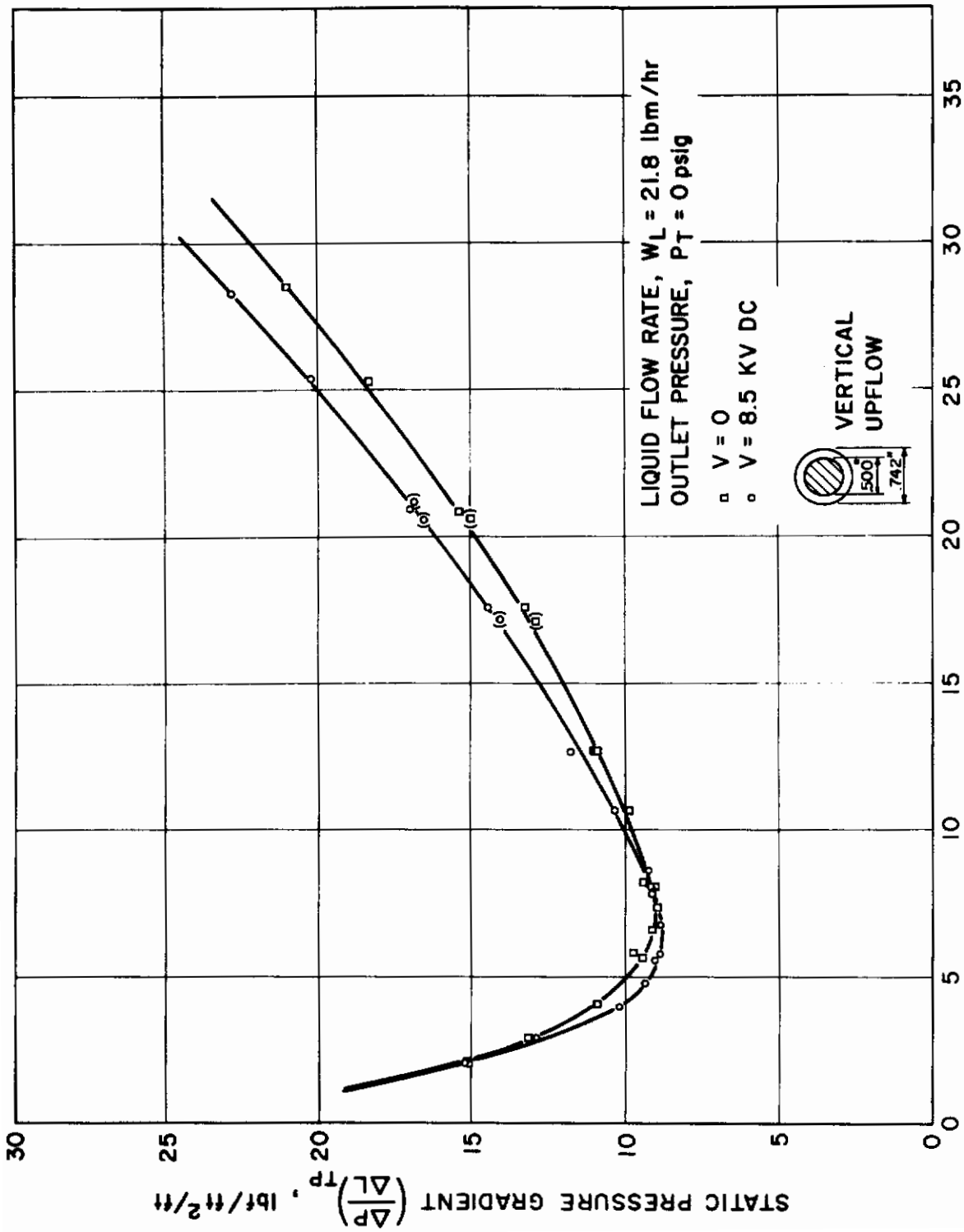

Fig. 12 Two Phase Flow Pressure Drop Versus Gas Flow Rate
W_L = 21.8 lbm / hr P_T = 0 psig

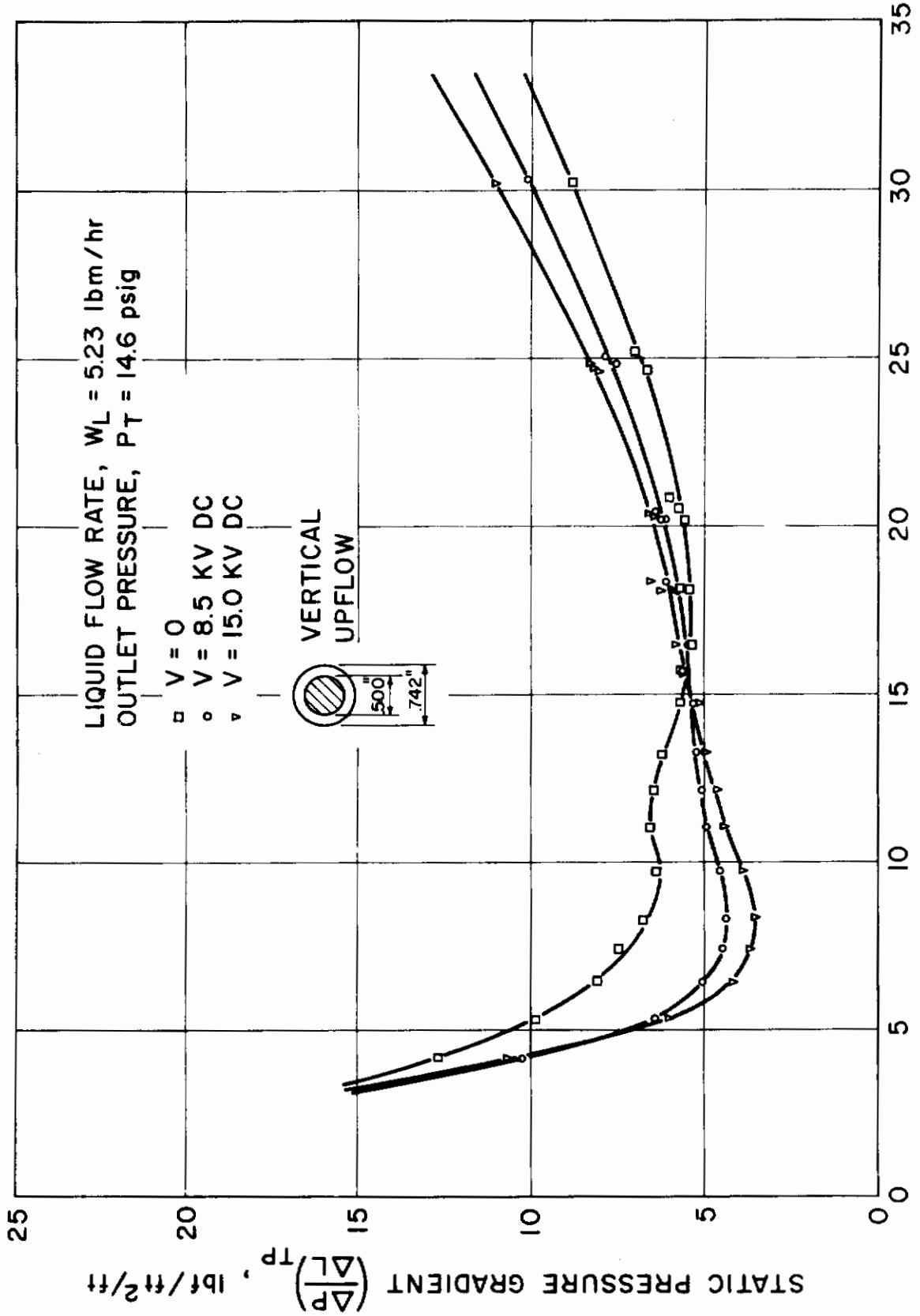

Fig. 13 Two Phase Flow Pressure Drop Versus Gas Flow Rate
w_L = 5.2 lbm/hr p_T=14.6 psig

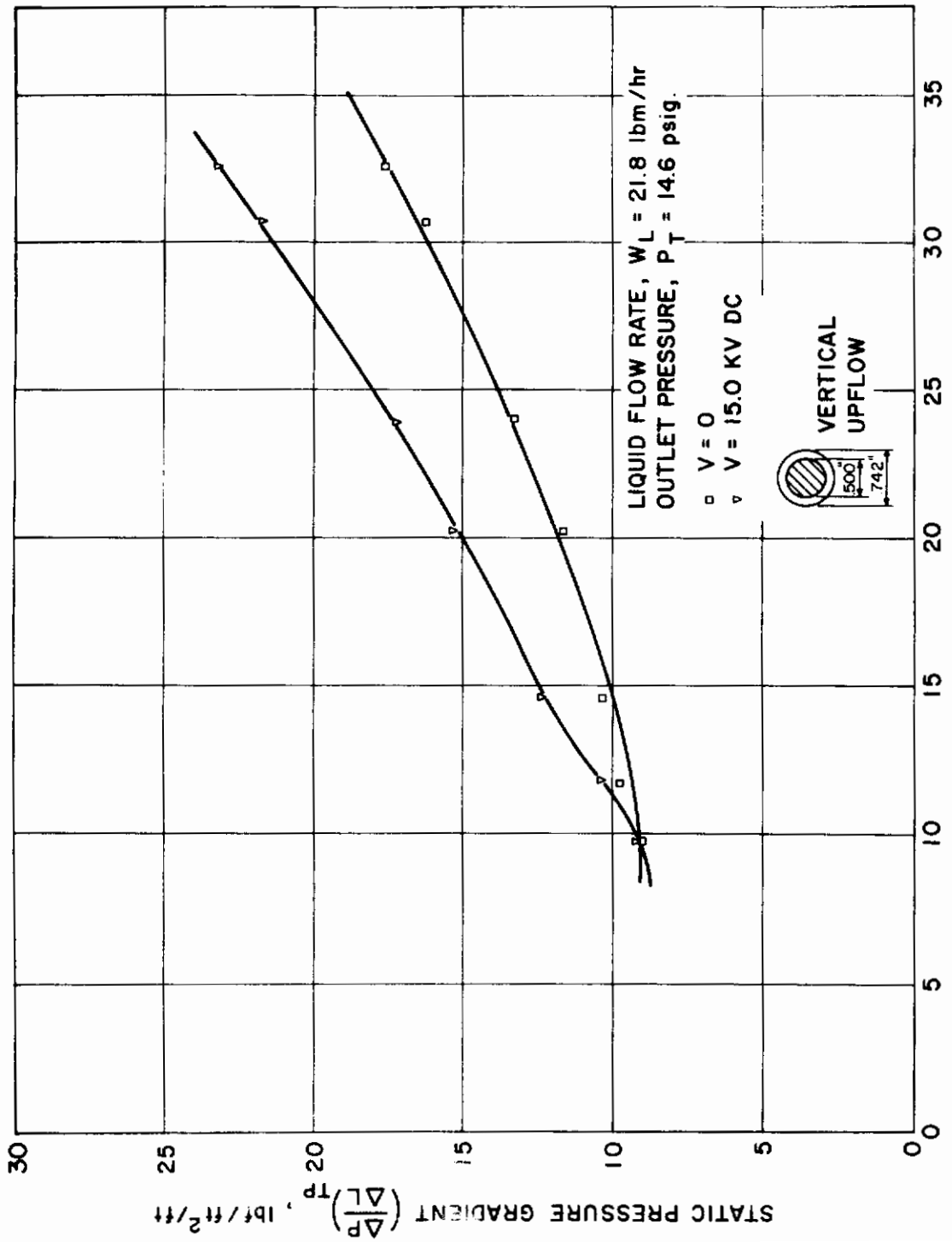

Fig. 14 Two Phase Flow Pressure Drop Versus Gas Flow Rate
W_L = 21.8 lbm/hr p_T = 14.6 psig

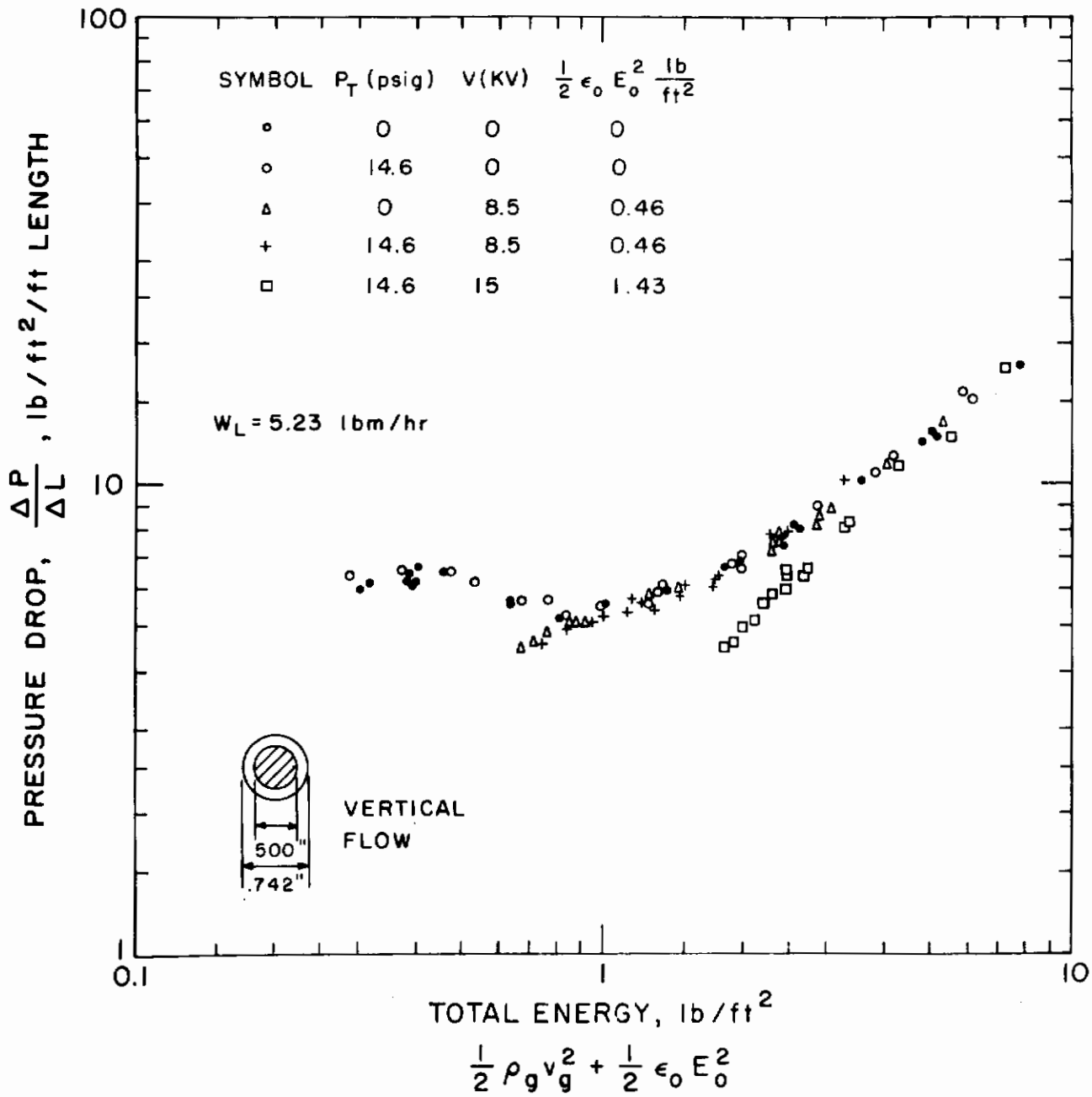

Fig. 15

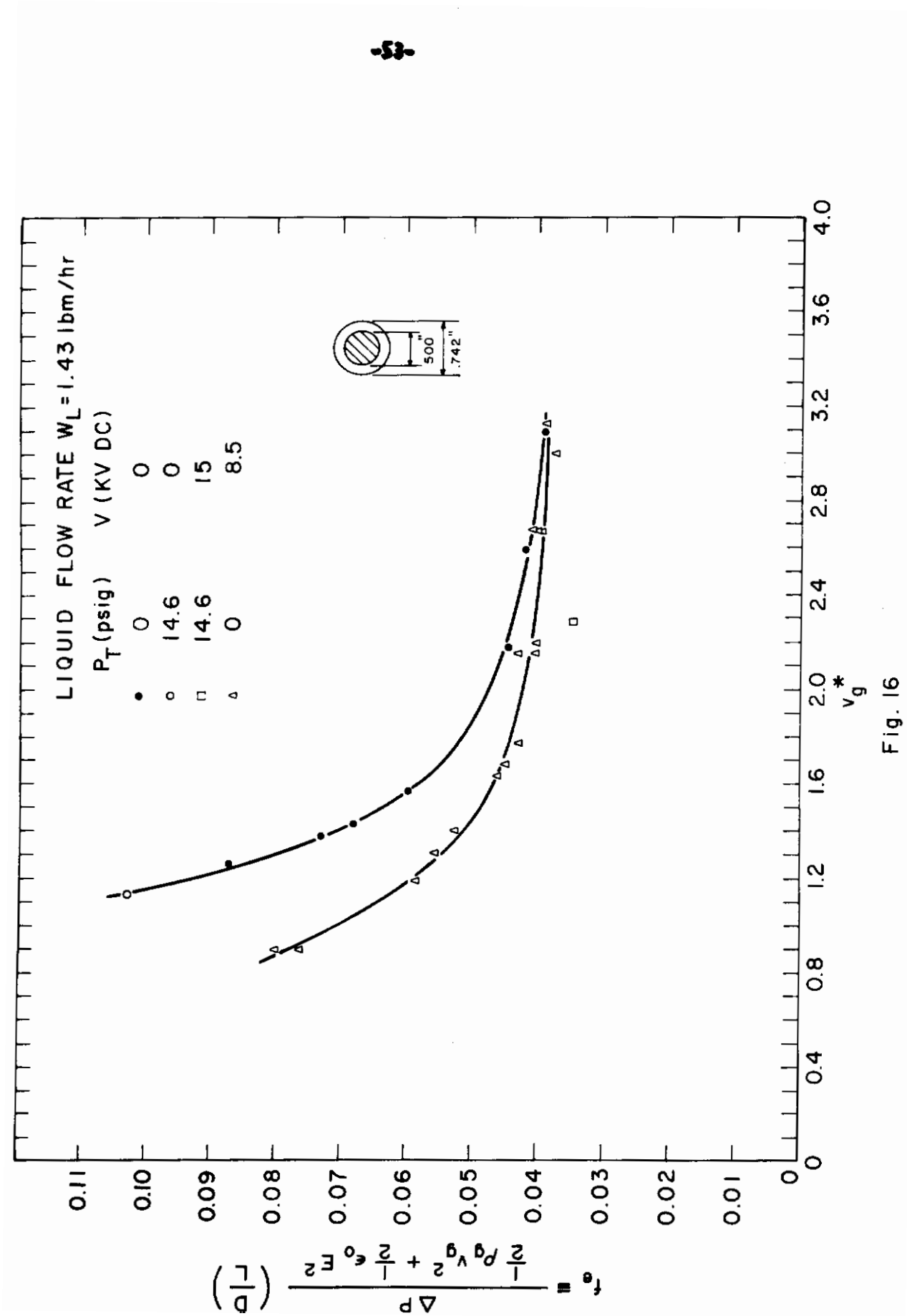

Fig. 16

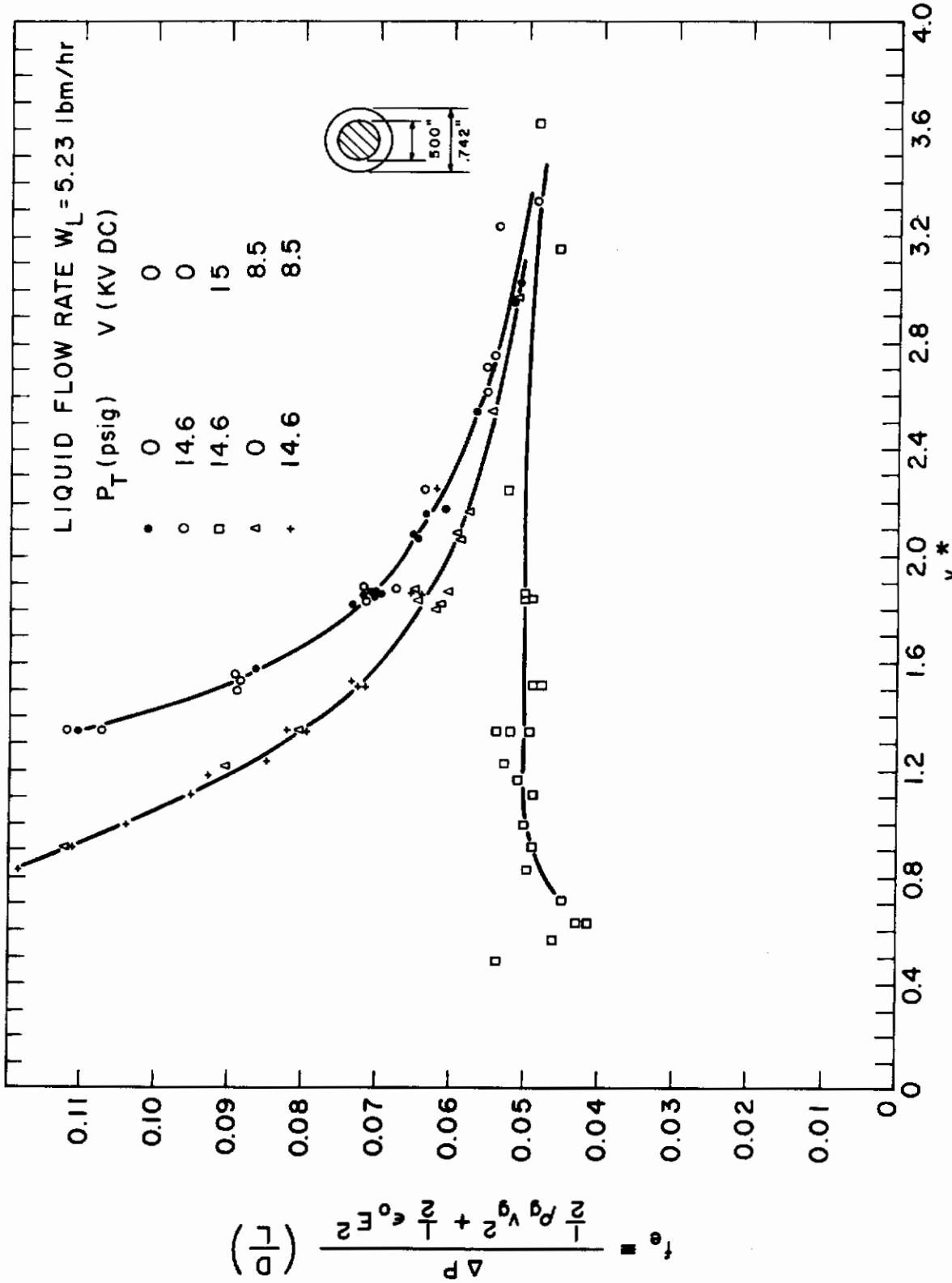

Fig. 17

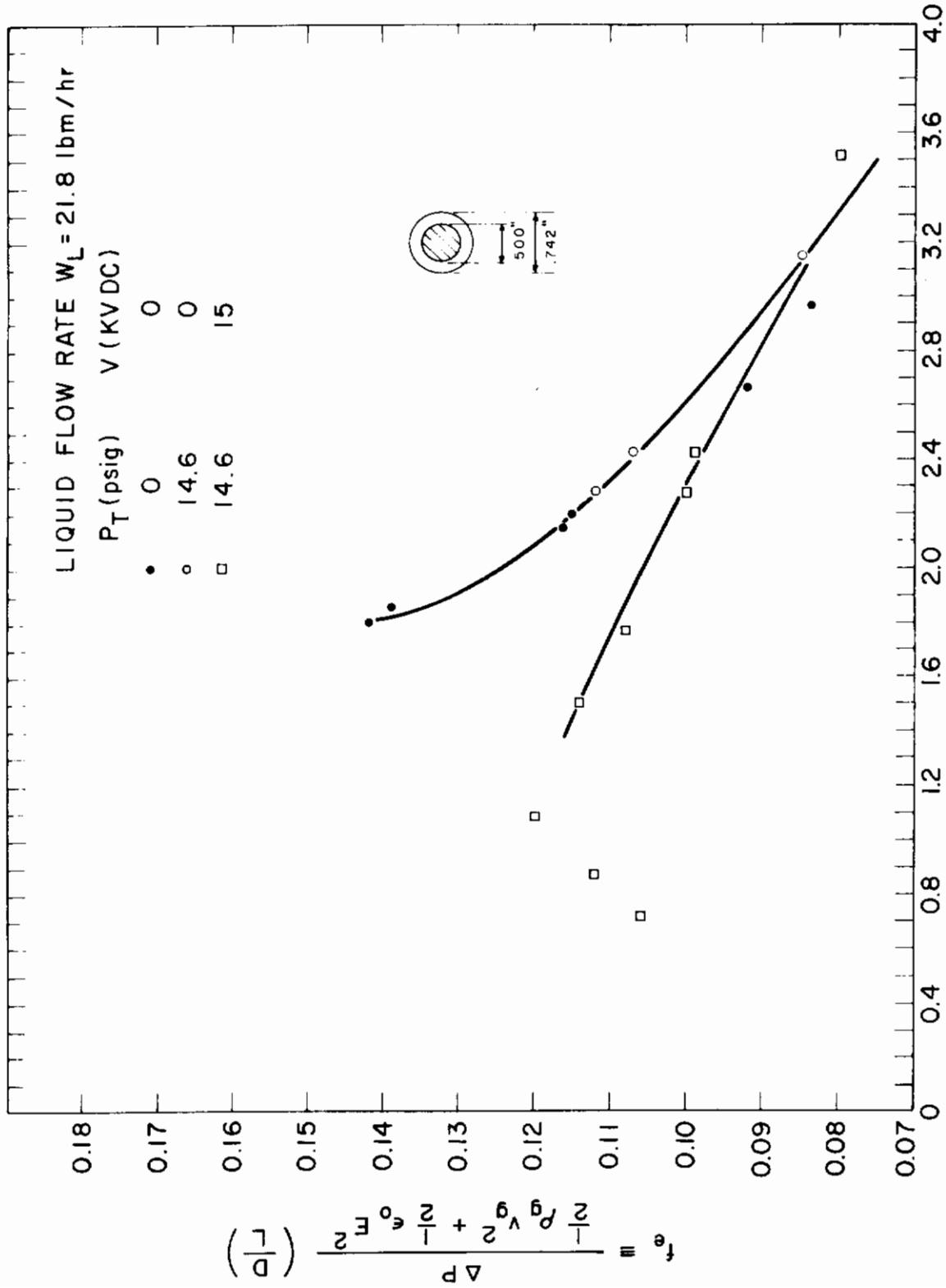

Fig. 18

SCHEMATIC DIAGRAM OF EHD CONDENSATION LOOP

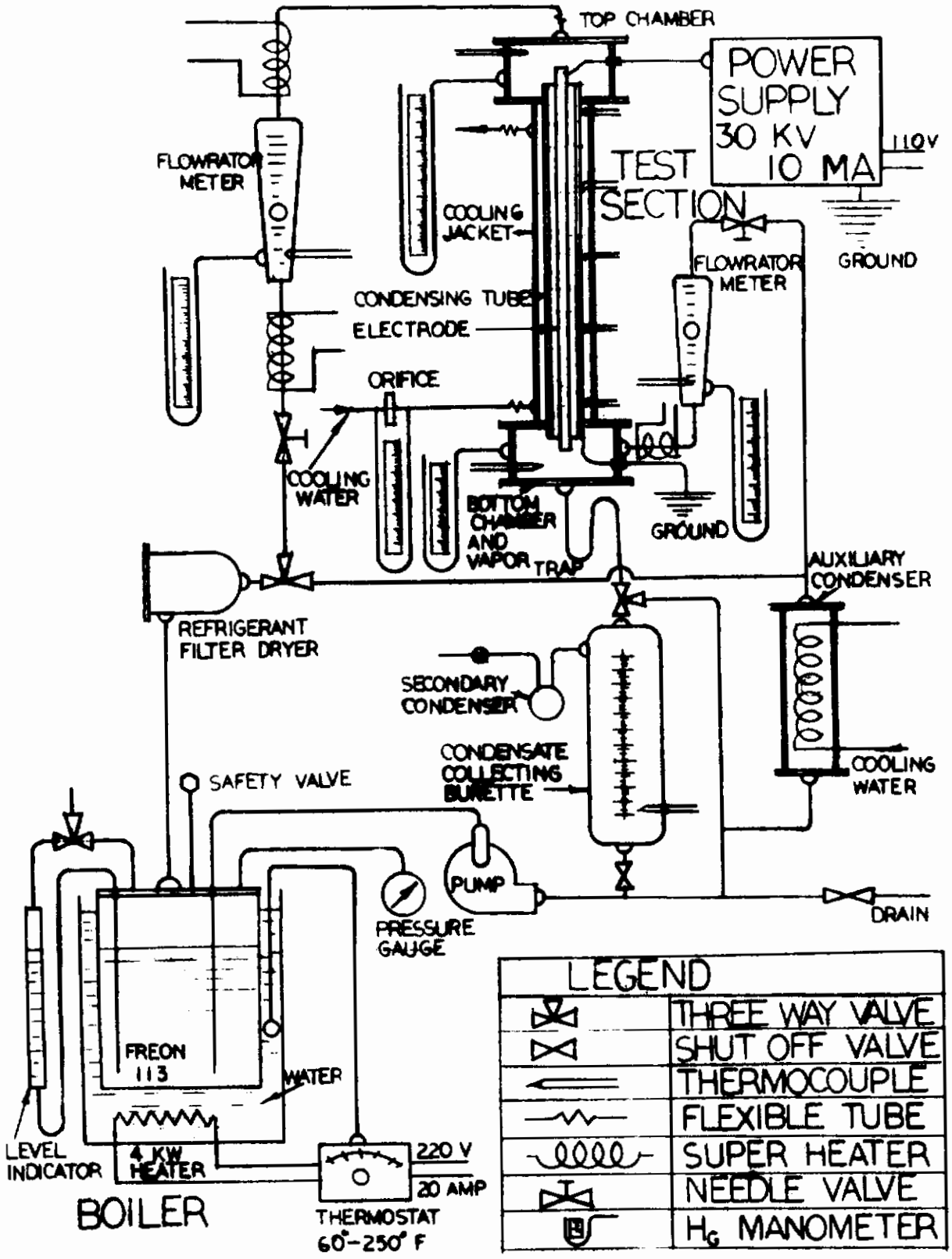

FIG. 19

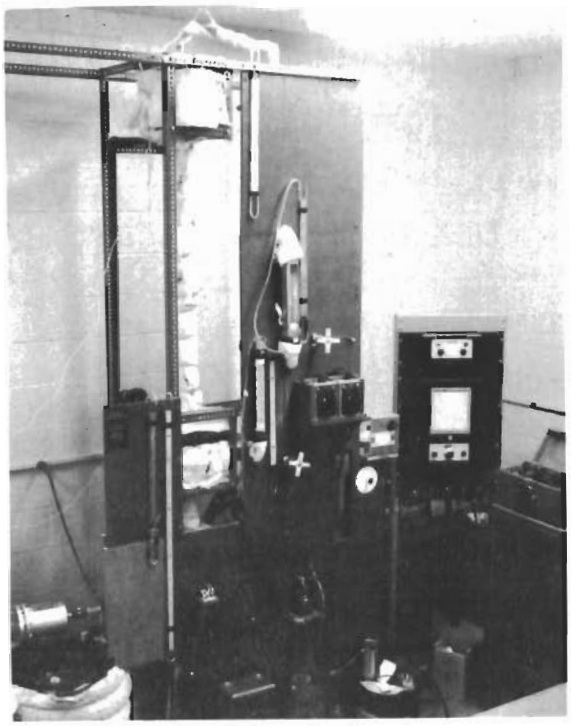

FIG. 20 OVER-ALL VIEW OF TEST LOOP

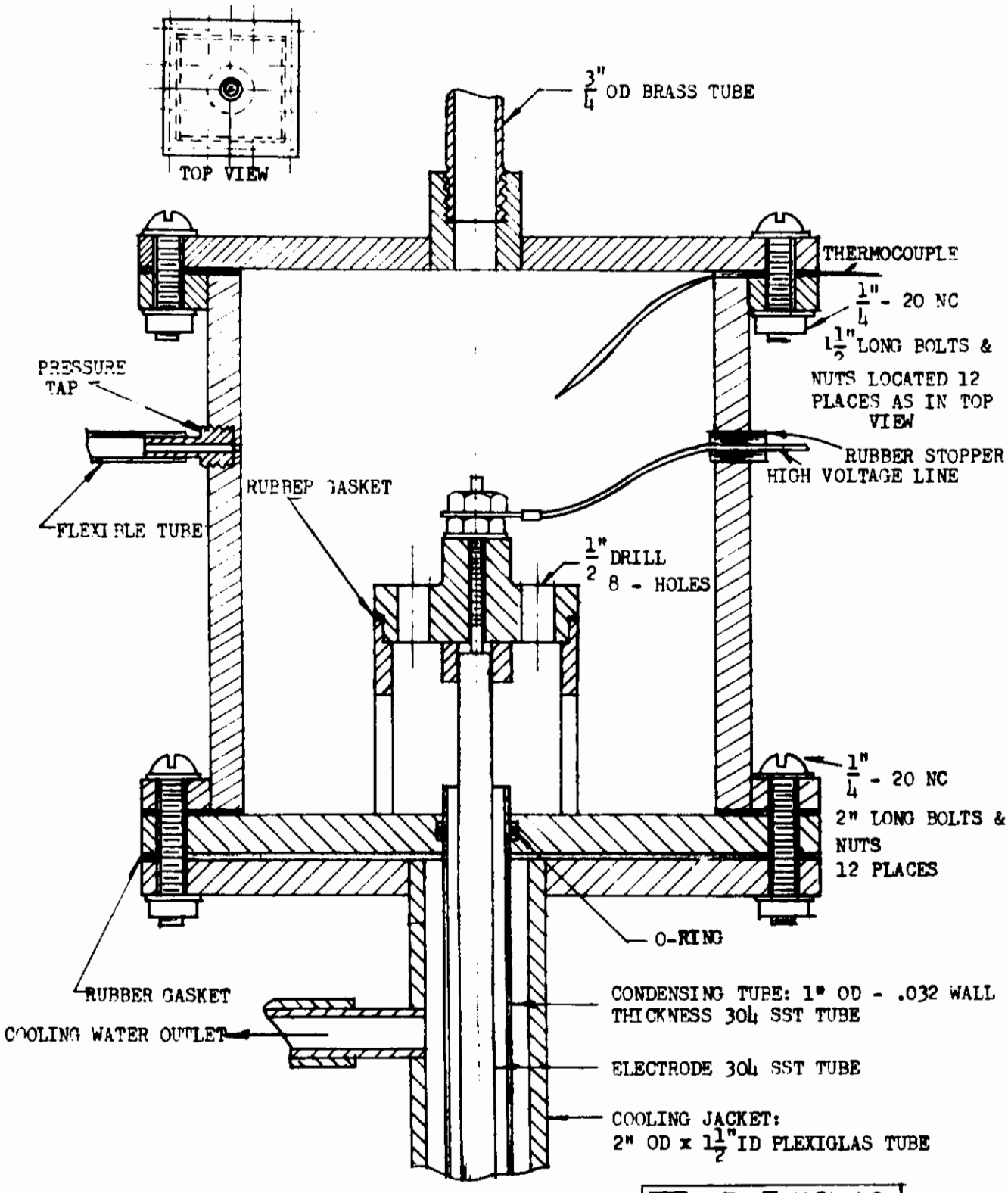

FIG. 21 TOP CHAMBER

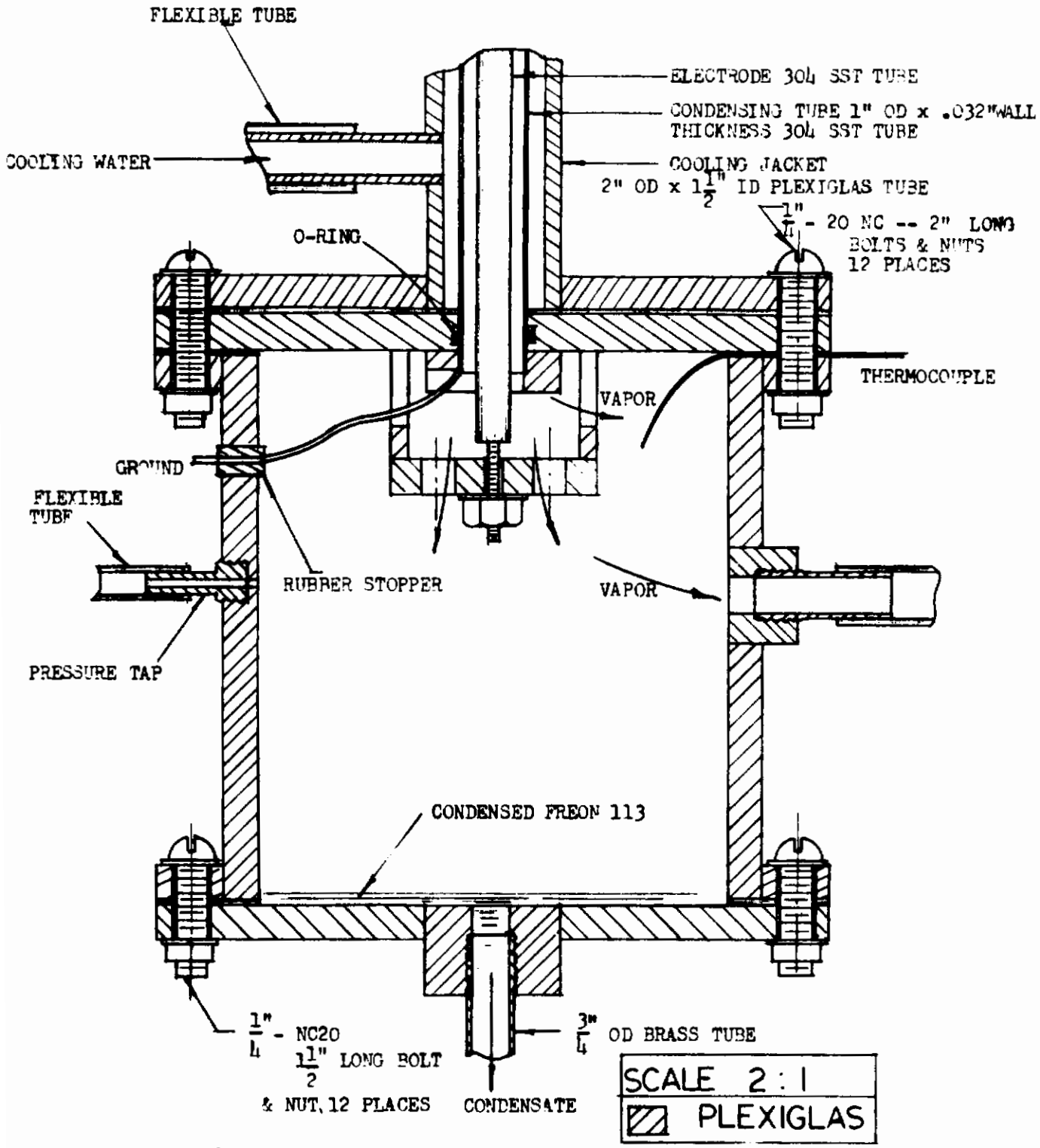

FIG. 22 BOTTOM CHAMBER AND VAPOR TRAP

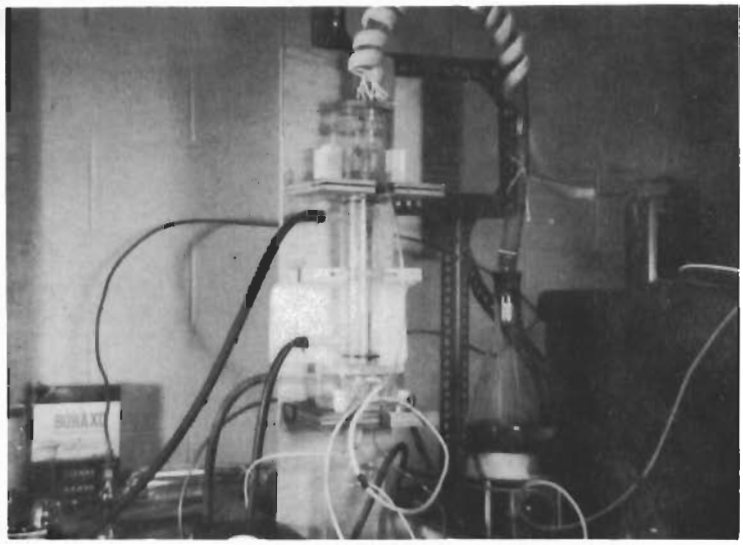

FIG. 23 APPARATUS FOR VISUAL STUDY OF EHD CONDENSATION

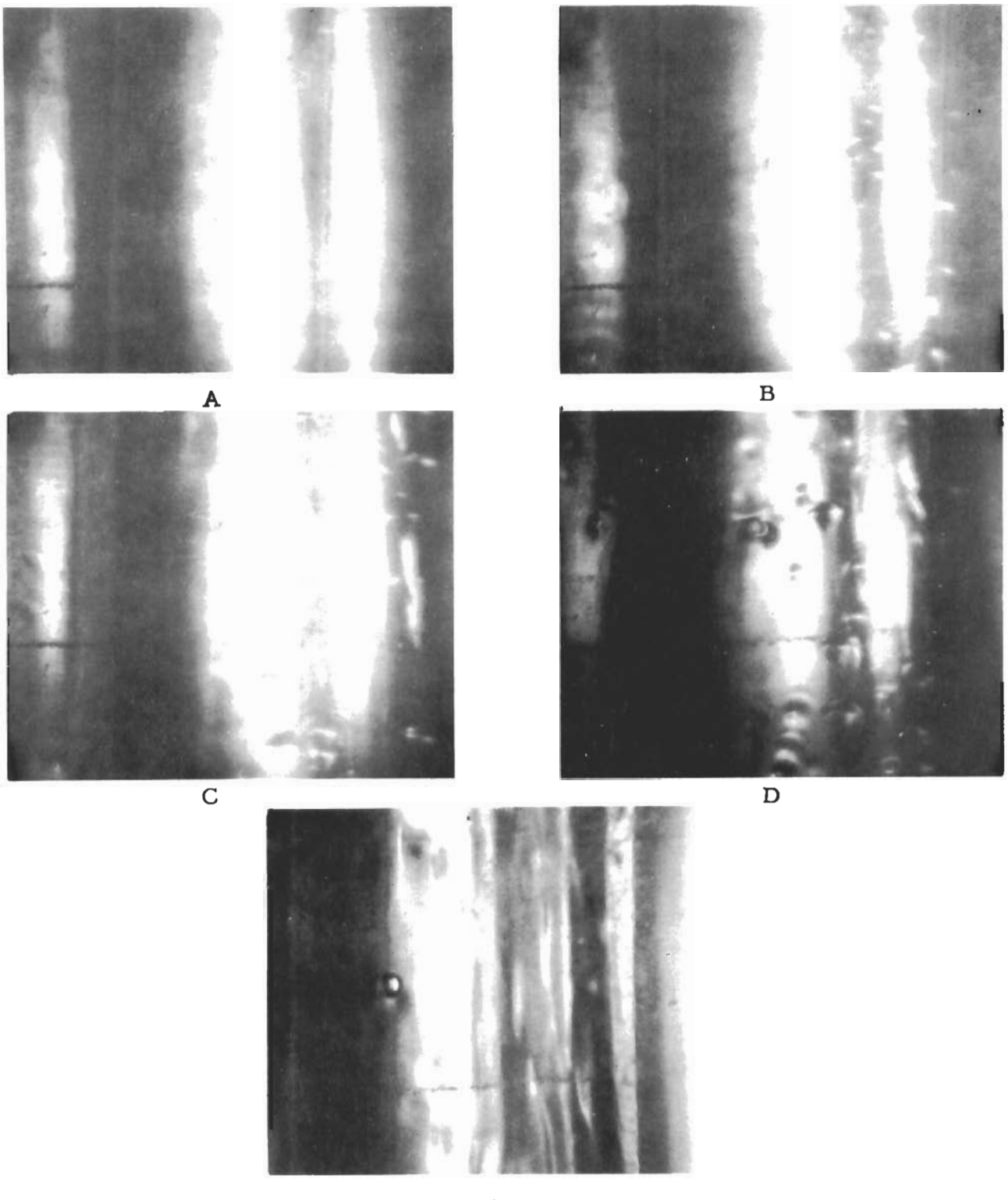

FIG. 24 PICTURES SHOWING CONDENSATE ON INNER WALL OF GLASS TUBE
Taken with strobe light at 4200 CPM. Sequence A to D shows increasing voltage from 0 to 30 KV. Electrode $\frac{1}{2}$" OD. Tube 1" ID. E was taken without strobe light at 30 KV.

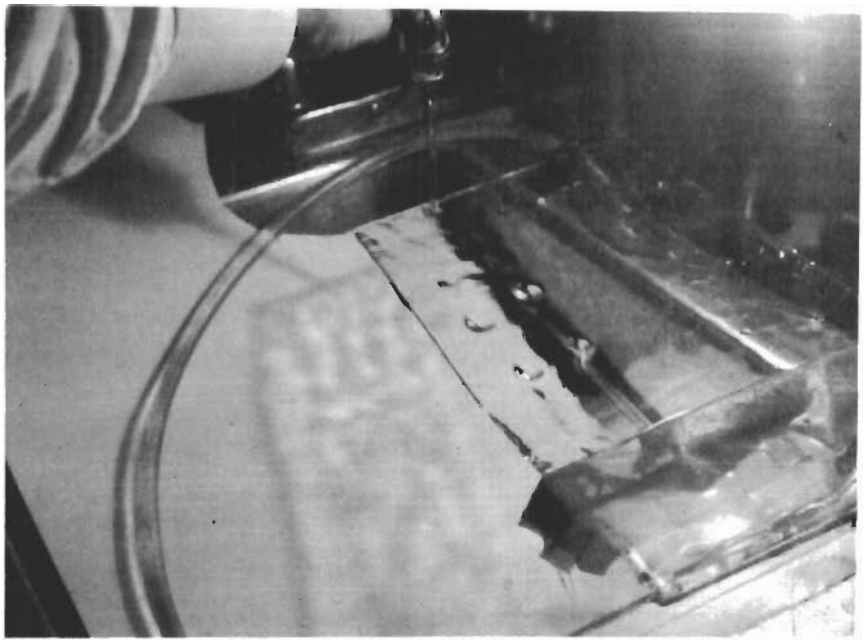

FIG. 25 GRAVITY FLOW UNDER A SLIGHTLY INCLINED GLASS PLATE

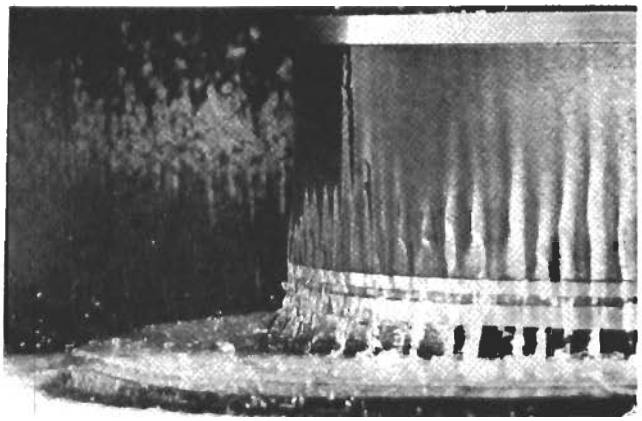

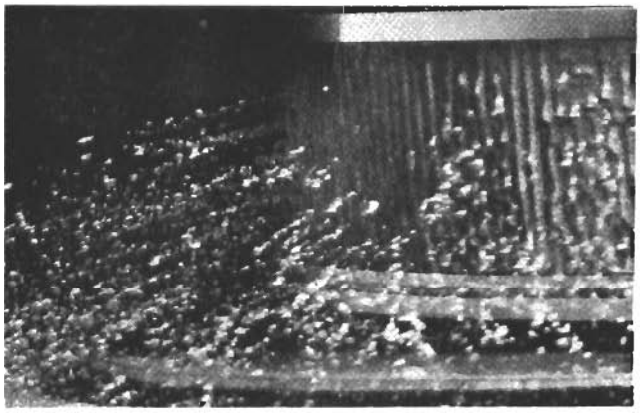

FIG. 26 Droplet Formation from a Liquid Film over a Rotating Cylinder
(Reproduced from Cheng and Cordero)

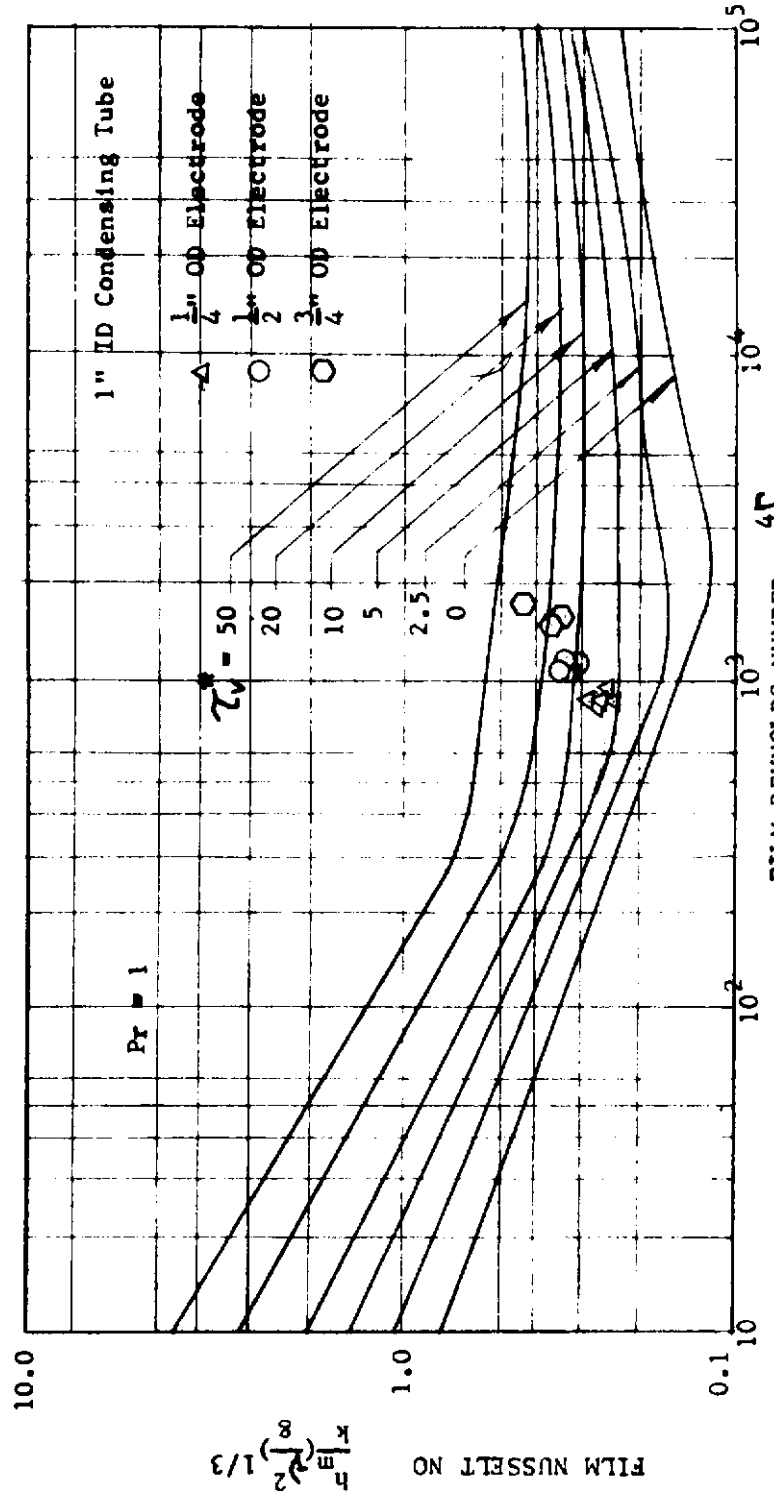

FIG. 27 NORMAL GRAVITY DATA WITH VARIOUS ANNULAR GEOMETRY

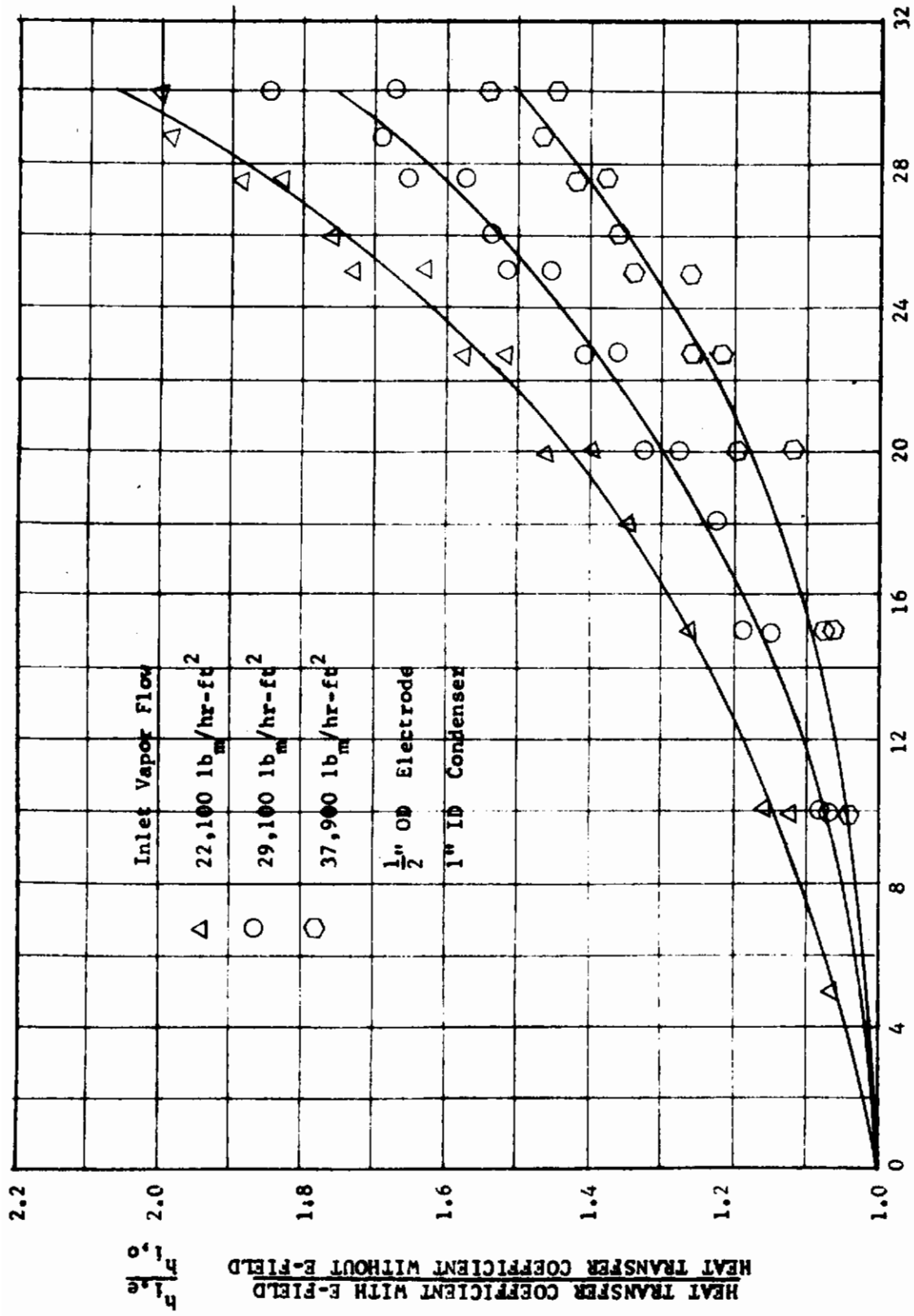

FIG. 28 AVERAGE HEAT TRANSFER COEFFICIENT RATIO vs APPLIED VOLTAGE

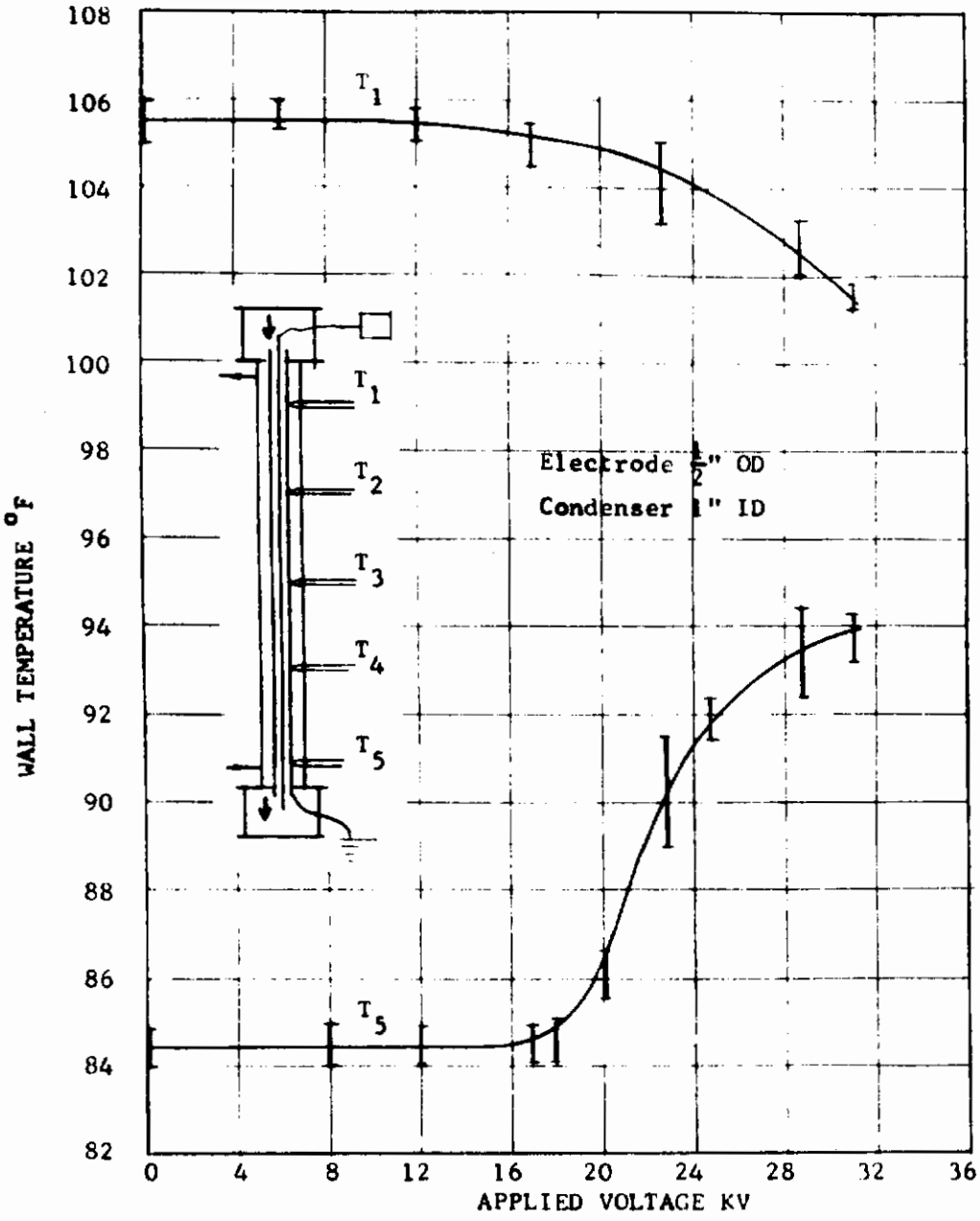

FIG. 29 VARIATION OF WALL TEMPERATURES (T_1 and T_5) WITH APPLIED VOLTAGE

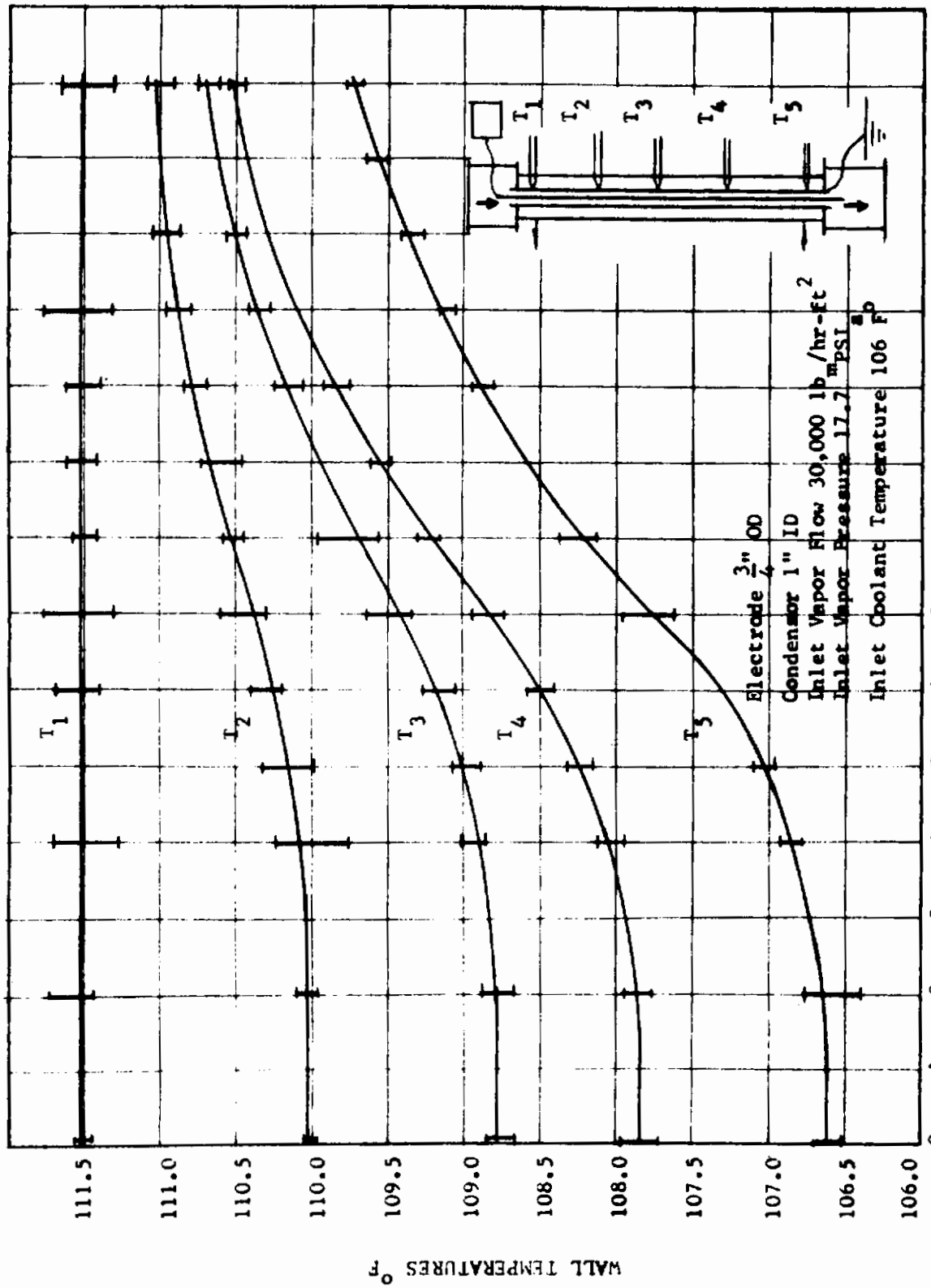

FIG. 30 WALL TEMPERATURE VARIATION vs APPLIED VOLTAGE WITHOUT SLUG FLOW

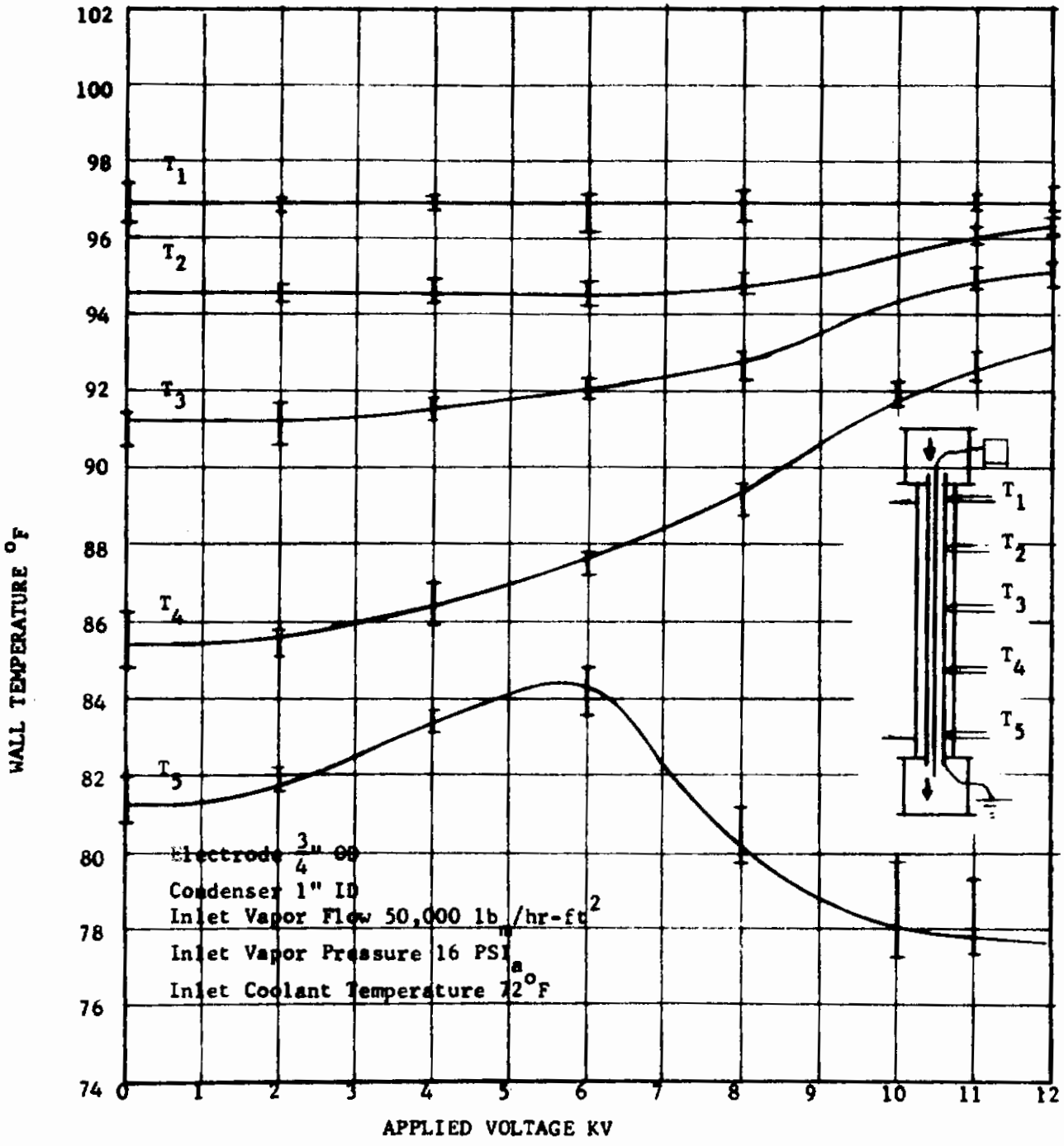

FIG. 31 WALL TEMPERATURE VARIATION vs APPLIED VOLTAGE WITH SLUG FLOW AT OUTLET OF CONDENSER

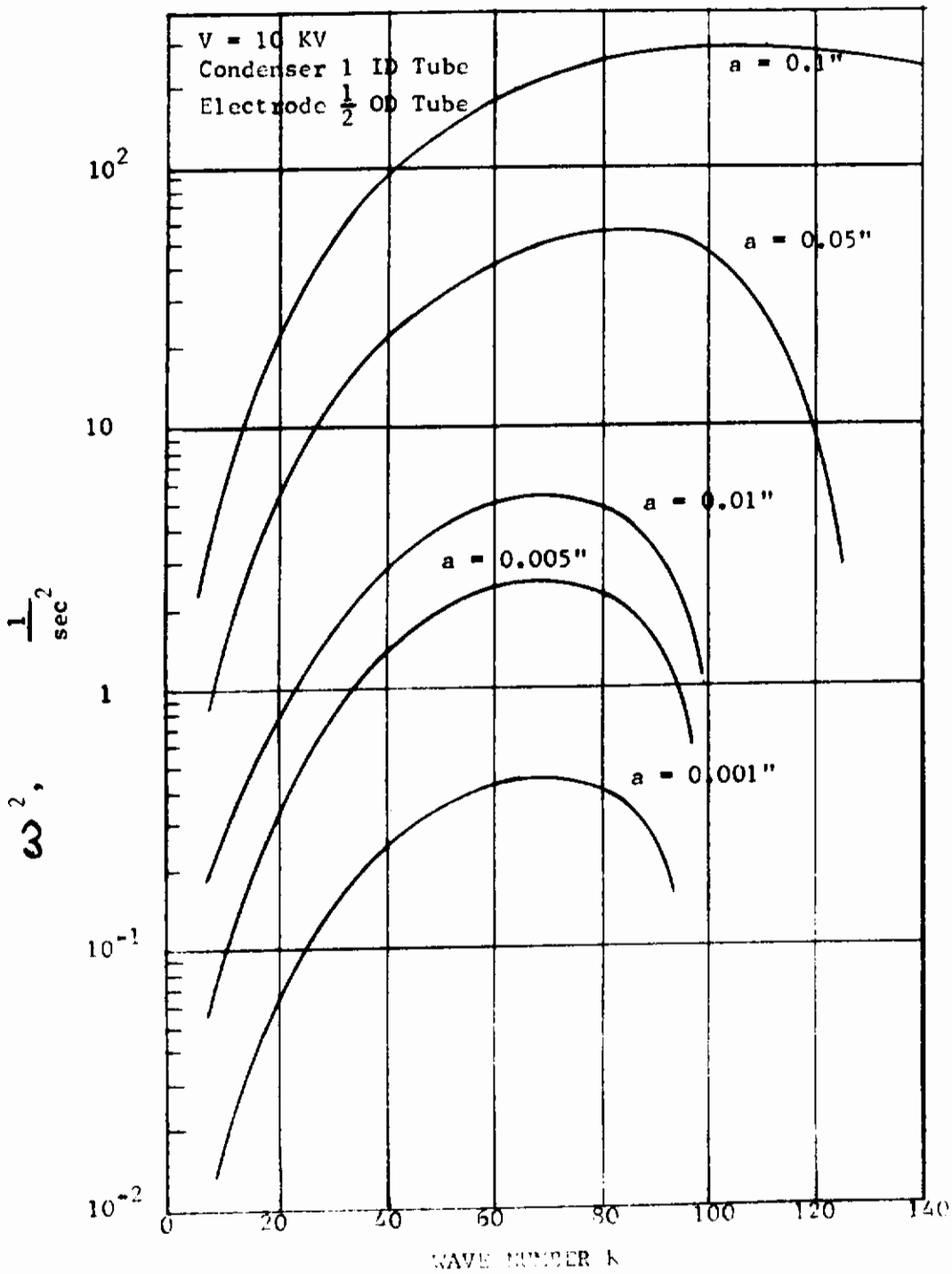

FIG. 32 ANGULAR FREQUENCY OF WAVE vs WAVE NUMBER
APPLIED VOLTAGE 10 KV

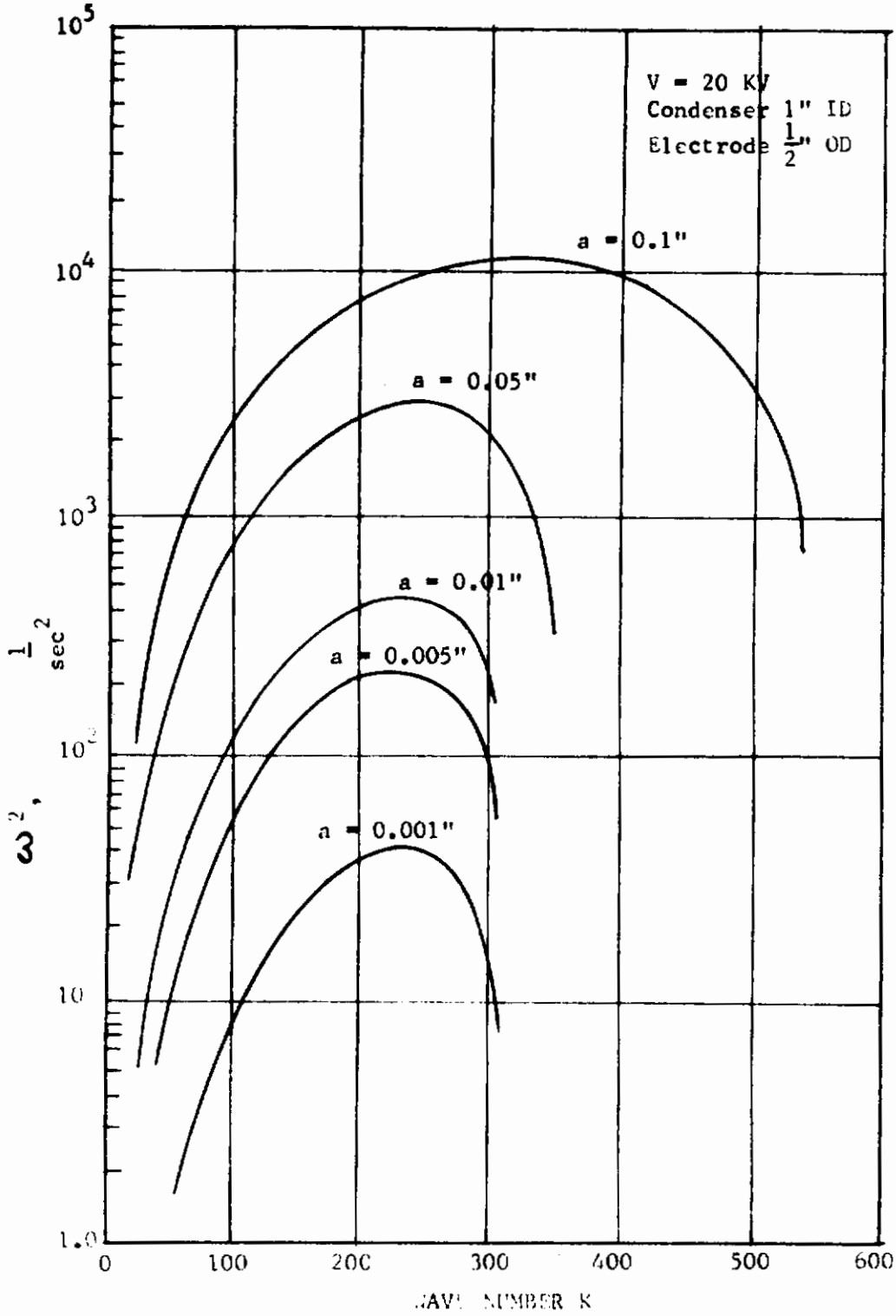

FIG. 33 ANGULAR FREQUENCY OF WAVE vs WAVE NUMBER
APPLIED VOLTAGE 20 KV

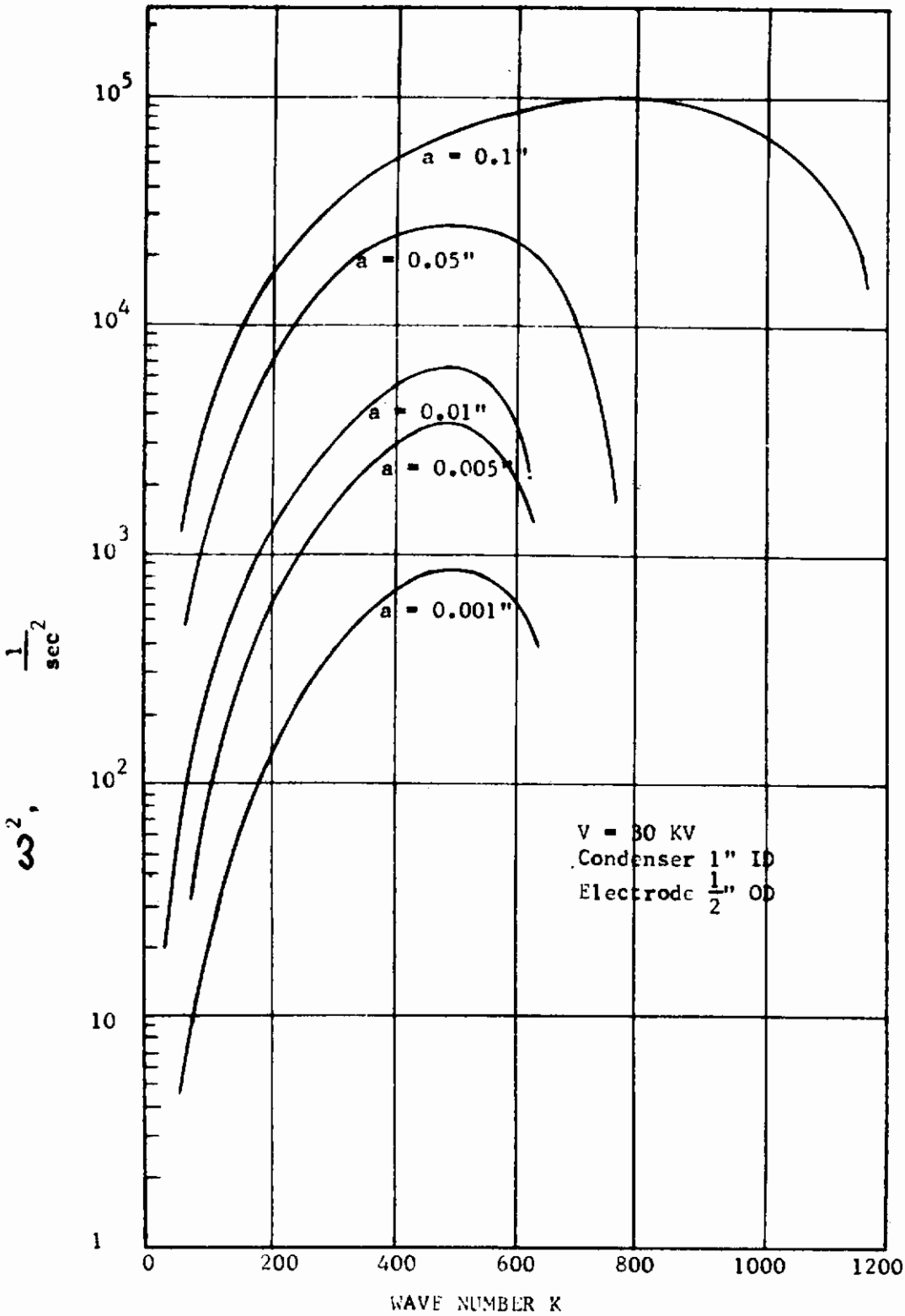

FIG. 34 ANGULAR FREQUENCY OF WAVE vs WAVE NUMBER
APPLIED VOLTAGE 30 KV

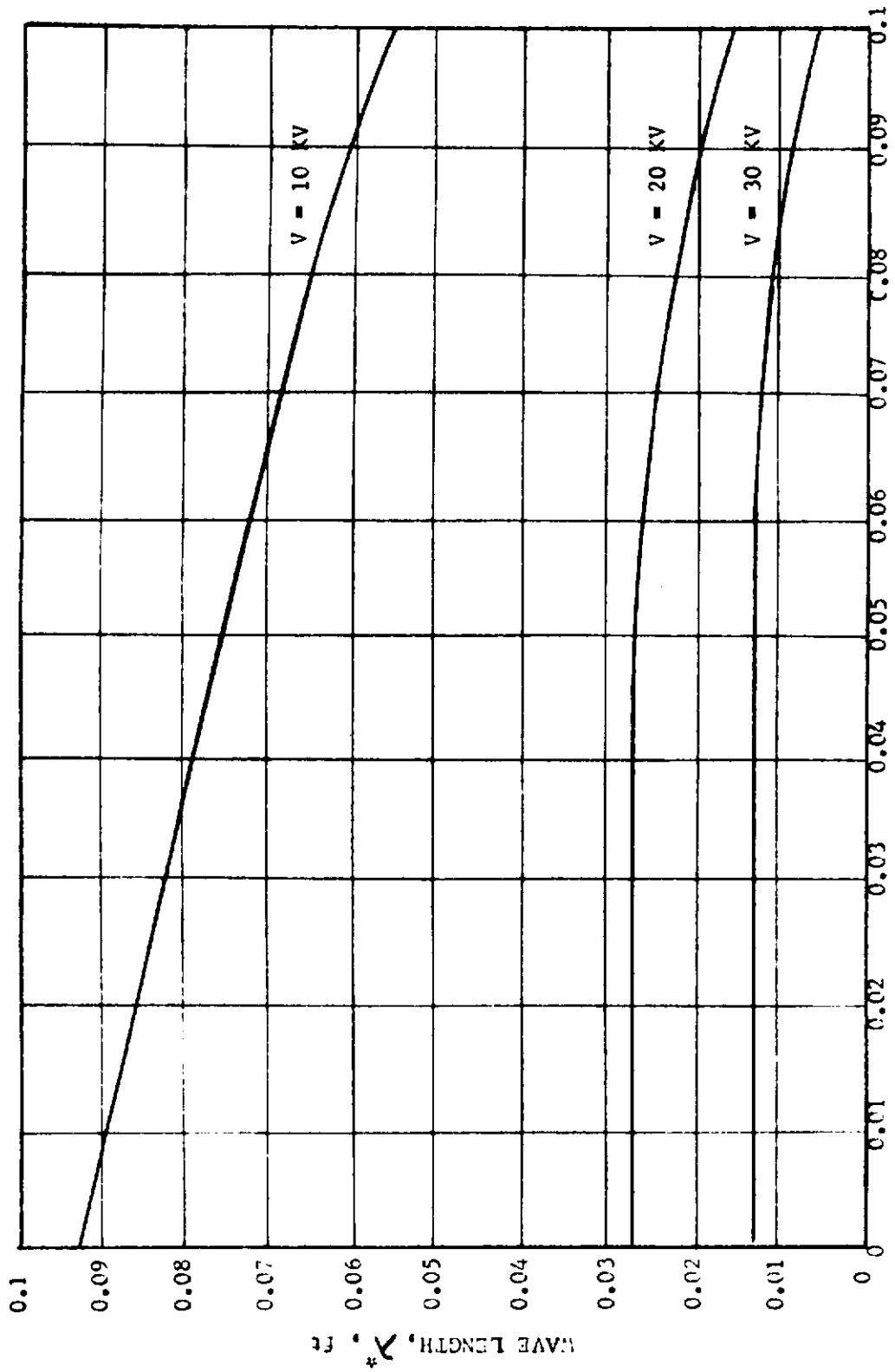

FIG. 35 FILM THICKNESS vs MOST UNSTABLE WAVE LENGTH

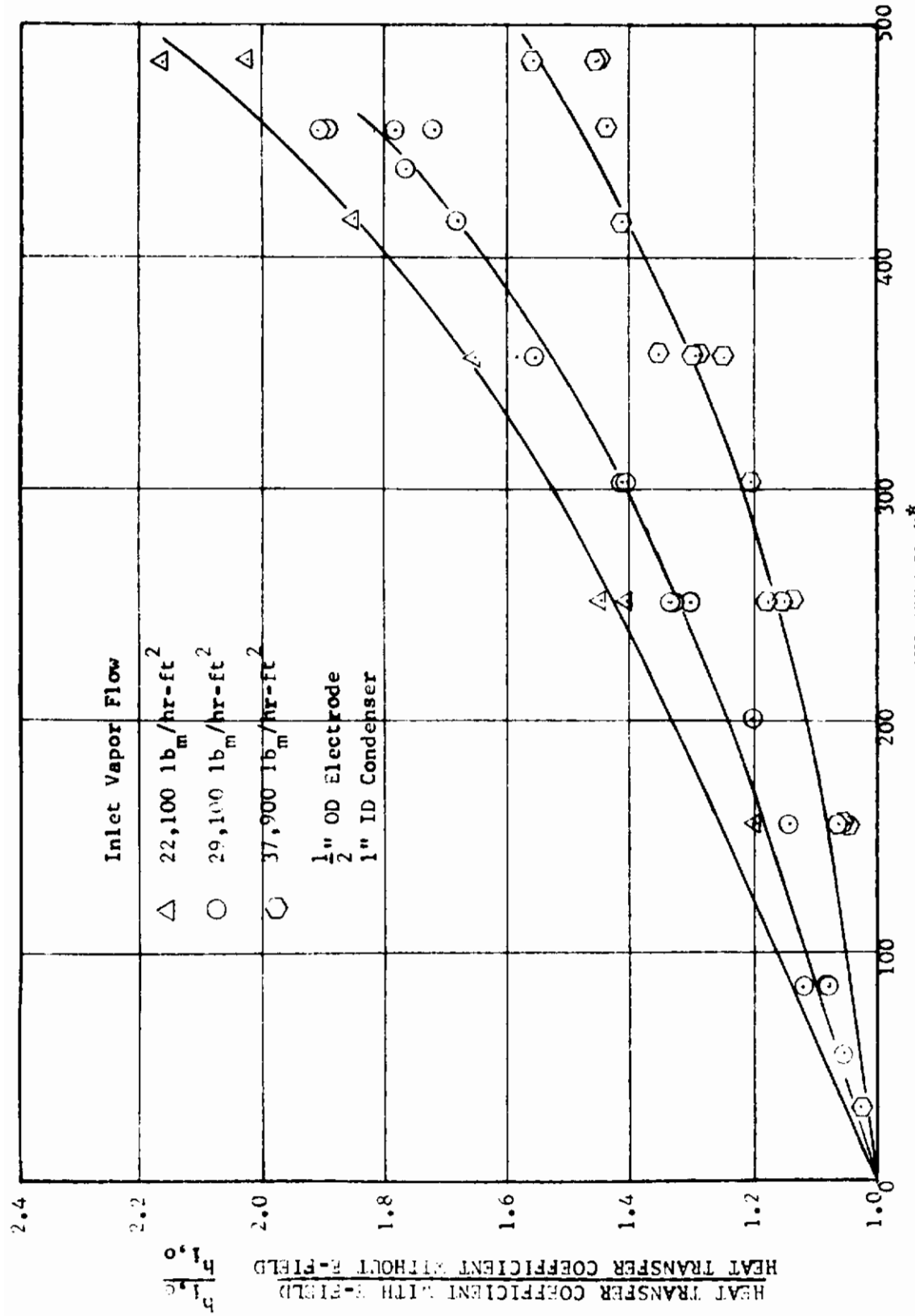

FIG. 36 AVERAGE HEAT TRANSFER COEFFICIENT RATIO vs K*

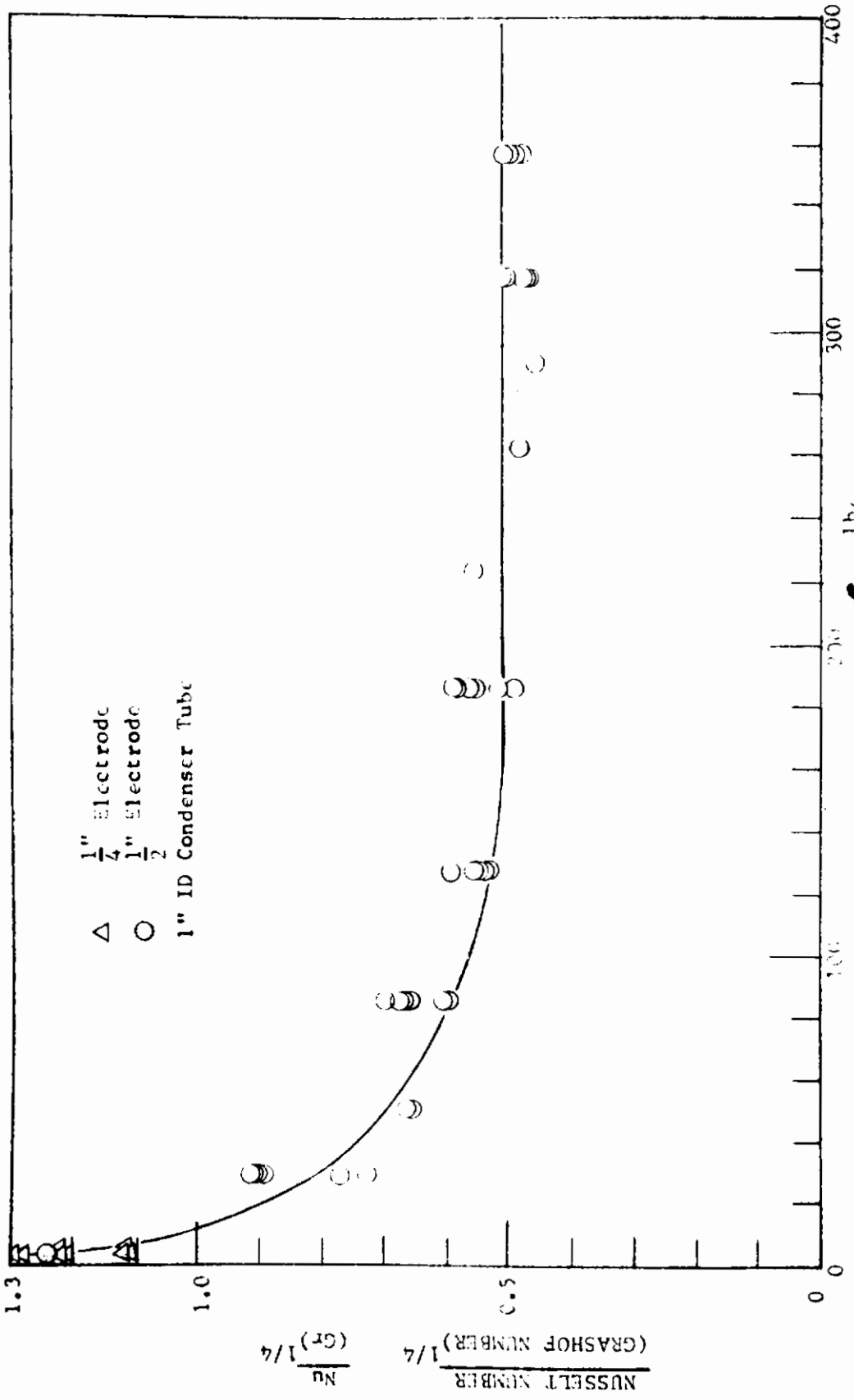

FIG. 37 CORRELATION OF HEAT TRANSFER DATA WITH ELECTRIC FIELD

REFERENCES

1. Gerstmann, J.,"Electrohydrodynamic Effects in Condensation", B.S. Thesis, Department of Mechanical Engineering, Tufts University, June, 1962.

2. Hall, W.E., "Two Phase Flow in a Non-Uniform Electric Field", B.S. Thesis, Department of Mechanical Engineering, Massachusetts Institute of Technology, June, 1962.

3. Margenau, H., Watson, W.W., and Montgomery, C.G., Physics, Principles and Applications, McGraw-Hill, 1949.

4. Landau, L.D. and Lifshitz, E.M., Electrodynamics of Continuous Media, Addison-Wesley Publishing Company,1960.

5. Stratton, J.A., Electromagnetic Theory, McGraw-Hill, 1941.

6. Wallis, G.B., "Flooding Velocities for Air and Water in Vertical Tubes", United Kingdom Atomic Energy Authority, AEEW-R123.

7. Melcher, J.R., Field Coupled Surface Waves, M.I.T. Press, Cambridge, Massachusetts, 1963.

8. Cheng, S.I. and Cordero, J., "Droplet Formation from Liquid Film over a Rotating Cylinder", AIAA Journal, 1,11, November 1963.

9. Rohsenow, W.M. et al, Trans. ASME, 78,1637 (1956).

10. Berenson, P.J. AIChE Paper No. 18, Heat Transfer Conference, Buffalo, August 1960.

11. Gerstmann, J., S.M. Thesis, Department of Mechanical Engineering, M.I.T., January, 1964.

APPENDIX A

Tabulated Test Data

Two-Phase Flow

Summary:

TABLE A0	Date, point identification numbers. Barometer readings p_B. Liquid inlet temperatures T_{LI}	
TABLES A1 - A6	Pressure drop $(\Delta p / \Delta L)_{TP}$, gas flow rate W_G and gas inlet temperature T_{IG}	
TABLE A1	W_L = 5.23 lbm/hr	P_T = 0 psig
	a. V = 0	b. V = 8.5 kV
TABLE A2	W_L = 5.23 lbm/hr	P_T = 14.6 psig
	a. V = 0 c. V = 15.0 kV	b. V = 8.5 kV
TABLE A3	W_L = 21.85 lbm/hr	P_T = 0 psig
	a. V = 0	b. V = 8.5 kV
TABLE A4	W_L = 21.85 lbm/hr	P_T = 14.6 psig
	a. V = 0	c. V = 15.0 kV
TABLE A5	W_L = 1.43 lbm/hr	P_T = 0 psig
	a. V = 0	b. V = 8.5 kV
TABLE A6	W_L = 1.43 lbm/hr	P_T = 14.6 psig
	a. V = 0	c. V = 15.0 kV

TABLE AO

Date	Points #	P_{B} "H_g	T_{Li} °F
12/11/63	1-18	-	80
12/12/63	19-35	-	77-80
12/15/63	36-48	-	74-75
12/17/63	49-61	-	75
12/20/63	62-74	29.66	77-80
12/26/63	75-92	29.68	75-78
12/27/63	93-105	29.87	74-76
12/28/63	106-114	30.00	75
12/30/63	115-136	30.49	76-80
1/2/64	137-152	29.60	78-80
1/3/64	153-172	29.80	78-82
1/6/64	173-178	29.80	78-80
1/7/64	179-192	29.80	75-77
1/8/64	193-207	29.70	77-79
1/20/64	208-218	29.60	78-80
1/21/64	219-232	29.55	78-82
1/22/64	233-245	30.00	79-80
2/6/64	246-251	---	78-79
2/7/64	252-272	29.30	76-80
2/11/64	273-278	30.20	76-77
3/3/64	279-286	30.00	77
3/4/64	287-288	30.00	80
3/5/64	289-293	29.55	80
3/6/64	293-295	30.20	79
5/8/64	296-305	29.90	80-88
5/11/64	306-307	30.11	82-86

TABLE A1-a

W_L = 5.23 lbm/hr P_T = 0 psig

V = 0

Point #	W_G lbm/hr	$(\Delta p/\Delta L)_{TP}$ lbf/ft^2/ft	T_{IG} °F
84	2.12	13.34	74
52	2.94	fluctuation	75
68	2.96	11.19	76
51	4.12	fluctuation	75
56	4.12	8.57	75
67	4.16	8.56	76
69	5.08	7.18	76
70	5.08	7.13	76
71	5.08	7.16	76
66	5.10	7.09	76
50	5.75	6.48	75
57	5.78	6.42	75
98	5.78	6.43	72
25	5.80	6.79	74
64	5.80	6.43	74
72	5.83	6.17	76
65	5.85	6.28	76
63	5.86	6.18	74
97	5.86	6.28	72
96	6.43	6.12	72
95	6.83	6.09	72
73	7.09	5.98	70
94	7.25	6.15	72
99	7.38	8.95	72
49	7.94	6.42	75
58	7.94	6.42	75
75	7.97	6.21	74
74	8.04	6.11	76
62	8.15	6.22	74
24	8.17	6.65	74
93	8.68	6.56	72
59	10.17	5.62	75
60	10.17	5.67	75
61	10.17	5.75	75

TABLE A1-a

(cont'd)

Point #	W_G lbm/hr	$(\Delta p/\Delta L)_{TP}$ lbf/ft^2/ft	T_{IG} °F
4	11.42	5.48	-
21	11.45	5.48	74
15	12.72	5.55	-
20	14.95	5.96	75
118	17.20	6.69	74
19	17.52	6.68	76
17	17.59	6.85	-
2	17.60	6.61	-
12	17.61	6.77	-
11	17.62	6.69	-
7	19.62	7.57	-
10	19.62	7.52	-
32	19.68	7.68	76
1	19.75	7.77	-
117	20.40	8.17	74
119	20.60	7.99	74
116	24.10	10.17	72
122	28.00	12.44	74
115	28.70	12.92	72
306	28.80	12.79	63
307	35.60	17.73	66

TABLE A1-b

W_L = 5.23 lbm/hr P_T = 0 psig

V = 8.5 kV

Point #	W_G lbm/hr	$(\Delta p/\Delta L)_{TP}$ lbf/ft^2/ft	T_{IG} °F
83	2.12	13.07	74
85	2.12	13.39	74
82	2.81	9.91	74
90	3.47	8.09	75
89	4.04	6.23	75
81	4.05	5.92	74
88	4.88	4.94	75
80	4.88	4.83	74
87	5.40	4.89	75
79	5.60	4.53	74
27	5.80	4.79	75
26	5.80	4.82	74
86	5.91	4.55	75
78	6.30	4.63	74
91	6.47	4.62	75
77	7.00	4.82	74
76	7.97	5.15	74
23	8.17	5.14	74
92	8.62	5.12	75
22	11.44	5.69	74
14	12.72	5.86	-
121	17.10	7.28	66
125	17.28	7.21	68
16	17.48	7.52	-
13	17.68	7.39	-
18	17.75	7.79	-
8	19.62	8.37	-
9	19.62	8.32	-
33	19.75	8.43	76
120	20.55	8.85	66
126	20.60	8.87	66
124	24.15	11.10	68
123	28.00	13.64	68

TABLE A2-a

W_L = 5.23 lbm/hr P_T = 14.6 psig

V = 0

Point #	W_G lbm/hr	$(\Delta p/\Delta L)_{TP}$ lbf/ft^2/ft	T_{IG} °F
243	4.15	12.62	76
256	5.31	9.85	77
240	6.47	8.09	76
237	7.44	7.55	76
252	8.30	6.78	77
233	9.72	6.39	99
230	11.07	6.55	76
265	12.17	6.47	72
227	13.23	6.20	76
259	14.72	5.64	74
209	15.70	5.73	76
208	15.90	5.73	76
270	16.49	5.37	71
266	18.10	5.41	72
223	18.12	5.65	76
276	20.20	5.56	70
219	20.55	5.73	70
226	20.85	5.99	76
296	24.60	6.66	77
273	24.65	6.69	64
215	25.20	7.00	70
212	30.20	8.92	76
297	35.10	10.66	72
301	36.40	11.44	60
303	36.90	11.51	58
299	43.40	15.77	63
298	44.60	15.24	53

TABLE A2-b

W_L = 5.23 lbm/hr P_T = 14.6 psig

V = 8.5 kV

Point #	W_G lbm/hr	$(\Delta p / \Delta L)_{TP}$ lbf/ft^2/ft	T_{IG} °F
244	4.15	10.25	76
257	5.34	6.42	77
241	6.47	5.04	76
238	7.44	3.69	76
253	8.32	4.39	77
234	9.72	4.94	79
235	9.75	4.56	79
231	11.07	4.95	76
264	12.17	5.08	72
228	13.30	5.21	74
260	14.72	5.32	74
210	15.70	5.63	76
271	16.49	5.44	70
267	18.08	5.78	71
224	18.35	6.11	76
222	20.20	6.24	70
277	20.22	6.15	66
220	20.45	6.41	73
274	24.85	7.55	62
216	25.05	7.86	70
213	30.30	10.12	70

TABLE A2-c

W_L = 5.23 lbm/hr P_T = 14.6 psig

V = 15 kV

Point #	W_G lbm/hr	$(\Delta p / \Delta L)_{TP}$ lbf/ft^2/ft	T_{IG} °F
245	4.15	10.66	76
258	5.37	6.03	77
242	6.47	4.18	76
239	7.44	3.69	76
254	8.32	3.38	77
255	8.32	3.52	77
236	9.74	3.88	76
232	11.07	4.50	75
263	12.17	4.61	72
229	13.30	4.95	74
261	14.72	5.13	72
211	15.60	5.61	76
272	16.48	5.84	64
268	18.08	5.97	71
269	18.08	6.30	71
225	18.32	6.63	76
278	20.25	6.42	64
221	20.35	6.62	73
218	24.60	8.04	64
217	24.70	8.25	64
275	24.85	8.30	62
214	30.20	11.04	70
302	36.40	12.68	58
300	43.60	17.87	56

TABLE A3-a

W_L = 21.85 lbm/hr P_T = 0 psig

V = 0

Point #	W_G lbm/hr	$(\Delta p / \Delta L)_{TP}$ lbf/ft^2/ft	T_{IG} °F
114	2.08	15.24	72
105	2.12	5.17	72
104	2.98	13.17	72
103	4.06	10.92	72
102	5.70	9.42	72
29	5.85	9.74	76
101	6.64	9.14	72
100	7.38	8.95	72
45	8.09	9.20	72
47	8.09	9.16	72
30	8.26	9.42	76
48	9.20	6.35	74
42	10.69	9.87	71
44	10.69	9.87	71
39	12.70	10.92	70
41	12.70	11.03	70
135	17.15	12.88	66
36	17.60	13.25	74
38	17.60	13.26	74
132	20.60	14.90	66
35	20.85	15.39	76
131	25.30	18.28	66
130	25.35	18.28	66
127	28.50	20.96	66

TABLE A3-b

W_L = 21.85 lbm/hr P_T = 0 psig

V = 8.5 kV

Point #	W_G lbm/hr	$(\Delta p / \Delta L)_{TP}$ lbf/ft^2/ft	T_{IG} °F
113	2.08	15.14	76
112	2.93	12.90	76
110	4.00	10.20	76
111	4.82	9.28	76
109	5.60	9.04	76
28	5.80	8.89	76
108	6.80	8.85	76
107	7.85	9.14	76
46	8.09	9.20	72
106	8.65	9.23	76
43	10.69	10.37	71
40	12.70	11.78	70
136	17.20	14.07	66
37	17.60	14.47	74
133	20.60	16.52	60
34	20.95	16.99	76
134	21.20	16.88	66
129	25.40	20.21	66
128	28.30	22.76	66

TABLE A4-a

W_L = 21.85 lbm/hr P_T = 14.6 psig

V = 0

Point #	W_G lbm/hr	$(\Delta p / \Delta L)_{TP}$ lbf/ft^2/ft	T_{IG} °F
281	9.75	9.06	75
289	11.77	9.80	-
279	14.60	10.32	75
283	20.20	11.60	75
285	24.00	17.22	75
291	30.70	16.21	-
288	32.60	17.60	72
304	42.20	23.37	57

TABLE A4-b

W_L = 21.85 lbm/hr P_T = 14.6 psig

V = 15 kV

Point #	W_G lbm/hr	$(\Delta p / \Delta L)_{TP}$ lbf/ft^2/ft	T_{IG} °F
282	9.75	9.06	75
290	11.82	10.37	-
280	14.60	12.42	75
284	20.20	15.25	75
286	23.90	17.18	75
297	30.70	21.70	-
287	32.60	23.20	72
305	42.30	27.97	54

TABLE A5-a

W_L = 1.43 lbm/hr P_T = 0 psig

V = 0

Point #	W_G lbm/hr	$(\Delta p / \Delta L)_{TP}$ lbf/ft^2/ft	T_{IG} °F
144	2.17	12.55	76
143	3.05	10.03	76
167	3.21	9.60	78
152	3.70	8.33	76
151	4.36	7.04	76
166	4.52	7.10	78
142	4.53	7.45	75
150	4.93	6.64	76
141	5.03	6.69	75
149	5.35	6.21	76
165	5.51	6.12	78
148	5.74	5.85	76
147	6.16	5.76	76
140	6.30	5.67	75
164	6.35	5.61	78
146	6.80	5.55	76
145	6.98	5.66	76
139	7.06	5.71	75
163	7.08	5.70	74
160	7.65	6.06	74
162	7.72	6.02	74
138	8.18	5.61	76
161	8.21	5.13	74
159	8.81	4.75	74
158	9.31	4.54	74
157	9.85	4.30	74
137	9.99	4.25	76
156	10.88	3.99	76
155	11.89	3.81	76
154	13.00	3.80	76
172	13.52	3.83	78
153	14.82	4.03	76
171	15.78	4.20	78
170	20.65	5.86	78
169	24.60	7.85	78
168	29.20	10.29	78

TABLE A5-b

W_L = 1.43 lbm/hr P_T = 0 psig

V = 8.5 kV

Point #	W_G lbm/hr	$(\Delta p / \Delta L)_{TP}$ lbf/ft^2/ft	T_{IG} °F
185	2.22	11.53	74
192	2.44	11.15	73
184	3.09	8.92	74
191	3.29	7.98	73
190	3.61	6.23	73
189	4.18	3.8[illegible]	74
183	4.35	3.81	74
207	4.71	3.33	71
188	4.80	3.88	74
182	5.08	3.21	74
187	5.55	3.28	74
181	6.25	3.35	74
206	6.54	3.42	70
186	6.72	3.57	74
180	7.15	3.54	74
205	7.92	3.94	70
179	8.15	3.55	74
204	8.53	3.54	70
203	9.72	3.57	70
202	10.16	3.65	64
178	11.29	3.64	66
201	12.37	3.89	64
177	13.30	4.07	66
200	15.48	4.47	64
176	15.92	4.54	66
199	16.80	4.74	66
198	20.40	6.52	64
197	20.40	6.12	64
175	20.80	6.35	65
174	25.10	9.43	65
196	25.30	8.62	64
195	25.30	8.86	64
194	25.40	9.09	66
193	28.40	10.15	73
173	29.65	11.46	65

TABLE A6-a

W_L = 1.43 lbm/hr P_T = 0 psig

V = 0

Point #	W_G lbm/hr	$(\Delta\rho/\Delta L)_{TP}$ lbf/ft^2/ft	T_{IG} °F
294	15.18	3.65	72

TABLE A6-b

W_L = 1.43 lbm/hr P_T = 14.6 psig

V = 15 kV

Point #	W_G	$\Delta\rho$	T_{IG}
295	15.18	2.94	-
293	30.70	7.51	-

APPENDIX B

TABULATED TEST DATA (CONDENSER)

TABLE B1 Test Series A, B

1/4" OD Electrode
1" ID Condenser
V = 0 to 20 KV
Vapor Generation Rate without E-Field =
90 to 120 lb_m/hr

TABLE B2 Test Series C, E, F, G, H

1/2" OD Electrode
1" IDCondenser
V = 0 to 30 KV
Vapor Generation Rate without E-Field=
90 to 155 lb_m/hr

TABLE B3 Test Series J, K

3/4" OD Electrode
1" ID Condenser
Vapor Generation Rate without E-Field =
90 to 155 lb_m/hr

The series numbers in the following table identify the data points in the original computation sheets of the IBM 1620 Computers.

TABLE B1

Series Number	Applied Voltage	Coolant Flow			Top Chamber		Bottom Chamber	
	V KV	T_{in}	T_{out} °F	Δh cm Hg	T_{top} °F	P_{top} cm Hg	T_{bottom} °F	P_{bottom} cm Hg
A-01	0	53.90	56.83	10.0	132.25	6.0	119.28	1.6
A-02	10	53.90	56.85	10.0	132.05	--	119.30	1.7
A-03	20	54.14	57.30	10.0	131.40	3.0	116.75	1.2
A-04	0	53.70	55.95	20.5	132.70	5.4	118.85	2.1
A-05	10	53.70	56.05	21.0	133.70	5.7	118.00	2.0
A-06	20	53.90	56.40	21.0	133.90	4.6	107.40	0.5
A-07	0	53.70	56.67	10.8	126.60	1.8	120.11	2.8
A-08	20	53.37	56.75	10.8	126.81	-0.3	118.00	2.2
A-09	10	53.45	56.60	10.8	127.21	1.7	120.55	1.6
A-10	0	53.23	55.38	25.5	127.23	1.9	119.70	1.4
A-11	10	53.00	55.24	25.5	127.23	1.7	120.54	1.7
A-12	20	53.00	55.24	25.5	126.60	1.3	119.50	1.3
A-13	0	53.00	54.82	35.0	127.02	3.9	120.95	2.3
A-14	10	52.75	54.73	35.0	127.02	2.5	120.54	2.5
A-15	20	53.21	55.21	35.0	127.23	0.8	118.65	0.7
A-16	0	53.91	57.02	9.7	123.90	3.0	120.54	2.6
A-17	10	54.50	57.61	10.0	124.69	2.0	119.7	2.5
A-18	17	54.37	57.66	10.0	120.89	-0.6	117.8	-1.2
A-22	0	40.43	44.12	9.6	129.10	2.5	120.6	2.5
A-23	5	40.55	44.25	9.5	125.78	2.4	120.95	2.4
A-24	20	40.75	44.55	9.5	125.55	2.3	120.25	2.3
A-25	0	40.90	44.41	9.5	125.45	1.7	119.39	1.7
A-26	20	40.91	44.50	9.8	125.10	2.1	119.92	2.1
B-01	0	46.60	49.90	9.5	126.69	3.1	119.35	3.0
B-02	0	46.42	49.60	9.5	126.10	2.5	119.00	2.3
B-03	5	46.47	49.75	9.5	125.89	3.2	119.40	3.1
B-04	9	46.89	50.22	9.5	125.83	2.2	119.60	2.1
B-05	15	46.80	50.20	9.5	125.32	2.7	118.72	2.0
B-06	20	46.52	50.09	9.5	124.70	0.6	117.2	0.5

Series Number	Wall Temperature			Condensed Freon	
	T_{w1} °F	T_{w3} °F	T_{w5} °F	$T_{cond.}$ °F	Time Sec
A-01	92.35	76.10	71.27	118.85	71.55
A-02	92.55	76.35	70.80	118.65	67.50
A-03	92.35	77.45	72.35	116.50	65.00
A-04	88.90	72.60	69.50	118.65	64.80
A-05	88.85	73.50	69.75	117.80	63.50
A-06	88.65	74.15	70.60	107.40	62.00
A-07	92.78	76.55	70.38	118.85	63.75
A-08	91.90	77.00	71.5	124.00	60.10
A-09	93.21	77.00	70.8	---	62.00
A-10	88.86	72.15	67.93	117.80	61.00
A-11	88.65	72.80	68.75	119.68	59.90
A-12	88.89	73.00	69.95	118.85	57.50
A-13	87.12	71.26	67.85	119.90	59.90
A-14	87.12	71.49	67.92	119.29	58.00
A-15	87.79	72.80	69.10	118.21	58.30
A-16	92.80	76.78	71.26	120.11	68.00
A-17	92.79	77.44	71.92	119.50	66.80
A-18	91.05	77.00	72.15	117.60	64.40
A-22	90.20	67.31	60.32	119.59	56.50
A-23	90.99	68.15	60.70	120.95	56.00
A-24	91.10	69.37	61.70	119.81	12.60
A-25	89.50	66.92	61.28	118.92	59.25
A-26	89.50	67.83	61.58	118.50	57.50
B-01	91.70	71.52	64.53	118.43	63.0
B-02	91.40	70.78	63.90	117.80	---
B-03	91.29	70.90	64.85	118.80	62.0
B-04	91.95	72.23	65.67	118.38	61.0
B-05	91.60	73.02	66.50	118.20	60.0
B-06	90.52	72.06	65.67	116.70	57.5

Series Number	Vapor Generation			Vapor Trap		
	ϕ %	T °F	P cm Hg	ϕ %	T °F	P cm Hg
A-01	36.5	123.70	4.0	15.0	159.70	0.8
A-02	36.5	122.85	0.4	9.0	165.10	1.0
A-03	36.5	122.00	4.0	0.0	169.55	1.0
A-04	34.0	140.35	4.0	0.0	182.50	1.0
A-05	36.0	124.90	4.0	---	180.90	---
A-06	36.0	125.55	---	0.0	176.75	0.0
A-07	47.5	122.65	6.6	49.0	126.80	2.5
A-08	47.5	124.3	4.0	40.0	128.30	0.3
A-09	47.0	124.70	5.5	42.0	129.32	2.7
A-10	47.5	124.70	5.5	42.5	129.50	1.8
A-11	47.0	124.52	5.0	35.0	130.59	1.6
A-12	46.5	124.10	4.6	26.0	132.25	1.2
A-13	45.0	123.50	7.1	28.0	133.30	3.8
A-14	46.5	124.52	5.9	30	133.30	2.4
A-15	47.0	124.31	4.2	19.5	135.60	0.7
A-16	37.5	122.00	5.3	19.0	138.29	2.7
A-17	39.0	121.80	5.2	20.0	138.08	2.5
A-18	37.5	120.10	1.6	7.5	142.40	-1.1
A-22	46.0	122.65	5.5	28.0	125.48	2.5
A-23	46.5	123.45	5.5	28.0	126.50	2.4
A-24	47.0	122.96	4.7	22.5	127.72	2.3
A-25	40.0	121.85	4.3	12.0	132.56	1.6
A-26	40.0	121.65	4.6	---	139.45	2.0
B-01	43.0	125.20	6.20	35.0	127.80	2.8
B-02	45.0	124.85	5.7	35.0	127.06	2.2
B-03	42.0	124.79	6.1	20.0	133.30	3.1
B-04	43.5	124.78	5.4	28.5	129.65	1.8
B-05	42.0	124.35	5.7	29.0	133.59	2.6
B-06	44.0	124.20	3.7	29.0	133.05	0.5

TABLE B2

Series Number	Applied Voltage	Coolant Flow			Top Chamber		Bottom Chamber	
	V KV	T_{in} °F	T_{out} °F	Δh cm Hg	T_{top} °F	P_{top} cm Hg	T_{bottom} °F	P_{bottom} °F
C-01	0	70.67	73.57	12.20	128.70	17.3	128.50	17.10
C-02	29	69.66	73.60	12.20	127.18	7.4	121.87	7.00
C-03	25	69.55	72.95	---	125.85	9.5	123.75	9.10
C-04	20	68.80	72.05	11.80	125.60	11.5	124.75	11.20
C-05	15	69.00	71.60	11.65	92.80	12.9	126.00	12.90
C-06	10	68.60	71.46	---	126.33	13.4	126.20	13.10
C-07	5	68.23	71.20	11.60	126.49	13.4	126.20	13.10
C-08	0	71.65	74.30	11.70	127.21	14.6	125.45	14.40
C-09	29	71.32	74.95	11.70	127.55	6.6	121.65	6.20
C-10	0	70.85	73.50	11.80	126.07	12.75	125.93	12.40
E-04	29	65.70	69.21	13.5	103.30	-0.10	114.7	-0.40
E-05	25	65.30	68.60	13.5	122.53	1.40	116.51	1.05
E-06	28.25	65.30	68.68	13.5	122.38	0.50	115.74	0.00
E-07	22.5	65.40	68.51	13.5	122.50	3.10	117.65	2.60
E-08	29	65.80	69.25	13.5	122.53	-0.10	115.14	-0.40
E-09	20	65.80	68.72	13.5	122.52	4.40	119.20	4.05
E-11	22.5	65.7	68.80	13.5	122.44	3.9	118.38	3.55
E-12	20	65.80	68.90	13.5	122.55	5.2	119.26	4.90
E-13	15	65.70	68.60	13.5	122.53	6.6	120.55	6.30
E-14	17.5	65.50	68.85	13.5	122.65	5.6	119.95	5.40
E-15	10	65.20	67.78	13.5	122.28	6.6	120.83	6.30
E-16	5	65.40	68.05	13.5	121.73	7.8	121.54	7.60
E-17	0	65.40	67.97	13.5	121.85	8.1	121.85	7.90
E-18	27.5	65.30	68.66	13.5	121.78	0.2	115.83	0.00
E-19	0	65.00	67.62	13.5	120.45	6.0	120.45	5.90
F-01	0	63.80	67.55	13.1	130.30	12.8	124.40	12.4
F-02	5	64.00	67.75	12.9	130.63	13.4	124.99	12.8
F-03	10	63.95	67.90	13.2	131.03	13.2	124.94	12.6
F-04	15	64.55	68.35	12.9	131.33	12.6	124.26	11.9
F-05	20	64.65	68.70	12.6	131.16	12.2	124.26	11.7
F-06	25	64.50	68.60	13.0	131.18	9.8	122.32	9.1
F-07	29	64.50	68.75	13.1	130.84	8.0	121.13	7.1
F-08	30	64.50	68.85	13.5	130.47	6.8	120.30	5.9
F-09	25	64.65	68.80	13.2	130.18	10.0	122.57	9.0
F-10	30	64.90	69.15	13.5	129.98	7.2	120.55	6.3
F-11	20	64.75	68.75	13.6	129.80	11.4	123.46	10.6
F-12	25	64.95	69.10	13.7	129.53	9.6	122.28	8.7
F-13	20	64.90	68.60	13.5	129.60	10.6	123.25	10.2
F-14	15	65.15	68.95	13.5	129.55	12.8	124.30	12.15
F-15	7.5	65.35	69.03	--	129.60	12.8	120.55	12.0
F-16	0	65.40	68.60	13.70	130.52	12.0	124.36	11.6

Series Number	Wall Temperature		Condensed Freon	
	T_{w1} °F	T_{w5} °F	$T_{cond.}$ °F	Time Sec
C-01	114.63	102.67	126.25	64.10
C-02	111.25	109.22	119.80	45.40
C-03	112.07	107.32	121.50	49.80
C-04	112.12	103.60	122.45	53.00
C-05	112.65	101.30	123.75	55.30
C-06	112.25	99.35	121.89	57.00
C-07	112.40	100.95	123.80	60.00
C-08	113.35	98.18	124.50	64.20
C-09	111.50	109.60	119.30	46.70
C-10	112.67	98.50	123.71	61.00
E-04	101.95	103.30	112.96	51.20
E-05	102.50	101.92	114.54	54.50
E-06	102.05	103.02	113.71	52.40
E-07	102.75	100.90	115.70	56.80
E-08	102.35	103.81	113.40	50.70
E-09	103.35	99.80	116.80	57.50
E-10	103.52	101.36	116.26	56.20
E-11	103.90	97.99	117.71	60.50
E-12	103.87	100.15	117.39	58.20
E-13	104.29	96.10	118.37	61.40
E-14	103.65	97.55	117.70	59.80
E-15	103.41	92.76	118.42	61.60
E-16	103.69	92.24	119.52	65.90
E-17	103.90	92.28	119.55	64.80
E-18	101.95	102.55	113.32	51.80
E-19	103.05	92.20	118.38	64.90
F-01	106.89	100.30	122.25	49.7
F-02	107.57	100.92	122.70	48.0
F-03	107.80	101.00	122.70	47.0
F-04	107.37	101.32	122.20	48.0
F-05	107.78	104.09	122.29	45.3
F-06	106.75	105.60	120.43	45.0
F-07	106.44	107.10	119.24	42.0
F-08	105.67	107.01	118.35	42.0
F-09	107.14	106.02	120.55	44.3
F-10	106.15	107.02	118.49	42.0
F-11	107.32	103.29	121.38	47.0
F-12	107.55	105.62	120.40	42.5
F-13	107.23	103.05	121.23	47.0
F-14	108.26	101.95	122.40	49.2
F-15	107.78	101.40	122.65	47.7
F-16	107.0	106.62	122.19	50.0

Series	Vapor Generation			Vapor Trap		
	ϕ %	T °F	P cm Hg	ϕ %	T °F	P cm Hg
C-01	42.0	130.32	20.4	32.0	132.82	17.1
C-02	51.0	128.00	11.2	16.0	133.33	6.6
C-03	49.5	137.65	13.1	21.5	130.15	9.1
C-04	45.9	127.25	14.3	--	132.15	10.7
C-05	45.8	128.25	16.0	29.0	131.50	12.5
C-06	43.5	128.20	16.4	29.5	131.20	12.8
C-07	46.0	128.50	16.5	31.3	129.95	13.0
C-08	42.0	129.76	17.6	39.0	129.95	14.4
C-09	52.0	128.81	10.4	22.0	129.95	5.6
C-10	43.0	128.22	16.7	35.5	132.50	12.4
E-04	52.5	123.15	3.4	22.0	136.10	-1.4
E-05	50.0	123.00	5.3	26.5	136.50	1.1
E-06	52.0	122.95	4.5	23.0	137.75	-0.1
E-07	48.0	122.85	6.4	27.0	137.20	2.2
E-08	52.0	123.15	4.0	21.0	137.05	-0.7
E-09	47.5	121.95	7.0	29.5	137.30	4.0
E-10	48.5	122.30	7.5	27.0	137.20	3.4
E-11	46.5	122.60	9.5	31.0	136.65	5.3
E-12	47.0	122.30	8.5	29.0	136.60	4.3
E-13	45.5	123.00	6.8	32.0	136.35	6.1
E-14	46.5	122.20	8.9	31.5	136.20	5.4
E-15	43.0	123.10	9.6	33.5	135.95	6.2
E-16	42.0	128.85	10.7	35.0	135.60	7.4
E-17	42.0	124.00	11.0	35.5	135.27	7.9
E-18	50.0	122.20	4.0	24.0	137.85	-0.2
E-19	43.3	122.80	9.3	38.5	134.55	5.8
F-01	56.7	130.73	17.3	50.0	133.75	12.1
F-02	58.0	131.00	18.0	51.5	133.95	12.8
F-03	57.7	131.47	17.8	50.0	134.15	12.6
F-04	56.7	131.95	16.0	47.5	134.35	11.8
F-05	58.9	131.80	17.1	46.5	134.50	11.5
F-06	59.0	132.15	14.5	42.0	134.70	8.9
F-07	61.8	131.80	12.1	38.5	134.80	7.1
F-08	61.5	131.53	11.9	36.0	135.05	5.8
F-09	60.5	131.15	14.8	43.0	134.60	9.0
F-10	61.0	130.75	12.1	36.5	135.10	6.2
F-11	59.0	130.67	16.1	46.5	134.55	10.6
F-12	60.3	130.13	14.2	42.5	134.50	8.6
F-13	57.2	130.25	15.2	45.0	134.31	10.0
F-14	58.8	130.40	17.7	50.0	134.20	12.1
F-15	49.5	129.95	17.1	49.5	134.20	12.1
F-16	56.0	130.87	16.3	49.5	134.75	11.4

Series Number	Applied Voltage	Coolant Flow			Top Chamber		Bottom Chamber	
	V KV	T_{in} °F	T_{out} °F	Δh cm Hg	T_{top} °F	P_{top} cm Hg	T_{bottom} °F	P_{bottom} cm Hg
G-02	20	79.85	82.30	12.6	121.05	-0.3	116.50	-0.6
G-03	30	79.00	81.70	12.7	120.97	-1.6	115.83	-1.8
G-04	25	78.15	80.70	12.7	121.35	2.4	117.60	2.1
G-05	30	77.50	80.40	12.7	120.98	-0.4	116.30	-0.7
G-06	20	78.15	80.45	13.1	121.25	4.6	119.70	4.2
G-07	0	78.00	80.05	13.1	121.17	7.2	121.22	6.8
G-08	15	77.80	80.10	13.0	122.42	5.8	121.00	5.7
G-09	0	78.30	80.55	12.8	121.03	7.0	121.03	6.8
G-10	22.5	78.10	80.75	12.5	122.62	3.1	118.88	2.8
G-11	27.5	77.60	80.05	--	122.65	0.5	117.32	0.2
H-01	0	65.10	68.40	11.7	130.30	12.8	125.55	12.3
H-02	15	65.55	69.05	11.8	130.00	12.1	124.87	11.7
H-03	25	65.85	69.60	11.6	129.80	8.45	122.43	8.0
H-04	0	66.30	70.40	11.8	128.66	5.75	120.40	4.8
H-05	27.5	66.60	70.60	11.9	128.53	7.6	121.80	6.9
H-06	22.5	65.85	69.35	12.7	128.83	9.5	123.23	9.0
H-07	0	65.65	68.95	12.5	129.80	12.9	125.23	12.4

Series Number	Wall Temperature		Condensed Freon	
	T_{w1} °F	T_{w5} °F	$T_{cond.}$ °F	Time Sec
G-02	106.90	101.20	114.00	63.4
G-03	105.96	108.00	112.00	63.5
G-04	106.97	106.77	111.65	72.3
G-05	106.27	108.35	113.50	65.5
G-06	107.15	105.47	116.83	75.1
G-07	107.47	99.85	118.73	86.5
G-08	107.65	102.6	118.15	80.7
G-09	107.85	100.20	118.15	90.5
G-10	107.29	106.6	116.06	71.8
G-11	106.24	107.02	114.89	66.6
H-01	108.16	100.83	122.58	50.3
H-02	108.47	101.43	122.55	51.3
H-03	107.65	105.70	120.60	48.0
H-04	106.70	108.10	118.37	43.5
H-05	107.78	107.67	119.87	46.2
H-06	107.79	104.45	120.60	48.5
H-07	108.22	100.95	123.06	53.8

Series Number	Vapor Generation			Vapor Trap		
	ϕ %	T °F	P cm Hg	ϕ %	T °F	P cm Hg
G-02	39.0	120.70	2.3	47.50	127.50	-0.6
G-03	41.3	120.30	1.4	25.00	130.85	-1.7
G-04	38.8	121.08	4.0	24.5	134.65	1.5
G-05	42.0	120.30	2.4	21.0	135.95	-0.6
G-06	36.5	121.80	6.3	28.0	136.13	3.8
G-07	33.0	123.17	8.9	32.0	134.52	6.5
G-08	35.0	122.85	8.2	31.0	134.70	5.7
G-09	33.0	123.05	9.1	34.0	134.45	6.5
G-10	37.0	122.40	5.1	25.0	135.70	2.8
G-11	39.0	121.65	3.0	--	137.85	0.4
H-01	52.0	128.61	16.7	40.5	135.90	12.3
H-02	52.0	128.53	16.0	38.5	125.05	11.6
H-03	53.7	129.80	12.6	31.0	126.78	7.9
H-04	56.5	128.64	9.9	24.5	138.22	4.7
H-05	55.0	128.50	11.9	29.0	138.05	7.0
H-06	53.3	128.50	13.4	33.5	137.22	8.8
H-07	51.7	128.30	16.7	40.5	125.10	12.4

TABLE B3

Series Number	Applied Voltage	Coolant Flow			Top Chamber		Bottom Chamber	
	V KV	T_{in}	T_{out} °F	Δh cm Hg	T_{top} °F	P_{top} cm Hg	T_{bottom} °F	P_{bottom} cm Hg
J-01	0	78.05	81.05	12.7	125.67	10.0	114.37	7.5
J-03	6	77.00	80.46	12.0	125.20	6.0	107.67	1.3
J-05	0	76.65	79.90	12.0	124.60	8.6	114.37	5.4
J-06	2	76.60	79.85	12.0	136.59	8.5	116.68	4.0
J-07	4	76.55	80.10	12.0	125.25	7.1	115.45	3.0
J-08	6	76.15	79.80	12.0	125.05	4.0	112.11	-0.4
K-01	0	72.21	76.30	12.5	130.7	12.3	121.40	7.1
K-02	0	71.90	76.16	11.8	134.5	11.6	121.50	6.3
K-03	4	71.90	76.10	12.5	129.82	10.4	120.15	4.2
K-04	6	72.10	76.41	12.0	129.60	8.9	117.83	2.2
K-05	7	71.95	76.35	12.1	129.60	8.5	116.3	1.1
K-06	8	71.95	76.40	12.2	129.25	7.3	113.2	-0.1
K-07	9	71.93	76.35	12.2	128.95	6.9	110.3	-0.5
K-08	10	71.97	76.41	12.5	128.60	7.3	106.6	-0.3
K-09	8	72.08	76.47	12.5	130.00	8.0	107.7	1.2
K-10	9	72.00	76.40	12.6	131.20	7.4	107.6	-0.15
K-11	6	71.97	76.25	12.7	131.50	8.5	111.80	2.5
K-12	0	71.93	75.95	12.5	132.00	13.5	118.56	7.2

Series Number	Wall Temperature					Condensed Freon	
	T_{w1} °F	T_{w2} °F	T_{w3} °F	T_{w4} °F	T_{w5} °F	$T_{cond.}$ °F	Time Sec
J-01	97.55	97.79	91.45	86.30	82.30	111.15	53.1
J-03	97.05	94.91	92.33	87.75	84.19	105.30	53.05
J-05	96.65	94.20	92.12	85.55	81.21	111.57	51.1
J-06	96.90	94.25	90.65	85.85	81.71	114.00	50.8
J-07	97.05	94.90	91.99	86.99	83.11	113.05	51.1
J-08	96.22	94.33	91.92	87.32	84.10	110.95	49.5
K-01	96.95	95.00	91.25	84.00	79.00	119.00	40.6
K-02	96.53	94.75	90.80	84.10	78.20	119.20	39.6
K-03	96.50	95.00	91.00	85.08	79.08	117.65	39.1
K-04	96.57	95.10	91.70	86.20	80.16	115.82	40.6
K-05	96.65	95.23	91.95	86.55	80.80	114.50	39.0
K-06	96.45	95.17	92.02	87.05	81.60	112.95	40.1
K-07	96.03	95.02	92.02	87.18	83.50	108.52	40.1
K-08	96.47	95.30	92.50	87.70	78.60	104.85	40.5
K-09	96.50	95.36	92.00	86.90	81.83	106.05	40.5
K-10	95.90	94.75	91.73	86.70	81.31	105.77	40.5
K-11	96.45	---	---	---	80.55	109.65	40.5
K-12	96.39	94.76	90.33	83.65	77.78	115.92	40.5

Series Number	Vapor Generation			Vapor Trap		
	ϕ %	T °F	P cm Hg	ϕ %	T °F	P cm Hg
J-01	42.0	126.33	12.8	0	153.32	7.8
J-03	44.5	123.60	8.7	0	152.60	1.7
J-05	41.5	125.00	11.2	0	153.95	5.3
J-06	43.0	124.55	10.1	0	154.28	4.1
J-07	42.0	124.65	10.1	0	154.00	2.9
J-08	40.0	129.30	7.2	0	153.90	-0.4
K-01	53.3	128.00	16.3			
K-02	52.5	128.20	15.3			
K-03	54.9	127.35	14.6			
K-04	55.5	126.25	13.2			
K-05	57.0	125.75	12.9			
K-06	57.2	125.53	11.9			
K-07	57.0	125.70	13.5			
K-08	56.7	125.23	11.7			
K-09	54.0	127.23	12.1			
K-10	55.0	128.30	11.6			
K-11	53.5	128.18	12.6			
K-12	52.5	128.20	16.4			

APPENDIX C

SOLUTION OF ELECTROHYDRODYNAMIC INSTABILITY IN CYLINDRICAL GEOMETRY

The solutions for electrohydrodynamic (EHD) waves have been obtained by Melcher (Ref. 7) for a plane fluid interface in a uniform electric field, and he identifies various types of EHD waves, depending upon whether the electric field is perpendicular or parallel to the interface and whether the interface has or does not have free charges.

In the following analysis, the solution for the EHD waves will be developed for a concentric cylinder geometry, with the inner cylinder ($r = R_1$) at some high potential and the outer cylinder ($r = R_o$) at ground potential. The fluid interface is at radius $r = R^*$; liquid flows in the region $R^* < r < R_o$, and gas or vapor in the region $R_1 < r < R^*$. In the analysis, superscript (1) denotes the liquid medium and superscript (2) denotes the gas or vapor medium. The subscripts r, θ, and z denote the vector components in the cylindrical coordinate system and $\vec{r}$, $\vec{\theta}$, and $\vec{z}$ denote the respective unit vectors. The analysis assumes a charge-free interface.

I Bulk Equations of Motion

The equations which govern the motion of the bulk of the fluids are as follows:

$$\nabla \cdot \vec{v} = 0 \qquad (C.1.1)$$

$$\rho\left[\frac{\partial \vec{v}}{\partial t} + (\vec{v}\cdot\nabla)\vec{v}\right] + \nabla p = 0 \qquad (C.1.2)$$

$$\nabla \times \vec{E} = 0 \qquad (C.1.3)$$

$$\nabla \cdot \epsilon\vec{E} = 0 \qquad (C.1.4)$$

II Solution to Bulk Equations

In the following solution, the three dependent variables appearing in the bulk equations are assumed to be representable by a power series in small perturbation parameter Δ. Thus

$$p = \overset{0}{p}(r,\theta,z,t) + \Delta \overset{1}{p}(r,\theta,z,t) + \Delta^2 \overset{2}{p}(r,\theta,z,t) + \cdots\cdots \quad (C.2.1)$$

$$\vec{V} = \overset{0}{\vec{V}}(r,\theta,z,t) + \Delta \overset{1}{\vec{V}}(r,\theta,z,t) + \Delta^2 \overset{2}{\vec{V}}(r,\theta,z,t) + \cdots\cdots \quad (C.2.2)$$

$$\vec{E} = \overset{0}{\vec{E}}(r,\theta,z,t) + \Delta \overset{1}{\vec{E}}(r,\theta,z,t) + \Delta^2 \overset{2}{\vec{E}}(r,\theta,z,t) + \cdots\cdots \quad (C.2.3)$$

where the overscripts 0, 1, 2 indicate the zero, first and second order terms. The perturbation analysis presumes that there is an equilibrium condition of the dependent variables which satisfies the equations of motion together with the boundary conditions. Any perturbation from this equilibrium is hopefully predicted by such an analysis if the perturbations are small. The parameter Δ indicates the amplitude of perturbation, and hence the order of the approximation considered. In the present problem, the solution will be limited to a first-order approximation. To find the differential equations and boundary conditions consistent with the approximation, the assumed solutions of the variables are substituted into the equations of motion. The problem is "linearized" by neglecting all products of perturbation variables. The solution follows.

A. Pressure and Velocity

Substitution of (C.2.1) and (C.2.2) into (C.1.1) and (C.1.2) gives

$$\nabla \cdot \overset{0}{\vec{V}} + \Delta (\nabla \cdot \overset{1}{\vec{V}}) + \text{----------} = 0 \quad (C.1.1a)$$

$$\vec{r}\left(\rho \frac{\partial \overset{0}{v_r}}{\partial t} + \rho \overset{0}{\vec{V}} \cdot \nabla \overset{0}{v_r} + \frac{\partial \overset{0}{p}}{\partial r}\right) + \vec{\theta}\left(\rho \frac{\partial \overset{0}{v_\theta}}{\partial t} + \rho \overset{0}{\vec{V}} \cdot \nabla \overset{0}{v_\theta} + \frac{1}{r} \frac{\partial \overset{0}{p}}{\partial \theta}\right)$$

$$+ \vec{z}\left(\rho \frac{\partial \overset{0}{v_z}}{\partial t} + \rho \overset{0}{\vec{V}} \cdot \nabla \overset{0}{v_z} + \frac{\partial \overset{0}{p}}{\partial z}\right) + \Delta \left[\vec{r}\left(\rho \frac{\partial \overset{1}{v_r}}{\partial t} + \rho \overset{0}{\vec{V}} \cdot \nabla \overset{1}{v_r} + \right.\right.$$

$$\rho \overset{1}{\vec{V}} \cdot \nabla \overset{0}{v_r} + \frac{\partial \overset{1}{p}}{\partial r}\Big) + \vec{\theta}\left(\rho \frac{\partial \overset{1}{v_\theta}}{\partial t} + \rho \overset{0}{\vec{V}} \cdot \nabla \overset{1}{v_\theta} + \rho \overset{1}{\vec{V}} \cdot \nabla \overset{0}{v_\theta} + \frac{1}{r} \frac{\partial \overset{1}{p}}{\partial \theta}\right)$$

$$\left. + \vec{z}\left(\rho \frac{\partial \overset{1}{v_z}}{\partial t} + \rho \overset{0}{\vec{V}} \cdot \nabla \overset{1}{v_z} + \rho \overset{1}{\vec{V}} \cdot \nabla \overset{0}{v_z} + \frac{\partial \overset{1}{p}}{\partial z}\right)\right] + \text{-------} = 0 \quad (C.1.2a)$$

Since Δ is a parameter, the coefficient of each power of Δ in the expansion of the bulk equation must vanish.

1) Zero order solution - The coefficients of the zero order term in Δ in (C.1.1a) and (C.1.2a) are equated to zero:

$$\nabla \cdot \mathring{\vec{V}} = 0 \qquad \text{(C.1.1b)}$$

$$\left.\begin{aligned} \rho \frac{\partial \mathring{V}_r}{\partial t} + \rho \mathring{\vec{V}} \cdot \nabla \mathring{V}_r + \frac{\partial \mathring{p}}{\partial r} &= 0 \\ \rho \frac{\partial \mathring{V}_\theta}{\partial t} + \rho \mathring{\vec{V}} \cdot \nabla \mathring{V}_\theta + \frac{1}{r}\frac{\partial \mathring{p}}{\partial \theta} &= 0 \\ \rho \frac{\partial \mathring{V}_z}{\partial t} + \rho \mathring{\vec{V}} \cdot \nabla \mathring{V}_z + \frac{\partial \mathring{p}}{\partial z} &= 0 \end{aligned}\right\} \qquad \text{(C.1.2b)}$$

Zero-order solutions that satisfy these conditions are

$$\mathring{\vec{V}} = \mathring{V}_z \vec{z} \quad \text{and} \quad \mathring{p} = \pi$$

where $\mathring{V}$ is the equilibrium velocity of each phase and π is a constant.

2) First order solution - The zero order solution is substituted into (C.1.1a) and (C.1.2a) and the coefficients of Δ are set equal to zero:

$$\nabla \cdot \mathring{\vec{V}} = \frac{1}{r}\frac{\partial}{\partial r}(r \mathring{V}_r) + \frac{1}{r}\frac{\partial \mathring{V}_\theta}{\partial \theta} + \frac{\partial \mathring{V}_z}{\partial z} = 0 \qquad \text{(C.1.1c)}$$

$$\left.\begin{aligned} \rho \mathring{V} \frac{\partial \mathring{V}_r}{\partial z} + \rho \frac{\partial \mathring{V}_r}{\partial t} + \frac{\partial \mathring{p}}{\partial r} &= 0 \\ \rho \mathring{V} \frac{\partial \mathring{V}_\theta}{\partial z} + \rho \frac{\partial \mathring{V}_\theta}{\partial t} + \frac{1}{r}\frac{\partial \mathring{p}}{\partial \theta} &= 0 \\ \rho \mathring{V} \frac{\partial \mathring{V}_z}{\partial z} + \rho \frac{\partial \mathring{V}_z}{\partial t} + \frac{\partial \mathring{p}}{\partial z} &= 0 \end{aligned}\right\} \qquad \text{(C.1.2c)}$$

The first order solutions are assumed to be of the form

$$p' = Re\left[\tilde{p}(r)\exp j\psi\right]$$

$$\vec{v}' = Re\left[(\tilde{v}(r)\vec{r} + \tilde{v}_\theta(r)\vec{\theta} + \tilde{v}_z(r)\vec{z})\exp j\psi\right]$$

where

$$\psi \equiv \omega t - K_\theta\theta - K_z z$$

Substitution of these solutions into (C.1.2c) gives

$$\tilde{v}_r = \frac{j}{(\omega - K_z\bar{v})\rho}\frac{d\tilde{p}}{dr}$$

$$\tilde{v}_\theta = \frac{K_\theta}{(\omega - K_z\bar{v})\rho r}\tilde{p}$$

$$\tilde{v}_z = \frac{K_z}{(\omega - K_z\bar{v})\rho}\tilde{p}$$

and the substitution of these velocity components, in turn, into (C.1.1c) yields the equation for $\tilde{p}$:

$$Re\left[\frac{j}{(\omega - K_z\bar{v})\rho}\left(\frac{d^2\tilde{p}}{dr^2} + \frac{1}{r}\frac{d\tilde{p}}{dr} - \frac{K_\theta^2}{r^2}\tilde{p} - K_z^2\tilde{p}\right)\exp j\psi\right] = 0$$

A solution here is

$$\tilde{p} = A_1 I_{K_\theta}(K_z r) + A_2 K_{K_\theta}(K_z r)$$

where A_1 and A_2 are arbitrary constants. The velocity components can now be written in terms of this solution:

$$\tilde{v}_r = \frac{j}{(\omega - K_z\bar{v})\rho}\left[A_1 I'_{K_\theta}(K_z r) + A_2 K'_{K_\theta}(K_z r)\right]$$

$$\tilde{v}_\theta = \frac{K_\theta}{(\omega - K_z\bar{v})\rho r}\left[A_1 I_{K_\theta}(K_z r) + A_2 K_{K_\theta}(K_z r)\right]$$

$$\tilde{v}_z = \frac{K_z}{(\omega - K_z\bar{v})\rho}\left[A_1 I_{K_\theta}(K_z r) + A_2 K_{K_\theta}(K_z r)\right]$$

B. Electric Field

Equation (C.2.3) is substituted into (C.1.3) and (C.1.4) and the same procedure is followed as was done previously for the velocity and the pressure. Then

$$\nabla \times \overset{\circ}{\vec{E}} = 0 \qquad \text{(C.1.3a)}$$

$$\nabla \cdot \epsilon \overset{\circ}{\vec{E}} = 0 \qquad \text{(C.1.4a)}$$

$$\nabla \times \overset{'}{\vec{E}} = 0 \qquad \text{(C.1.3b)}$$

$$\nabla \cdot \epsilon \overset{'}{\vec{E}} = 0 \qquad \text{(C.1.4b)}$$

1) Zero order solution - The solution is identical to that for a cylindrical capacitor. Therefore,

$$\overset{\circ}{\vec{E}} = \frac{\Phi_0}{r} \vec{r}$$

where

$$\Phi_0 = V_0 / \epsilon \left[\frac{1}{\epsilon''} \ln \frac{R_0}{R^*} + \frac{1}{\epsilon'''} \ln \frac{R^*}{R_i} \right]$$

2) First order solution -

Assume a solution of the form

$$\overset{'}{\vec{E}} = Re\left[\left(\tilde{E}_r(r) \vec{r} + \tilde{E}_\theta(r) \vec{\theta} + \tilde{E}_z(r) \vec{z} \right) \exp j\psi \right]$$

Substitution of this into (C.1.3b) gives

$$\frac{1}{r} \begin{vmatrix} \vec{r} & r\vec{\theta} & \vec{z} \\ \frac{\partial}{\partial r} & \frac{\partial}{\partial \theta} & \frac{\partial}{\partial z} \\ Re(\tilde{E}_r e^{j\psi}) & Re(r\tilde{E}_\theta e^{j\psi}) & Re(\tilde{E}_z e^{j\psi}) \end{vmatrix} = 0$$

Then

$$Re\left\{\left[\vec{r}\left(-jK_\theta \tilde{E}_z + rjK_z \tilde{E}_\theta\right) + r\vec{\theta}\left(-jK_z \tilde{E}_r - \frac{d\tilde{E}_z}{dr}\right)\right.\right.$$
$$\left.\left. + \vec{z}\left(\tilde{E}_\theta + r\frac{d\tilde{E}_\theta}{dr} + jK_\theta \tilde{E}_r\right)\right] \exp j\psi\right\} = 0$$

This is satisfied by setting

$$\tilde{E}_r = \frac{j}{K_z}\frac{d\tilde{E}_z}{dr}$$

$$\tilde{E}_\theta = \frac{K_\theta}{rK_z}\tilde{E}_z$$

Substitution of these expressions into (C.1.4b) then yields the equation for $\tilde{E}_z$:

$$Re\left[\frac{\epsilon j}{K_z}\left(\frac{d^2\tilde{E}_z}{dr^2} + \frac{1}{r}\frac{d\tilde{E}_z}{dr} - \frac{K_\theta^2}{r^2}\tilde{E}_z - K_z^2\tilde{E}_z\right)\exp j\psi\right] = 0$$

A solution is

$$\tilde{E}_z = C_1 I_{K_\theta}(K_z r) + C_2 K_{K_\theta}(K_z r)$$

where C_1 and C_2 are arbitrary constants. Since the remaining components have been written in terms of $\tilde{E}_z$, their solutions are

$$\tilde{E}_r = \frac{j}{K_z}\left[C_1 I_{K_\theta}'(K_z r) + C_2 K_{K_\theta}'(K_z r)\right]$$

$$\tilde{E}_\theta = \frac{K_\theta}{rK_z}\left[C_1 I_{K_\theta}(K_z r) + C_2 K_{K_\theta}(K_z r)\right]$$

The general solutions for the pressure, velocity and electric field have been obtained valid to the first order in Δ . Again since Δ is small, all higher order terms are omitted in writing the boundary conditions and finding particular solutions.

III Description of Interface

A. The general equation of an interface is the surface described by $Y(r,\theta,z,t) = 0$

Assume

$$Y = R^* - r + \eta(\theta, z, t)$$

The differential equation of the interface,

$$\left(\frac{\partial Y}{\partial t} + \vec{V} \cdot \nabla Y\right)_{Y=0} = 0$$

then becomes

$$\left(\frac{\partial \eta}{\partial t} - V_r + \frac{V_\theta}{r}\frac{\partial \eta}{\partial \theta} + V_z \frac{\partial \eta}{\partial z}\right)_{r=R^*+\eta} = 0$$

As was done for the dependent variables, let η be represented by a power series in Δ :

$$\eta = \mathring{\eta} + \Delta \acute{\eta} + \Delta^2 \hat{\eta} + \text{-------}$$

Expansion of the interface differential equation in powers of Δ gives

$$\left(\frac{\partial \mathring{\eta}}{\partial t} - \mathring{V}_r + \frac{\mathring{V}_\theta}{r}\frac{\partial \mathring{\eta}}{\partial \theta} + \mathring{V}_z \frac{\partial \mathring{\eta}}{\partial z}\right)_{r=R^*} +$$

$$\Delta\left(\frac{\partial \acute{\eta}}{\partial t} - \acute{V}_r + \frac{\acute{V}_\theta}{r}\frac{\partial \mathring{\eta}}{\partial \theta} + \frac{\mathring{V}_\theta}{r}\frac{\partial \acute{\eta}}{\partial \theta} + \mathring{V}_z \frac{\partial \acute{\eta}}{\partial z} + \acute{V}_z \frac{\partial \mathring{\eta}}{\partial z}\right)_{r=R^*+\mathring{\eta}}$$

$$+ \text{----------} = 0$$

It is noted that $\mathring{\eta} = 0$ is a solution which causes the zero order coefficient to vanish. Then the requirement that the first order coefficient vanish becomes

$$\left(\frac{\partial \acute{\eta}}{\partial t} - \acute{V}_r + \mathring{V}_z \frac{\partial \acute{\eta}}{\partial z}\right)_{r=R^*+\mathring{\eta}} = 0 \qquad (C.3.1)$$

Next assume $\dot{\eta} = \tilde{\eta} \exp j\psi$

Substitution of this into (C.3.1) gives

$$\tilde{\eta} = \left[\frac{\tilde{V}_r}{j(\omega - K_z \dot{v})} \right]_{r=R^*} = \text{constant}$$

B. It is convenient to state the boundary conditions in terms of a unit normal vector $\vec{n}$. Since $\vec{n}$ depends only on the orientation of the surface, it is a function only of Y. The unit normal vector is defined as follows:

$$\vec{n} = \frac{\nabla Y}{|\nabla Y|} = \frac{-\vec{r} + \frac{1}{r}\frac{\partial \eta}{\partial \theta}\vec{\theta} + \frac{\partial \eta}{\partial z}\vec{z}}{\sqrt{1 + \left(\frac{1}{r}\frac{\partial \eta}{\partial \theta}\right)^2 + \left(\frac{\partial \eta}{\partial z}\right)^2}}$$

Substitution of the power series in Δ of η into the above expression yields, at $r = R^* + \eta$

$$\vec{n} = -\left\{ \vec{r} + \Delta Re\left[\left(\vec{\theta}\frac{K_\theta}{R^*}\tilde{\eta} + \vec{z} K_z \tilde{\eta} \right) j \exp j\psi \right] \right\} + \text{----} + \text{---} \qquad (C.3.2)$$

IV Boundary Conditions

There are a total of eight independent boundary conditions - two at each electrode and four at the interface leading to a solution of the eight arbitrary constants $A_1^{(1)}$, $A_2^{(1)}$, $A_1^{(2)}$, $A_2^{(2)}$, $C_1^{(1)}$, $C_2^{(1)}$, $C_1^{(2)}$, $C_2^{(2)}$.

A. The tangential components of the electric field at $r = R_1$ must vanish. Thus

$$\tilde{E}_z^{(2)}\Big|_{r=R_i} = C_1^{(2)} I_{K_\theta}(K_z R_i) + C_2^{(2)} K_{K_\theta}(K_z R_i) = 0 \qquad (C.4.1)$$

Also the radial component of the velocity is zero

$$\tilde{V}_r^{(2)}\Big|_{r=R_i} = \frac{j}{(\omega - K_z \dot{v}^{(2)})\rho^{(2)}} \left[A_1^{(2)} I'_{K_\theta}(K_z R_i) + A_2^{(2)} K'_{K_\theta}(K_z R_i) \right] = 0 \qquad (C.4.2)$$

B. The same conditions exist at the other electrode

$$\tilde{E}_z^{(i)}\Big|_{r=R_0} = C_1^{(i)} I_{K_\theta}(K_z R_0) + C_2^{(i)} K_{K_\theta}(K_z R_0) = 0 \qquad (C.4.3)$$

$$\tilde{V}_r^{(i)}\Big|_{r=R_0} = \frac{j}{(\omega - K_z \mathring{V}^{(i)})\,\rho^{(i)}}\left[A_1^{(i)} I'_{K_\theta}(K_z R_0) + A_2^{(i)} K'_{K_\theta}(K_z R_0)\right] = 0 \qquad (C.4.4)$$

C. Interfacial boundary conditions* - These boundary conditions are found by integrating the bulk equations (C.1.1) to (C.1.4) across the interface.

1) Continuity boundary condition

$$\vec{n} \cdot \left[\left[\vec{V}\right]\right]_{r=R^*+\eta} = 0$$

This condition is satisfied by requiring that

$$\tilde{\eta}^{(1)} = \tilde{\eta}^{(2)}$$

or

$$\frac{\tilde{V}_r^{(1)}}{j(\omega - K_z \mathring{V}^{(1)})}\Bigg|_{r=R^*} = \frac{\tilde{V}_r^{(2)}}{j(\omega - K_z \mathring{V}^{(2)})}\Bigg|_{r=R^*}$$

Then

$$\frac{A_1^{(1)} I'_{K_\theta}(K_z R^*) + A_2^{(1)} K'_{K_\theta}(K_z R^*)}{(\omega - K_z \mathring{V}^{(1)})^2\,\rho^{(1)}} = \frac{A_1^{(2)} I'_{K_\theta}(K_z R^*) + A_2^{(2)} K'_{K_\theta}(K_z R^*)}{(\omega - K_z \mathring{V}^{(2)})^2\,\rho^{(2)}} \qquad (C.4.5)$$

* $[[\,]]$ denotes the difference of the double-bracketed quantity evaluated in the regions (2) and (1).

2)

$$\vec{n} \cdot [[\epsilon \vec{E}]]_{r=R^*+\eta} = 0$$

or

$$(\epsilon^{(2)} E_r^{(2)} - \epsilon^{(1)} E_r^{(1)})_{r=R^*} = 0$$

Therefore,

$$C_1^{(2)} \epsilon^{(2)} I'_{K_\theta}(K_z R^*) + C_2^{(2)} \epsilon^{(2)} K'_{K_\theta}(K_z R^*)$$

$$- C_1^{(1)} \epsilon^{(1)} I'_{K_\theta}(K_z R^*) - C_2^{(1)} \epsilon^{(1)} K'_{K_\theta}(K_z R^*) = 0 \qquad (C.4.6)$$

3)

$$\vec{n} \times [[\vec{E}]]_{r=R^*+\eta} = 0$$

or

$$\begin{vmatrix} \vec{r} & \vec{\theta} & \vec{z} \\ -1 & \mathrm{Re}\left[-\frac{\Delta K_\theta}{R^*} \tilde{\eta} j e^{j\psi}\right] & \mathrm{Re}\left[-\Delta K_z \tilde{\eta} j e^{j\psi}\right] \\ \frac{[[\Phi_0]]}{R^*} + \Delta [[E'_r]]_{r=R^*} & \Delta [[E'_\theta]]_{r=R^*} & \Delta [[E'_z]]_{r=R^*} \end{vmatrix} = 0$$

therefore,

$$K_z \tilde{\eta} j e^{j\psi} \frac{[[\Phi_0]]}{R^*} = [[E'_z]]_{r=R^*}$$

and

$$\frac{K_\theta}{R^*} \tilde{\eta} j e^{j\psi} \frac{[[\Phi_0]]}{R^*} = [[E'_\theta]]_{r=R^*}$$

But since $E'_\theta = \frac{K_\theta}{K_z} E'_z$ the two equations are not independent and the single relation is

$$C_1^{(2)} I_{K_\theta}(K_z R^*) + C_2^{(2)} K_{K_\theta}(K_z R^*) - C_1^{(1)} I_{K_\theta}(K_z R^*) - C_2^{(1)} K_{K_\theta}(K_z R^*)$$

$$- \frac{[[\Phi_0]] K_z j}{R^* \rho^{(1)}(\omega - K_z v^{(1)})^2} A_1^{(1)} I'_{K_\theta}(K_z R^*) - \frac{[[\Phi_0]] K_z j}{R^* \rho^{(1)}(\omega - K_z v^{(1)})^2} \cdot$$

$$\cdot A_2^{(1)} K'_{K_\theta}(K_z R^*) = 0 \qquad (C.4.7)$$

4) Momentum boundary conditions

$$n_\alpha \left[\!\left[p\right]\!\right]_{r=R^*+\eta} = n_\beta \left[\!\left[\Sigma_{\alpha\beta}\right]\!\right]_{r=R^*+\eta}$$

where α and β take on the values r, θ, z.

$\Sigma_{\alpha\beta}$ (total stress tensor) = $\Sigma_{\alpha\beta}^{\text{Mech.}} + \Sigma_{\alpha\beta}^{\text{elect.}}$

where (ref. 7)

$$\left[\!\left[\Sigma_{\alpha\beta}^{\text{mech.}}\right]\!\right] = \delta_{\alpha\beta}\,\sigma\left[\frac{1}{R^*} - \frac{1}{R^{*2}}\left(\eta + \frac{\partial^2\eta}{\partial\theta^2}\right) - \frac{\partial^2\eta}{\partial z^2}\right]$$

$$\left[\!\left[\Sigma_{\alpha\beta}^{\text{elect.}}\right]\!\right] = \epsilon E_\alpha E_\beta - \frac{1}{2}\epsilon\,\delta_{\alpha\beta} E_\gamma E_\gamma$$

a) Momentum condition for α = r

$$-\left[\!\left[\pi\right]\!\right]_{r=R^*} - \Delta\left[\!\left[p'\right]\!\right]_{r=R^*} = -\frac{\sigma}{R^*} - \Delta\sigma\,Re\left[\left(\frac{K_\theta^2-1}{R^{*2}} + K_z^2\right)\eta\right]$$
$$-\frac{\epsilon^{(2)}}{2}\left(\frac{\bar{\phi}_o^{(2)}}{r} + \Delta E_r^{(2)}\right)^2_{r=R^*+\eta} + \frac{\epsilon^{(1)}}{2}\left(\frac{\bar{\phi}_o^{(1)}}{r} + \Delta E_r^{(1)}\right)^2_{r=R^*+\eta}$$

Zero order:

$$\left[\!\left[\pi\right]\!\right] = \frac{\sigma}{R^*} + \frac{1}{2}\frac{\left[\!\left[\epsilon\bar{\phi}_o^2\right]\!\right]}{R^{*2}}$$

First order:

$$\left[\!\left[\tilde{p}\right]\!\right]_{r=R^*} = \sigma\left(\frac{K_\theta^2-1}{R^{*2}} + K_z^2\right)\tilde{\eta} + \frac{\left[\!\left[\epsilon\bar{\phi}_o\tilde{E}_r\right]\!\right]}{R^*} + \frac{\left[\!\left[\epsilon\bar{\phi}_o^2\right]\!\right]\tilde{\eta}}{R^{*3}}$$

or

$$A_1^{(2)} I_{K_\theta}(K_z R^*) + A_2^{(2)} K_{K_\theta}(K_z R^*)$$

$$+ A_1^{(1)}\left\{-I_{K_\theta}(K_z R^*) - \frac{\sigma\left[(K_\theta^2-1)/R^{*2} + K_z^2\right] + \left[\!\left[\epsilon\bar{\phi}_o^2\right]\!\right]/R^{*3}}{(\omega - K_z\bar{v}^{(1)})^2\,\mathcal{J}^{(1)}} I'_{K_\theta}(K_z R^*)\right\}$$

$$+ A_2^{(1)}\left\{-K_{K_\theta}(K_z R^*) - \frac{\left[(K_\theta^2-1)/R^{*2} + K_z^2\right] + \left[\!\left[\epsilon\bar{\phi}_o^2\right]\!\right]/R^{*3}}{(\omega - K_z\bar{v}^{(1)})^2\,\mathcal{J}^{(1)}} K'_{K_\theta}(K_z R^*)\right\}$$

$$-\frac{\epsilon^{(2)}\bar{\phi}_o^{(2)} j}{R^* K_z}\left[C_1^{(2)} I'_{K_\theta}(K_z R^*) + C_2^{(2)} K'_{K_\theta}(K_z R^*)\right]$$

$$+\frac{\epsilon^{(1)}\bar{\phi}_o^{(1)} j}{R^* K_z}\left[C_1^{(1)} I'_{K_\theta}(K_z R^*) + C_2^{(1)} K'_{K_\theta}(K_z R^*)\right] = 0 \qquad \text{(c.4.8)}$$

b) The momentum conditions for $\alpha = \theta$ and $\alpha = z$ reduce identically to (C.4.7) and are therefore not independent conditions.

V Dispersion Equation

The eight independent boundary conditions (C.4.1) to (C.4.8) give eight homogeneous equations in the constants $(A_1^{(1)} \rightarrow C_2^{(2)})$. For a nontrivial solution to exist the determinant of the coefficients must vanish. This requirement gives the dispersion relation between ω and K_θ, K_z.

$$\omega = \left\{ \frac{K_z (\rho_{eq}^{(1)} \mathring{V}^{(1)} + \rho_{eq}^{(2)} \mathring{V}^{(2)})}{\rho_{eq}} \pm \left[\frac{\sigma \left(\frac{K_\theta^2 - 1}{R^{*2}} + K_z^2 \right) K_z}{\rho_{eq}} + \frac{E_o^{(1)} E_o^{(2)} (\epsilon^{(1)} - \epsilon^{(2)}) K_z}{\rho_{eq}} \left(\frac{1}{R^*} - \frac{(\epsilon^{(1)} - \epsilon^{(2)}) K_z}{\epsilon_{eq}} \right) - K_z^2 \frac{(\mathring{V}^{(1)} - \mathring{V}^{(2)})^2 \rho_{eq}^{(1)} \rho_{eq}^{(2)}}{(\rho_{eq})^2} \right]^{\frac{1}{2}} \right\} \quad \text{(C.5.1)}$$

where

$$\rho_{eq}^{(1)} = K_z \rho^{(1)} \frac{I'_{K_\theta}(K_z R_o) K_{K_\theta}(K_z R^*) - I_{K_\theta}(K_z R^*) K'_{K_\theta}(K_z R_o)}{I'_{K_\theta}(K_z R^*) K'_{K_\theta}(K_z R_o) - I'_{K_\theta}(K_z R_o) K'_{K_\theta}(K_z R^*)}$$

$$\rho_{eq}^{(2)} = K_z \rho^{(2)} \frac{I'_{K_\theta}(K_z R_i) K_{K_\theta}(K_z R^*) - I_{K_\theta}(K_z R^*) K'_{K_\theta}(K_z R_i)}{I'_{K_\theta}(K_z R_i) K'_{K_\theta}(K_z R^*) - I'_{K_\theta}(K_z R^*) K'_{K_\theta}(K_z R_i)}$$

$$\rho_{eq} = \rho_{eq}^{(1)} + \rho_{eq}^{(2)}$$

$$\epsilon_{eq} = K_z \left[\epsilon^{(1)} \frac{I_{K_\theta}(K_z R^*) K_{K_\theta}(K_z R_i) - I_{K_\theta}(K_z R_i) K_{K_\theta}(K_z R^*)}{I'_{K_\theta}(K_z R^*) K_{K_\theta}(K_z R_i) - I_{K_\theta}(K_z R_i) K'_{K_\theta}(K_z R^*)} + \epsilon^{(2)} \frac{I_{K_\theta}(K_z R_o) K_{K_\theta}(K_z R^*) - I_{K_\theta}(K_z R^*) K_{K_\theta}(K_z R_o)}{I'_{K_\theta}(K_z R^*) K_{K_\theta}(K_z R_o) - I_{K_\theta}(K_z R_o) K'_{K_\theta}(K_z R^*)} \right]$$

$$E_o^{(1)} = \Phi_o^{(1)} / R^* = V_o / \epsilon^{(1)} R^* \left[\frac{1}{\epsilon^{(1)}} \ln \frac{R_o}{R^*} + \frac{1}{\epsilon^{(2)}} \ln \frac{R^*}{R_i} \right]$$

$$E_o^{(2)} = \Phi_o^{(2)} / R^* = V_o / \epsilon^{(2)} R^* \left[\frac{1}{\epsilon^{(1)}} \ln \frac{R_o}{R^*} + \frac{1}{\epsilon^{(2)}} \ln \frac{R^*}{R_i} \right]$$

Equation (C.5.1) is greatly simplified if it is assumed that $R_o - R_1$ remains finite and R^* becomes infinite. This essentially reduces the problem from the cylindrical to the plane case.

Then for any two radii R_1 and R_2 having values between R_i and R_o,

$$\frac{I'_{K_\theta}(K_z R_2)K_{K_\theta}(K_z R_1) - I_{K_\theta}(K_z R_1)K'_{K_\theta}(K_z R_2)}{I'_{K_\theta}(K_z R_1)K'_{K_\theta}(K_z R_2) - I'_{K_\theta}(K_z R_2)K'_{K_\theta}(K_z R_1)} \longrightarrow \frac{\coth K_z(R_2 - R_1)}{K_z}$$

$$\frac{I_{K_\theta}(K_z R_1)K_{K_\theta}(K_z R_2) - I_{K_\theta}(K_z R_2)K_{K_\theta}(K_z R_1)}{I'_{K_\theta}(K_z R_1)K_{K_\theta}(K_z R_2) - I_{K_\theta}(K_z R_2)K'_{K_\theta}(K_z R_1)} \longrightarrow \frac{\tanh K_z(R_1 - R_2)}{K_z}$$

This reduces the dispersion equation to the following form:

$$\left[\omega - \frac{K_z(\rho_{eq}^{(1)}V^{(1)} + \rho_{eq}^{(2)}V^{(2)})}{\rho_{eq}}\right]^2 = \frac{\sigma K_z^3}{\rho_{eq}} - \frac{(\epsilon^{(2)} - \epsilon^{(1)})^2 E_o^{(2)} E_o^{(1)} K_z^2}{\rho_{eq}\cdot\epsilon_{eq}} - K_z^2 \frac{(V^{(1)} - V^{(2)})^2 \rho_{eq}^{(1)}\rho_{eq}^{(2)}}{\rho_{eq}^2} \quad (C5.2)$$

where

$$\rho_{eq}^{(1)} = \rho^{(1)} \coth K_z(R_o - R^*) \qquad \rho_{eq}^{(2)} = \rho^{(2)} \coth K_z(R^* - R_i)$$

$$\rho_{eq} = \rho_{eq}^{(1)} + \rho_{eq}^{(2)}$$

$$\epsilon_{eq} = \epsilon^{(1)} \tanh K_z(R^* - R_i) + \epsilon^{(2)} \tanh K_z(R_o - R^*)$$

$$E_o^{(1)} = V_o/\epsilon^{(1)}\left[\frac{1}{\epsilon^{(1)}}(R_o - R^*) + \frac{1}{\epsilon^{(2)}}(R^* - R_i)\right]$$

$$E_o^{(2)} = V_o/\epsilon^{(2)}\left[\frac{1}{\epsilon^{(1)}}(R_o - R^*) + \frac{1}{\epsilon^{(2)}}(R^* - R_i)\right]$$

Equation (C.5.2) may be compared with that obtained by Melcher (Ref. 7) who treated the case of a plane horizontal interface in a gravitational field with no parallel motion of the fluids. His dispersion equation is presented in terms of the phase velocities of the gravity, capillary and EHD waves:

$$\omega^2 = K^2(v_g^2 + v_c^2 + v_e^2)$$

where $$v_g^2 = \frac{g(\rho^{(1)} - \rho^{(2)})}{\rho_{eq} K} \qquad (C.5.3)$$

$$v_c^2 = \frac{\sigma K}{\rho_{eq}}$$

$$v_e^2 = (\epsilon^{(2)} - \epsilon^{(1)})^2 E_o^{(2)} E_o^{(1)} / \rho_{eq} \epsilon_{eq}$$

It is readily seen that (C.5.2) and (C.5.3) are identical if, in the former equation, the parallel motion is neglected ($V^{(1)} = V^{(2)} = 0$), and in the latter equation, the gravitational term is neglected.

In the two-phase flow and condensing systems, superscript $^{(1)}$ refers to the liquid and superscript $^{(2)}$ to the gas or the vapor. Therefore, $\rho^{(2)} \ll \rho^{(1)}$. Further, if the liquid layer is thin and the vapor layer is sufficiently thick, the following assumptions should hold:

$$\frac{2\pi(R_0 - R^*)}{\lambda} \ll 1$$

$$\frac{2\pi(R^* - R_i)}{\lambda} > 2$$

the dispersion equation (C.5.2) then reduces to

$$(\omega - K V_\ell)^2 \cong \frac{(R_0 - R^*) K^3}{\rho_\ell} \left[\sigma K - (1 - \frac{\epsilon_g}{\epsilon_\ell})^2 \epsilon_g E_g^2 - \rho_g (V_\ell - V_g)^2\right] \qquad (C.5.4)$$

If the relative velocity term ($V_l - V_g$) were small enough to be negligible, then (C.5.4) further reduces to

$$(\omega - KV_l)^2 = \frac{(R_0 - R^*)K^3}{\rho_l}\left[\sigma K - (1 - \frac{\epsilon_g}{\epsilon_l})^2 \epsilon_g E_g^2\right] \qquad (C.5.5)$$

To obtain the characteristic wave numbers K^*, the right hand side of (C.5.4) or (C.5.5) is differentiated with respect to K, equated to zero and solved for K^*. The results are

$$K^* = \frac{3}{4\sigma}\left[(V_l - V_g)^2 \rho_g + (1 - \frac{\epsilon_g}{\epsilon_l})^2 \epsilon_g E_g^2\right] \qquad (C.5.6)$$

if the relative velocities were significant, and

$$K^* = \frac{3}{4\sigma}\left[(1 - \frac{\epsilon_g}{\epsilon_l})^2\right] \epsilon_g E_g^2 \qquad (C.5.7)$$

if the relative velocities can be neglected.

APPENDIX D1

COMPUTER PROGRAM (FLOW CHART) FOR CALCULATION OF NUSSELT NUMBER AND GRASHOF NUMBER

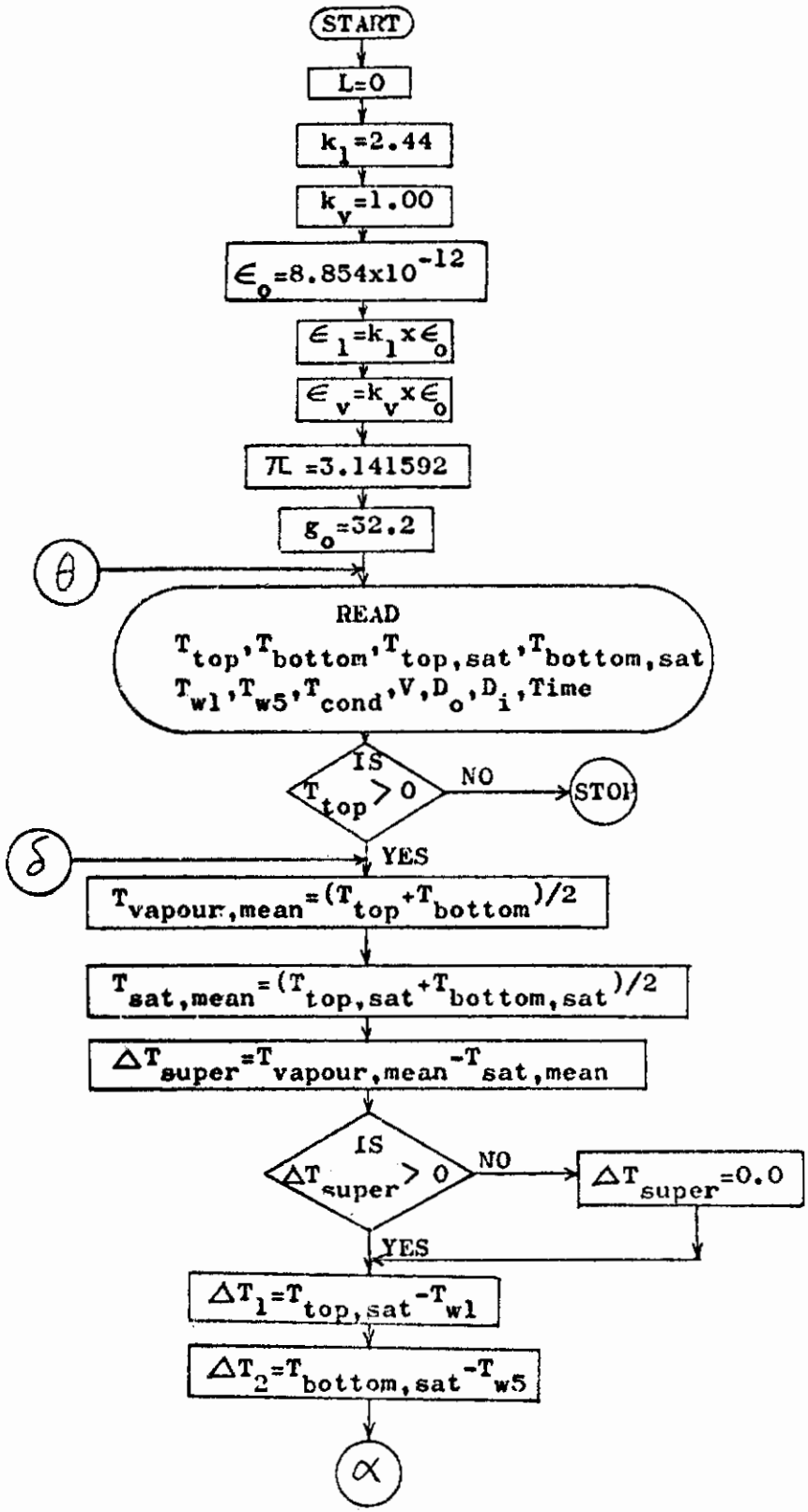

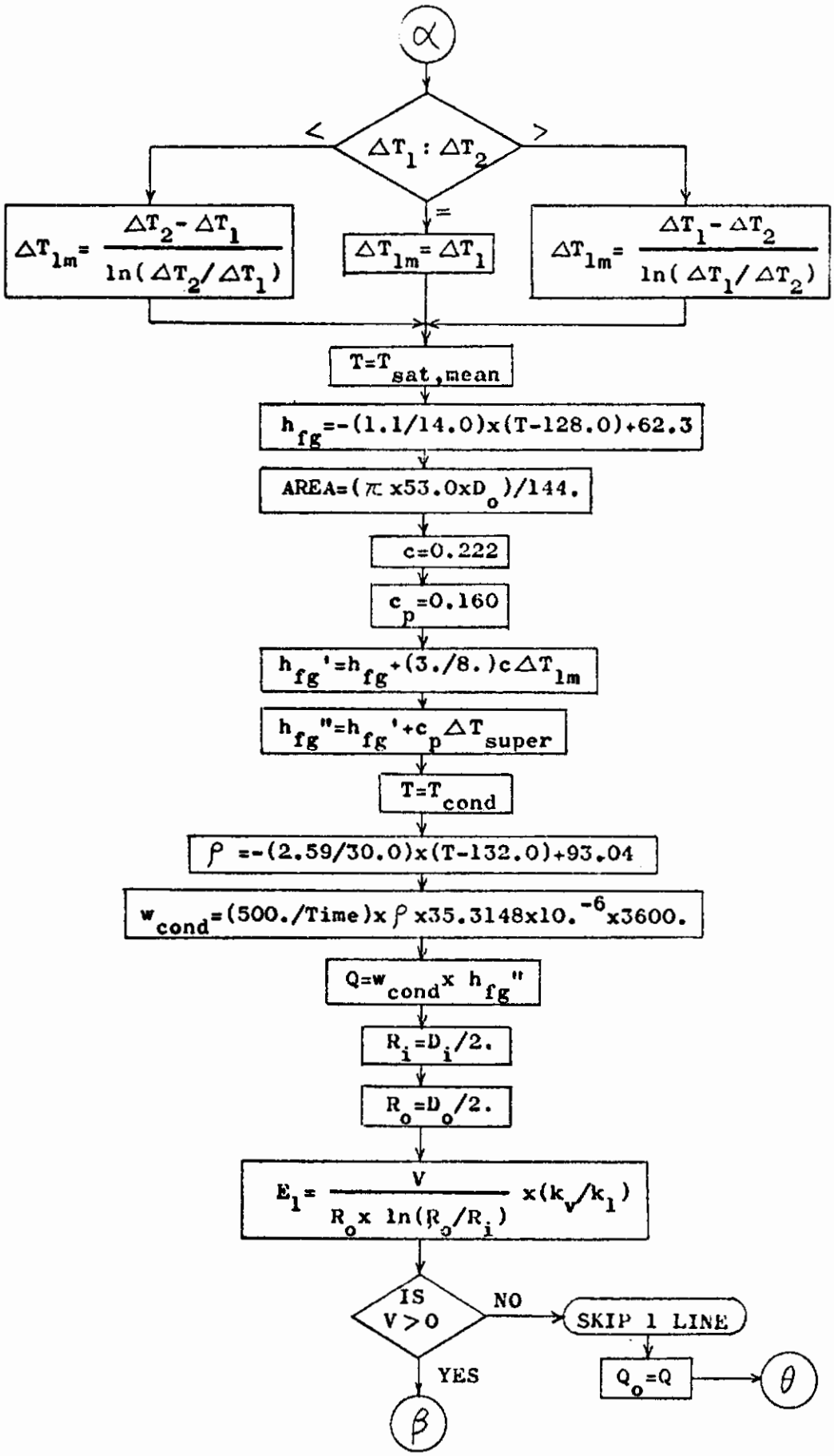

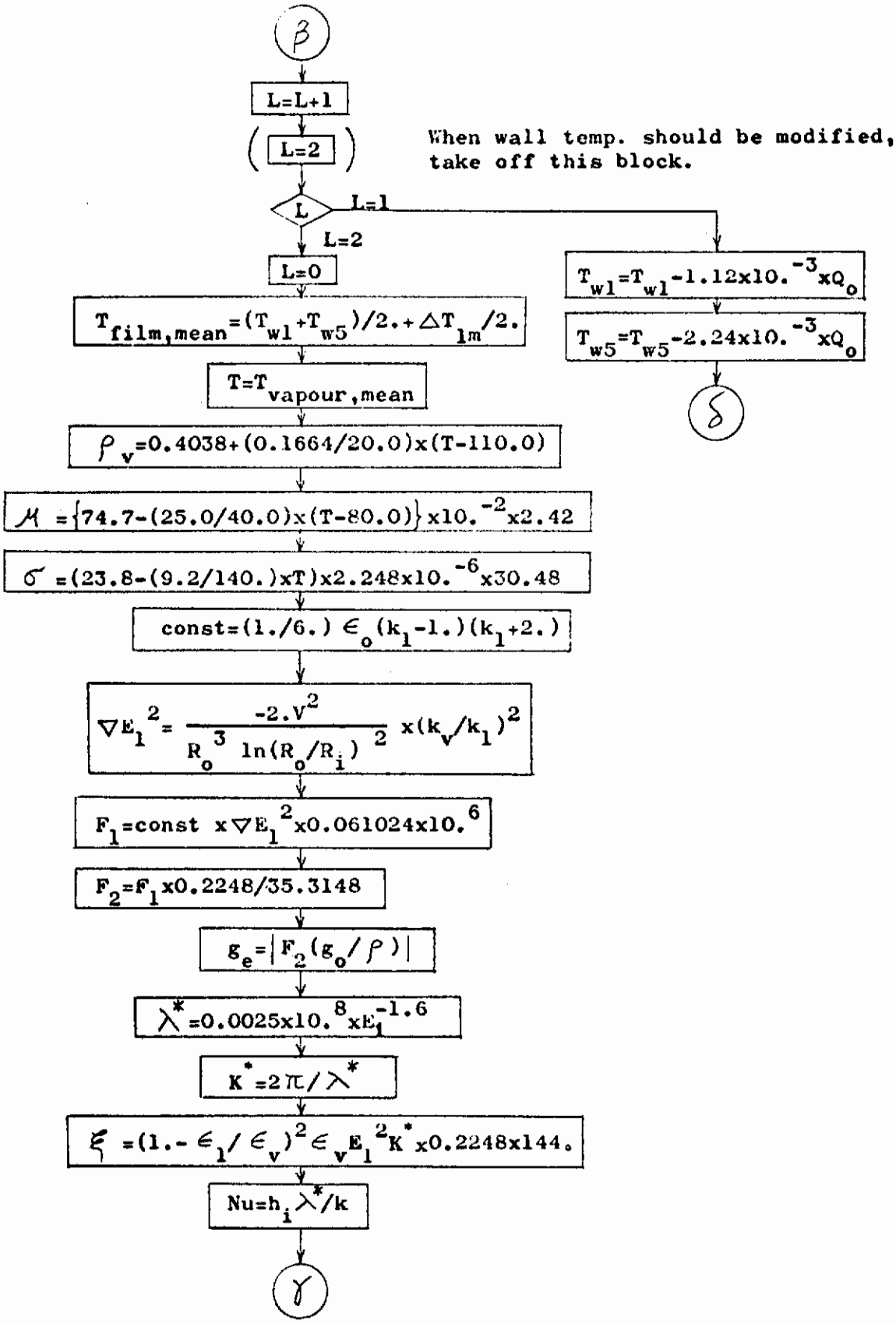

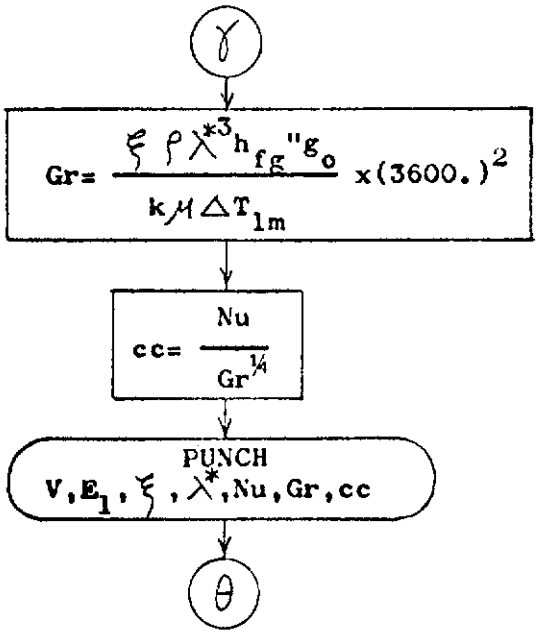

APPENDIX D2

COMPUTER PROGRAM (FLOW CHART) FOR CALCULATION OF ANGULAR FREQUENCY

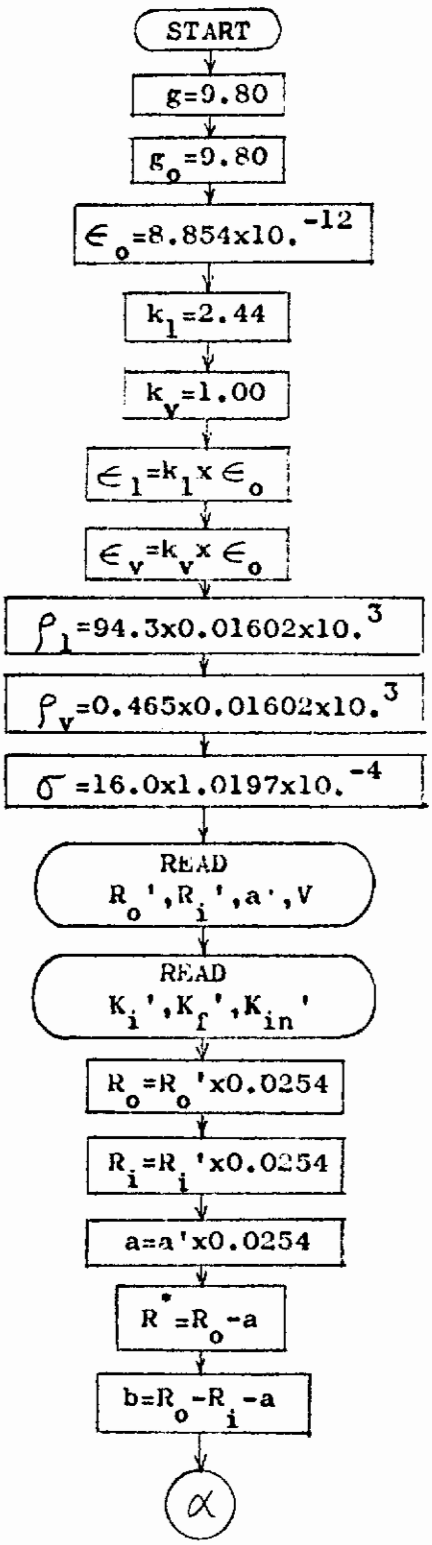

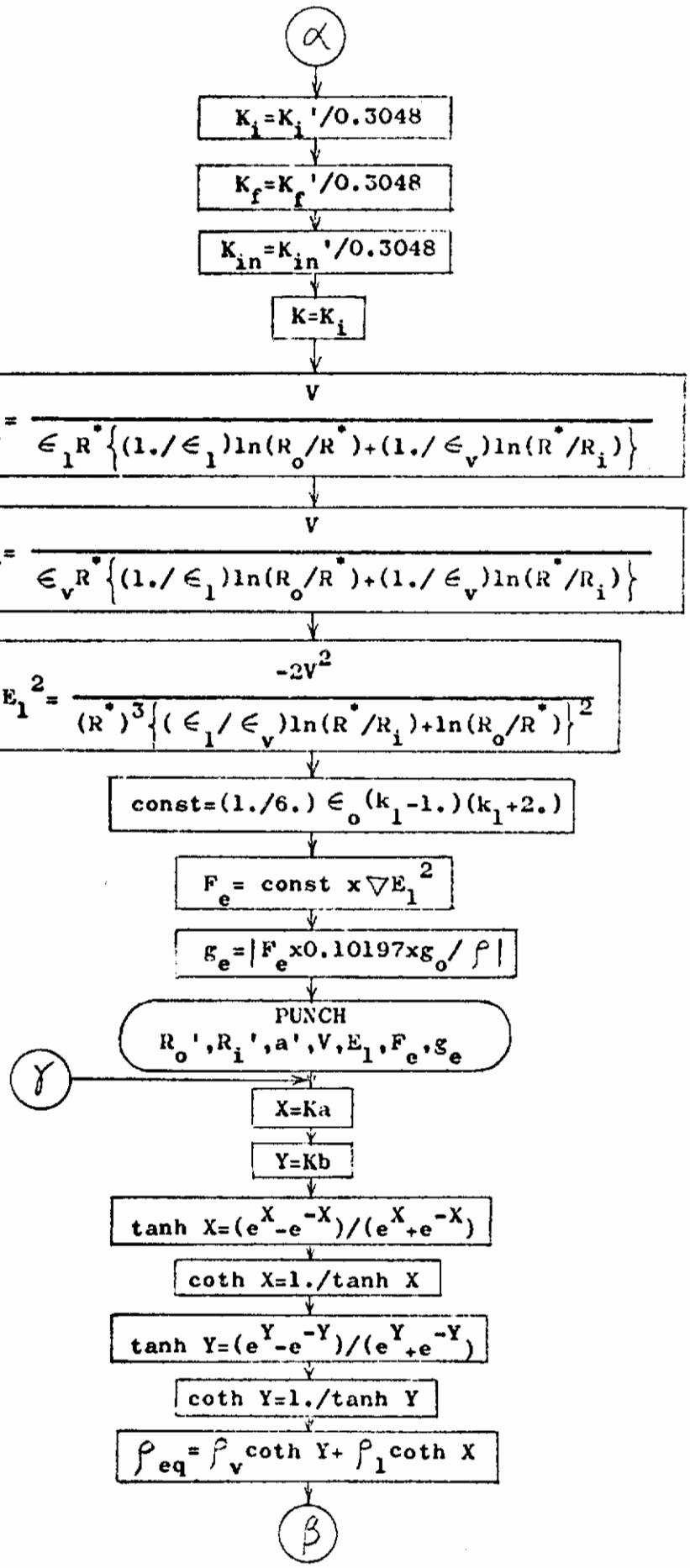

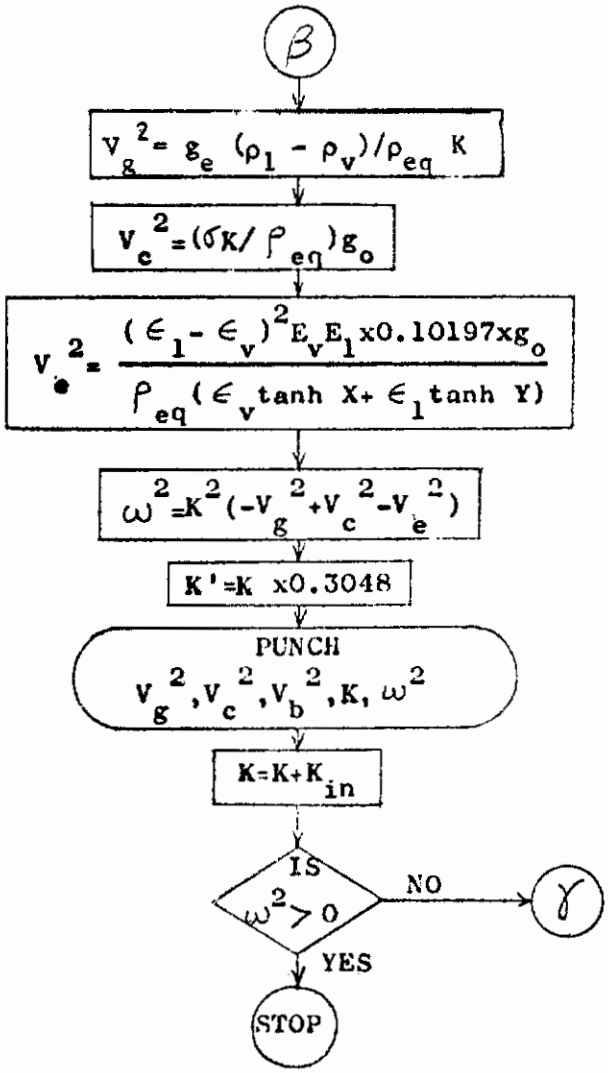

UNCLASSIFIED
Security Classification

DOCUMENT CONTROL DATA - R&D
(Security classification of title, body of abstract and indexing annotation must be entered when the overall report is classified)

1. ORIGINATING ACTIVITY *(Corporate author)*
Tufts University
Medford 55, Massachusetts

2a. REPORT SECURITY CLASSIFICATION
UNCLASSIFIED

2b. GROUP

3. REPORT TITLE
Study of Electrostatic Effects on Condensing Heat Transfer

4. DESCRIPTIVE NOTES *(Type of report and inclusive dates)*
Final Report

5. AUTHOR(S) *(Last name, first name, initial)*
Choi, Harry Y., Reynolds, John M.

6. REPORT DATE	7a. TOTAL NO. OF PAGES	7b. NO. OF REFS
May 1965	124	11

8a. CONTRACT OR GRANT NO.
AF33(657)-10908
b. PROJECT NO. 6146
614615
c.
d.

9a. ORIGINATOR'S REPORT NUMBER(S)
None

9b. OTHER REPORT NO(S) *(Any other numbers that may be assigned this report)*
AFFDL-TR-65-51

10. AVAILABILITY/LIMITATION NOTICES
This report will be available through DDC to all qualified DDC users.

11. SUPPLEMENTARY NOTES

12. SPONSORING MILITARY ACTIVITY
Air Force Flight Dynamics Laboratory
Research and Technology Division
Wright-Patterson Air Force Base, O.

13. ABSTRACT

A study on the effects of strong electric fields on condensation heat transfer and two-phase flow has confirmed that significant changes in the flow regimes and heat transfer are possible with negligible electrical power expenditure. Over 100 per cent increase in heat transfer has been attained with pressure drop increases which are of the order of 15 per cent in the annular flow regime.

Results show that the slug flow regime is substantially suppressed. In essence, slug flow occurs only in the region of very low gas flows in which the system is almost entirely gravity dependent. The increase in heat transfer rates is gradual up to a certain threshold value of the applied voltage; beyond this value, the increase is steep. Some progress has been made in analytical and physical modeling of the phenomenon both from the viewpoint of determining pressure drop and heat transfer and of aiding in the determination of the fluid configuration at the heat transfer surface.

DD FORM 1 JAN 64 1473

UNCLASSIFIED
Security Classification

UNCLASSIFIED
Security Classification

14. KEY WORDS	LINK A		LINK B		LINK C	
	ROLE	WT	ROLE	WT	ROLE	WT
1. Heat Transfer						
2. Condensation						
3. Heat Exchanger Design						
4. Fluid Mechanics						

INSTRUCTIONS

1. ORIGINATING ACTIVITY: Enter the name and address of the contractor, subcontractor, grantee, Department of Defense activity or other organization *(corporate author)* issuing the report.

2a. REPORT SECURITY CLASSIFICATION: Enter the overall security classification of the report. Indicate whether "Restricted Data" is included. Marking is to be in accordance with appropriate security regulations.

2b. GROUP: Automatic downgrading is specified in DoD Directive 5200.10 and Armed Forces Industrial Manual. Enter the group number. Also, when applicable, show that optional markings have been used for Group 3 and Group 4 as authorized.

3. REPORT TITLE: Enter the complete report title in all capital letters. Titles in all cases should be unclassified. If a meaningful title cannot be selected without classification, show title classification in all capitals in parenthesis immediately following the title.

4. DESCRIPTIVE NOTES: If appropriate, enter the type of report, e.g., interim, progress, summary, annual, or final. Give the inclusive dates when a specific reporting period is covered.

5. AUTHOR(S): Enter the name(s) of author(s) as shown on or in the report. Enter last name, first name, middle initial. If military, show rank and branch of service. The name of the principal author is an absolute minimum requirement.

6. REPORT DATE: Enter the date of the report as day, month, year; or month, year. If more than one date appears on the report, use date of publication.

7a. TOTAL NUMBER OF PAGES: The total page count should follow normal pagination procedures, i.e., enter the number of pages containing information.

7b. NUMBER OF REFERENCES: Enter the total number of references cited in the report.

8a. CONTRACT OR GRANT NUMBER: If appropriate, enter the applicable number of the contract or grant under which the report was written.

8b, 8c, & 8d. PROJECT NUMBER: Enter the appropriate military department identification, such as project number, subproject number, system numbers, task number, etc.

9a. ORIGINATOR'S REPORT NUMBER(S): Enter the official report number by which the document will be identified and controlled by the originating activity. This number must be unique to this report.

9b. OTHER REPORT NUMBER(S): If the report has been assigned any other report numbers *(either by the originator or by the sponsor)*, also enter this number(s).

10. AVAILABILITY/LIMITATION NOTICES: Enter any limitations on further dissemination of the report, other than those imposed by security classification, using standard statements such as:

(1) "Qualified requesters may obtain copies of this report from DDC."

(2) "Foreign announcement and dissemination of this report by DDC is not authorized."

(3) "U. S. Government agencies may obtain copies of this report directly from DDC. Other qualified DDC users shall request through _____."

(4) "U. S. military agencies may obtain copies of this report directly from DDC. Other qualified users shall request through _____."

(5) "All distribution of this report is controlled. Qualified DDC users shall request through _____."

If the report has been furnished to the Office of Technical Services, Department of Commerce, for sale to the public, indicate this fact and enter the price, if known.

11. SUPPLEMENTARY NOTES: Use for additional explanatory notes.

12. SPONSORING MILITARY ACTIVITY: Enter the name of the departmental project office or laboratory sponsoring *(paying for)* the research and development. Include address.

13. ABSTRACT: Enter an abstract giving a brief and factual summary of the document indicative of the report, even though it may also appear elsewhere in the body of the technical report. If additional space is required, a continuation sheet shall be attached.

It is highly desirable that the abstract of classified reports be unclassified. Each paragraph of the abstract shall end with an indication of the military security classification of the information in the paragraph, represented as *(TS), (S), (C), or (U)*.

There is no limitation on the length of the abstract. However, the suggested length is from 150 to 225 words.

14. KEY WORDS: Key words are technically meaningful terms or short phrases that characterize a report and may be used as index entries for cataloging the report. Key words must be selected so that no security classification is required. Identifiers, such as equipment model designation, trade name, military project code name, geographic location, may be used as key words but will be followed by an indication of technical context. The assignment of links, rules, and weights is optional.

UNCLASSIFIED
Security Classification